Université catholique de Louvain
Institut de Recherche Expérimentale et Clinique
Pôle de Morphologie

Influence of hyaluronidase Spam1 in the pathogenesis of osteoarthritis

Sébastien Lafont

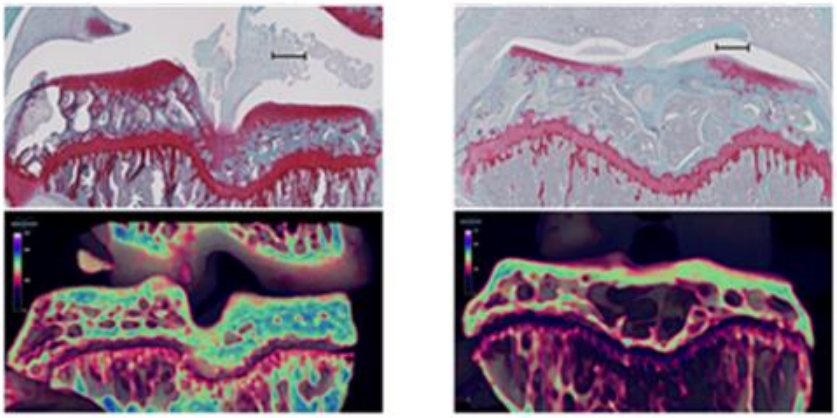

Wild Type OA Spam1$^{-/-}$ OA

Promoteur : Prof. Catherine Behets
Co-promoteur : Prof. Daniel Manicourt

Thèse présentée en vue de l'obtention du grade de Docteur en Sciences Biomédicales et Pharmaceutiques

Novembre 2020

“A hero can be anyone.
Even a man doing something as simple and reassuring as putting a coat around a young boy’s shoulders to let him know the world hadn’t ended.”
B. W.

Composition of the thesis jury

Promoter:	**Prof. Catherine Behets** Pôle de morphologie, Institut de Recherche Expérimentale et Clinique, UCLouvain
Co-promoter:	**Prof. Daniel Manicourt** Faculté de médecine et médecine dentaire, UCLouvain
Jury chairman:	**Prof. Étienne Marbaix** Pôle de biologie cellulaire, Institut de Duve, UCLouvain
Members:	**Prof. Miikka Vikkula** Pôle de génétique, Institut de Duve, UCLouvain
	Prof. Frédéric Lecouvet Pôle d'imagerie médicale, Institut de Recherche Expérimentale et Clinique, UClouvain
	Prof. Emmanuel Thienpont Neuro Musculo Skeletal Lab, Institut de Recherche Expérimentale et Clinique, UClouvain
External members:	**Prof. Frank Luyten** Division of Rheumatology, Department of Musculoskeletal Sciences, KU Leuven
	Prof. Ivan Martin Department of Biomedicine, University of Basel
Author:	**Sébastien Lafont** Pôle de morphologie, Institut de Recherche Expérimentale et Clinique, UClouvain 52, Avenue Mounier – B1.52.04 B-1200 Brussels, Belgium

Remerciements

Avant toutes choses, je tiens à remercier ma famille proche qui aura quasiment vécu cette expérience de façon aussi intensive que moi.

Évidemment, je tiens à remercier mes promoteurs, la Professeur Catherine Behets et le Professeur Daniel Manicourt pour m'avoir donné l'opportunité que réalise ma thèse au sein du laboratoire de Morphologie. Je vous remercie également pour votre encadrement durant toutes ces années et les longues heures que vous avez passées à relire et bonifier mon travail. Je tiens également à remercie Madame Gilda Manicourt qui aura été d'un grand soutien surtout dans les derniers mois de la thèse, merci pour vos appels téléphoniques afin de prendre de mes nouvelles et de me rassurer, merci pour votre bienveillance ! Je remercie évidemment les membres de mon jury pour votre temps et les conseils avisés lors des différentes réunions que nous avons pu faire.

Je tiens également à remercier la Professeur Marie-Christine Many et le Professeur/Docteur Honoris Causa Benoit Lengelé. Vous êtes tous les deux des modèles pour les générations futures. Votre patience, votre dévotion envers les étudiants, votre passion pour l'enseignement, votre perfectionnisme et votre expertise vous mettent et vous mettront encore en lumière pour de nombreuses années. Je suis extrêmement reconnaissant de toutes les choses que vous m'avez transmis et enseigné durant toutes ces années, c'est une grande fierté de pouvoir dire que je vous ai côtoyé durant toutes ces années.

Je remercie également mes collègues directes Michael, Thomas et Antoine. Merci pour nos collaborations et moments festifs afin de décompresser de l'ambiance du laboratoire. Je remercie également Joanna, Hrag, Vincent, Thibaut, Loic, Laurent et Marc pour avoir su décanter l'ambiance au quatrième avec nos parties de baby-foot rondement menées, merci pour cette soupape de décompression ! Je remercie encore Joanna pour son soutien ces derniers mois, pour tes remarques intelligentes et le temps que tu as passé à relire le manuscrit.

Je remercie également Christine et Adeline pour votre excellent travail. Vous n'avez jamais rechigné à la tâche et m'avez toujours aidé avec le sourire. C'était très agréable de travailler avec vous, j'en garderai d'excellents souvenirs.

Je tiens également à remercier tous les autres membres du labo (Michelle, Lies, Walter, Louis) qui ont toujours répondu de façon positive lorsque j'avais besoin de leur aide.

Durant les moments difficiles, il était toujours possible de se réfugier dans le bureau des « filles ». Nous y étions toujours bien accueillis grâce à la bonne humeur de Gaëlle, Dorothée, Marco, Julie et Virginie. Merci pour ces bulles d'oxygène que vous saviez redonner dans les moments opportuns. Julie, « maman » de cette équipe, je te remercie pour tes bons conseils et ton expérience qui ont permis de calmer le jeu et de réaliser cette thèse en douceur malgré les embuches.

Je remercie tout particulièrement mes amis Bernard et Nicolas. Trop peu souvent mis en valeur, vous réalisez un boulot colossal pour l'organisation des travaux pratiques en Anatomie et pour le bon fonctionnement du service du don de corps. Ce fut un agréable plaisir de faire votre connaissance et d'avoir pu partager autant de choses avec vous. Ce sera toujours avec plaisir que je viendrai vous rendre visite par la suite. Merci pour votre boulot, merci pour votre bonne humeur et les petites blagues matinales qui m'ont permis de tenir le coup toutes ces années !

Un remerciement particulier pour Tac, Vincent Watteyne et Edouard Uten. Malgré le temps et la distance, vous avez su rester présents quand il le fallait pour me changer les idées ! Je remercie également David Thomson pour ton écoute et tes conseils pertinents et avisés !

Je remercie également Daela Xhema pour son expertise et son soutien depuis mon premier mémoire en CHEX. Tu as toujours répondu présente pour un petit conseil ou une oreille attentive, je te remercie !

Je tiens particulièrement à remercier mes parents, ainsi que Marleen et Giovanni, car sans vous, rien de tout ceci n'aurait pu être possible. Vous m'avez toujours soutenu et encouragé dans mes projets, qu'ils soient bons ou moins bons, vous ne m'avez jamais jugé et avez toujours été présents. Je vous suis extrêmement reconnaissant pour tout ce que vous m'avez transmis ! Je remercie évidemment ma sœur Déborah pour son soutien à toute épreuve malgré la difficulté de la distance. Je remercie également Grammy, Tante Arlette, Marraine et Jean-Phil qui ont toujours cru et été là pour moi.
Tant que nous sommes dans la famille, je remercie évidemment Virginie pour tout ce que tu as fait pour moi. C'est toi qui m'auras quasiment tout appris en ce qui concerne la recherche scientifique et ses procédés. Tu as pris le temps de m'aider comme personne n'a su le faire et je t'en serai éternellement reconnaissant ! Je te remercie également pour la confiance et le rôle que vous m'avez demandé, avec Tom, de jouer dans l'éducation de votre fils. Vous pouvez compter sur moi pour mouvementer son éducation !

Évidemment je remercie Leslie qui aura subi cette thèse de façon aussi intensive que moi !

List of abbreviations

ABC transporters:	ATP-binding cassette transporters
ACL:	anterior cruciate ligament
ACLT:	transection of anterior cruciate ligament
ADAMTS:	a disintegrin and metalloproteinase with thrombospondin motifs
BMD:	bone mineral density
BMLs:	bone marrow lesions
BMP:	bone morphogenic protein
BMU:	bone multicellular unit
BV/TV:	bone volume fraction (bone volume/total volume)
CACTC:	cyclic articular cartilage tibial compression
Ch:	chondroitin
ChS:	chondroitin sulfate
DAMPs:	damage associated molecular patterns
dKO:	double knock-out
DMM:	destabilization of the medial meniscus
DNA:	desoxyribonucleic acid
ECM:	extracellular matrix
GAG:	glycosaminoglycan
GLUC:	β-D-glucuronidase
GPI-anchored:	glycosyl phosphatidylinositol-anchored
GWAS:	genome wide association studies
HA:	hyaluronan
HABP:	hyaluronan binding protein
HARE:	hyaluronan receptor for endocytosis
HAS:	hyaluronan synthase
HEX:	β-hexosaminidase
HMW:	high molecular weight
HYALs:	hyaluronidases
HYALP1:	hyaluronidase pseudogene 1
IFP:	infrapatellar fat pad
IHC:	immunohistochemistry
IL:	interleukin
IRS:	immunoreactive score
KIAA1199:	also named CEMIP (cell migration inducing protein), hyaluronan-binding protein
LMW:	ow molecular weight
LYVE-1:	ymphatic vessel endothelial hyaluronan receptor 1
MIA:	mono-iodoacetate
Micro-CT:	micro-computed tomography
MM:	molecular mass
MMPs:	matrix-metalloproteinases
mRNA:	messenger ribonucleic acid

MS:	Mankin score
MSCs:	mesenchymal stem cells
MW:	molecular weight
NHE1:	sodium-hydrogen antiporter 1
OA:	osteoarthritis
PCC:	pericellular coat
pQCT:	peripheral Quantitative Computed Tomography
PTOA:	post-traumatic OA
qPCR:	quantitative polymerase chain reaction
RNA:	ribonucleic acid
ROI:	region of interest
ROM:	range of motion
ROS:	reactive oxygen species
SPAM1:	sperm adhesion molecule 1
Tb.N:	trabecular number
Tb.Sp:	trabecular separation
Tb.Th:	trabecular thickness
TGF-β1:	transforming growth factor beta 1
TMEM2:	transmembrane protein 2
TNF-α:	tumor necrosis factor alpha
VEGFA:	vascular endothelium growth factor A
WT:	wild type

Table of contents

Introduction

Osteoarthritis (OA) is a highly prevalent joint disorder characterized by cartilage degradation and abnormal bone remodelling. More precisely, micro- and macro-injuries initiate cell stress and extracellular matrix (ECM) degradation as well as maladaptive repair responses involving pro-inflammatory pathways. The symptoms of OA are joint pain, swelling and stiffness that lead to activity limitations, participation restrictions, sleep interruption, depressed mood, loss of independence and reduced quality of life (1). The burden and global impact of OA constitute a major challenge for health system in the coming years because OA is expected to increase (2).

All joints can be affected by OA but mainly those that support the weight of the body and those that are often used. Among these, the knee, hip, and small joints of the fingers are typical diarthrodial joints, which are organized into distinct structural elements including subchondral bone, articular cartilage, fibrous and synovial membranes, ligaments and tendons (3). These structural elements contribute to a functional articular organ that is uniquely adapted to permit constrained motion. The osteochondral unit is composed of articular cartilage, calcified cartilage and subchondral bone is the functional unit of the joint capable of absorbing shocks and transferring loads. Any alteration in the structure or composition of those tissues results in loss of function and disruption of joint integrity, such as encountered in OA.

1. The osteochondral unit

The osteochondral unit is composed of articular cartilage, calcified deep layer, subchondral bone plate and subchondral trabecular bone (Figure 1.A). This organization not only ensures structural and functional cohesion between these tissues, but also constitutes a protective junction between bone and cartilage. The crosstalk or dynamic relationship between cartilage and bone is crucial to maintain overall joint health and integrity and is disturbed in OA development (4).

1.1. Articular cartilage

Hyaline cartilage is the major cartilage type in human body and covers the bone surfaces of diarthrodial joints. This articular cartilage provides a gliding smooth surface with a low coefficient of friction and absorbs compressive loads far heavier than body weight while distributing them to the subchondral bone (5, 6). Mature articular cartilage is organized in four superimposed distinct areas: the superficial, intermediate, radial and calcified zones (Figure 1.B). The superficial zone is composed of collagen fibrils and one or two layers of flattened chondrocytes, both oriented tangentially to the surface. Just beneath, the intermediate zone is composed of round chondrocytes dispersed in a non-oriented collagen network. In the third, radial, zone, the chondrocytes are organized in longitudinal columns and collagen fibrils are perpendicular to the surface. These three zones form the non-calcified cartilage. Right under the radial zone, the calcified cartilage makes the transition with subchondral bone. It is separated from the radial zone by the tidemark delimitating the mineralization front. The calcified

cartilage presents hypertrophic chondrocytes and a unique matrix composition and mineralization (see 1.2). Moreover, this zone is innervated and vascularized (7, 8).

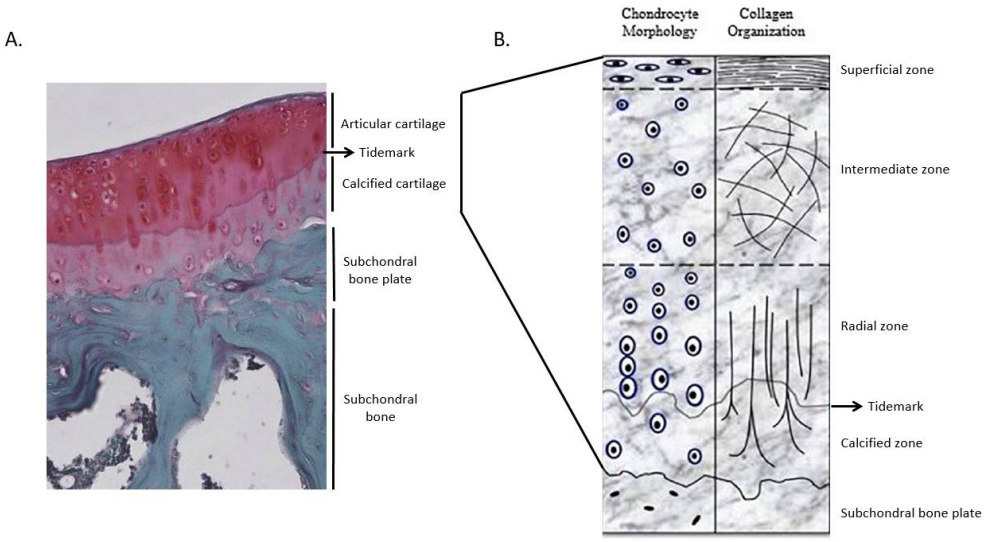

Figure 1 : Organization of the cartilage in a healthy joint
(A.) Histological representation of the osteochondral unit, composed of articular cartilage, calcified deep layer, subchondral bone plate and subchondral trabecular bone (mouse knee). (B.) In a healthy human joint, cartilage comprises four different areas: articular cartilage divided into three zones (superficial, intermediate and radial) and calcified cartilage which each express their own characteristics in terms of cells and collagen fibres orientation. This calcified cartilage interacts with the non-mineralized cartilage, from which it is separated by the tidemark, and the subchondral bone. Adapted from "3D bioprinting of cartilage for orthopedic surgeons: reading between the lines" by Di Bella, C., et al. 2015, Front Surg., Aug 13;2:39. (9)

Cartilage is a solid dense connective tissue composed of extracellular matrix (ECM) with up to 85% of water, produced by chondrocytes (10). This only cell type in articular cartilage represents 1–2% of the total cartilage volume (10, 11). Chondrocytes are considered quiescent cells. Their activity resides essentially in synthesizing the ECM proteins and maintaining a very low turnover rate (12). Deprived of blood and lymph vessels as well as nerves,

cartilage has poor intrinsic repair capacity and chondrocytes live in a hypoxic environment (5, 10). Under this normal hypoxic condition, chondrocytes accumulate and synthesize more type II collagen and aggrecan than in normoxia (13). Chondrocytes energy resources, such as nutrients and oxygen, are supplied by blood vessels in the subchondral bone, the synovium and the joint capsule (14). Chondrocytes are considered mechano- and chemosensory cells thanks to their primary cilium, a microtubule-based signaling organelle (14). This structure, with its calcium channels and integrins, allows interaction with ECM and acts in cartilage homeostasis by regulating the ECM production (15, 16).

The ECM main components, water (60-85%), type II collagen (15-22%), and proteoglycan complex including hyaluronan (HA) (4-7%), are organized in a specific porous and permeable matrix (3, 17-19) (Figure 2).

Collagen type II fibrils are the major component of the ECM of articular cartilage (Figure 2). They are coassembled with collagen XI and covalently crosslinked to collagen IX to form an organized network which can trap the negatively charged proteoglycan aggregates (14, 20-22). The mechanical properties of articular cartilage are determined by the fibrillar collagen network whose stability and strength provide the tissue with integrity and resiliency to stress whereas the entrapped proteoglycan aggregates ensure compressive resilience (22-24).

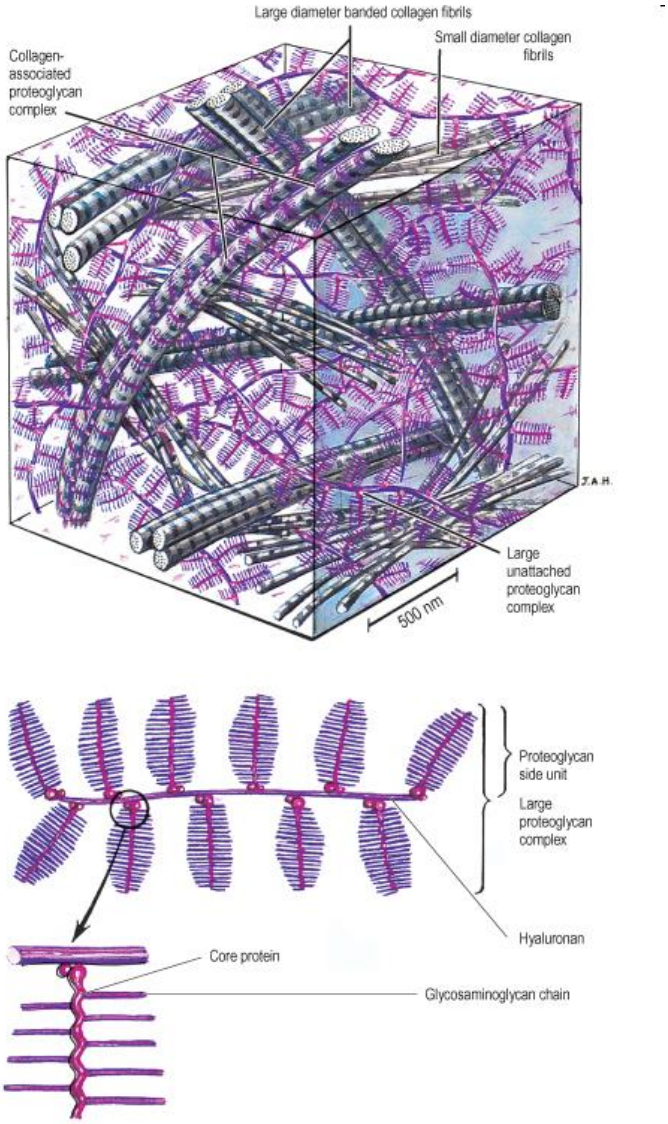

Figure 2: Organization of hyaline cartilage matrix.

The square box offers a schematic representation of the different components of the cartilage ECM. Depicted are large proteoglycan complexes and collagen fibres (cross-banded and of different diameters). Proteoglycan complexes bind to these fibres via their monomeric sidechains and link them together. Large proteoglycan complex is constituted of proteoglycan units anchored to hyaluronan.

Damage to the fibrillar meshwork, mediated by matrix-metalloproteinases (MMPs), may be a critical event in the pathology of arthritis due to the low collagen turnover within the cartilage (22). Among the other types of collagen, type VI collagen is present in the chondrocyte pericellular matrix (PCM). It allows chondrocyte integrity and attachment to the ECM by binding to type II collagen fibrils (25). Type IV collagen seems to be involved in maintaining chondrocyte phenotype or viability (26). Type X collagen is mainly present in calcified cartilage (27) (see section 1.2).

Proteoglycans (Figure 2) are a family of glycoconjugates with a central core protein to which one or more glycosaminoglycan (GAG) side chains are covalently linked post-translationally (28). Most of the proteoglycans exist as aggregates formed by their non-covalent association with HA and link protein (29). Aggrecan is the major proteoglycan in articular cartilage. By its interaction with HA and link protein in order to form a stable ternary complex in the ECM, aggrecan provides a hydrated gel structure that endows the cartilage with load-bearing properties and dissipation of mechanical load (14, 19). During compression, the numerous water molecules associated with the hydrophilic GAG chains are extruded. When compression stress is released, the proteoglycans fixed charges allow to osmotically reabsorb the water and thereby to restore the original cartilage dimensions. Joint motion and mechanical loading induce movement of synovial fluid across the cartilage, facilitating the diffusion of molecules and providing nutrition (3). The superficial frictionless property of the cartilage ECM is facilitated by a boundary layer of lubricants, lubricin and HA produced by synovial cells and chondrocytes (30).

HA belongs to glycosaminoglycans (GAGs), a group of heteropolysaccharides, which include heparan sulfate, heparin, chondroitin sulfate, keratan sulfate and dermatan sulfate. It plays diverse roles, notably, in embryonic development, joint cavity formation, longitudinal bone growth, normal homeostasis and wound healing. It is distributed around cells (the pericellular coat - PCC) and in ECM of connective tissues (31-34). A 70 kg human being has approximatively 15g of HA of which a third is renewed every day.

1.1.1. Hyaluronan biology

HA is an unbranched and linear chain of repeating disaccharides units (N-acetyl-D-glucosamine and D-glucuronic acid) linked by β-1,4-glycosidic bonds; disaccharide components are linked by β1,3-glycosidic bond (Figure 3). HA can reach a very high molecular weight (>10^6Da) (35-39).

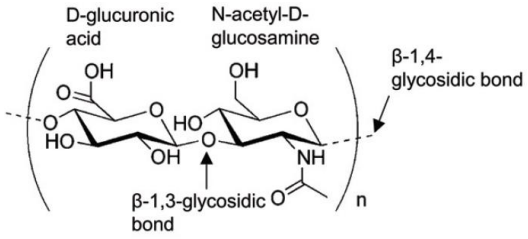

Figure 3 : Structural formula of HA disaccharide unit (D-glucuronic acid and N-acetyl-D-glucosamine).

HA is an unbranched and linear chain of repeating disaccharide units linked by β-1,4-glycosidic bonds and disaccharides components are linked by β1,3-glycosidic bonds. Adapted from "Hyaluronan: towards novel anti-cancer therapeutics" by Karbownik, M., 2013, Pharmacological Reports, 65, 1056-1074. (40)

1.1.1.1 HA synthesis by hyaluronan synthases

HA is synthesized at the inner side of the plasma membrane (Figure 4) by three transmembrane glycosyltransferase isoenzymes named hyaluronan synthases (HAS) (41-43). HAS gene sequences are located on different chromosomes but share a high degree of homology (44, 45). HAS biochemical and synthetic properties differ in the rate, length and stability of the HA they produce (45). For instance, HAS3 is the most active enzyme but produces HA with the lowest molecular weight (MW) (up to 10^6Da); HAS1 is the least active but produces HA with a MW at least twice that synthesized by HAS3. As for HAS2, it produces the highest MW HA and is finely regulated because it is the main hyaluronan synthase in normal adult cells (45, 46).

Unlike other GAGs, HA does not require to be linked to a core protein to initiate polymerisation (41). Once synthesized, HA can stay attached to the HA synthases and/or bind to other HA receptors at the cell surface (CD44) to form PCC or be released into the extracellular space via ABC transporters (41-43, 47, 48). The PCC also contains hyaladherins, proteins that can specifically bind to HA and modify the morphology and physicochemical properties of HA assemblies (18, 48).

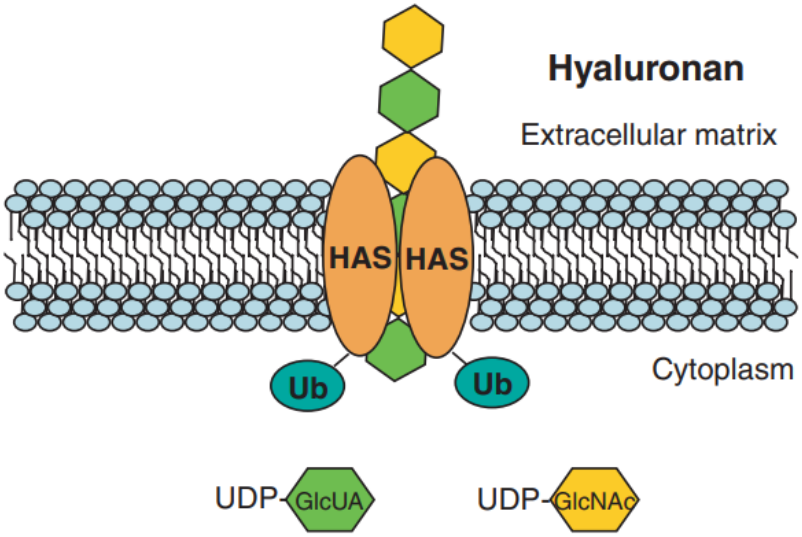

Figure 4 : Schematic representation of HA synthesis by HAS at the inner membrane surface.
Uridine diphosphate (UDP)-linked sugar substrates, glucuronic acid (GlcUA, green) and N-acetylglucosamine (GlcNAc, yellow), are sequentially added to the reducing end of the growing HA chain at the cytoplasmic aspect of the cell membrane through the action of hyaluronan synthases (HAS). The resulting sugar polymer is extruded into the ECM surrounding the cell. Adapted from "Transcriptional and post-translational regulation of hyaluronan synthesis" by Tammi, R.H., 2011, FEBS Journal, 278(9): 1419-28. (49)

1.1.1.2. HA degradation by hyaluronidases (HYALs)

Usually, HA is enzymatically cleaved by hyaluronidases, although it can also be non-specifically degraded by the action of oxygen free radicals (50, 51). The hyaluronidases degrade predominantly hyaluronan but also chondroitin (Ch) and chondroitin sulfates (ChS) at a slower rate. These endo-β-*N*-acetyl-hexosaminidases hydrolyse HA by cleaving the β1,4 glycosidic bond (52-54). The human genome counts six hyaluronidase-like sequences clustered on two chromosomal sites (32). Chromosome 3p21.3 regroups the sequences for HYAL1, HYAL2 and HYAL3, whereas chromosome 7q31.3 contains the

sequences for HYAL4, PH20/SPAM1 (sperm adhesion molecule1) and HYALP1, a pseudogene (Figure 5).

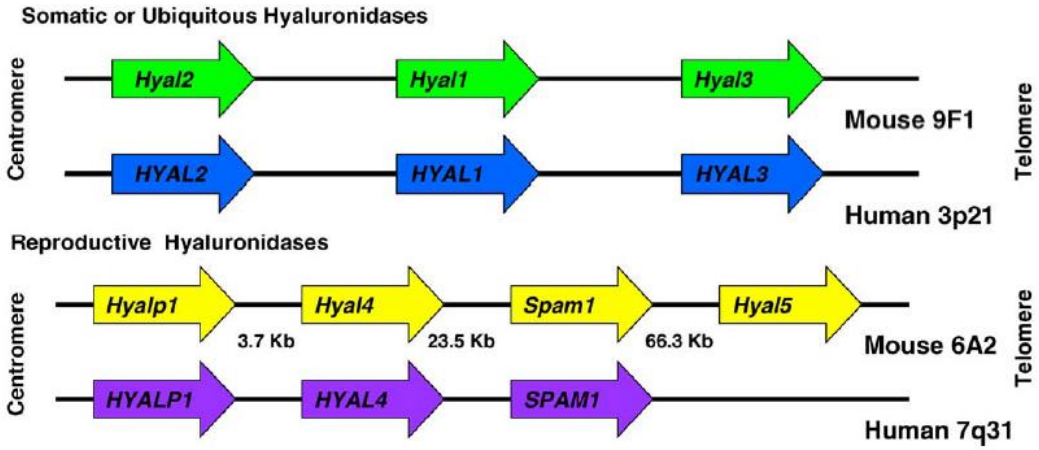

Figure 5 : Hyaluronidase genes in human and mouse genomes.
Mammalian genomes contain two clusters of tightly linked hyaluronidase genes. Both human and mouse have three genes (HYAL1/Hyal1, HYAL2/Hyal2, and HYAL3/Hyal3) in the somatic or ubiquitous cluster, on human 3p21/mouse 9F1. The reproductive cluster, located on human 7q31/mouse 6A2, includes HYALP1/Hyalp1, HYAL4/Hyal4, SPAM1/Spam1 and Hyal5 (in mouse), which are abundantly expressed in the testis. Among them, the protein SPAM1 is the most widely conserved mammalian sperm membrane protein and the only functional hyaluronidase in the "reproductive cluster". Taken from "Epididymal SPAM1 and its impact on sperm function" by Martin-DeLeon, P.A., 2006, Mol Cell Endocrinol., 250(1-2):114-21. (55)

The same genomic organization is present in mouse, with an additional hyaluronidase on the second chromosome: hyal1-3 are clustered on 9F1 - F2 and hyal4, Spam1, hyalp1 and hyal5 constitute the "reproductive cluster" on 6A2. The homology between similar sequences in mouse and human genomes is far greater than that between individual members of the paralog (52). The degree of homology between the pairs of orthologs of human and

mouse HYAL1, HYAL2 and SPAM1 is much greater than between the six human paralogs (32). Therefore, we will present human hyaluronidases as representative of all vertebrate ones.

The expression of hyaluronidases appears tissue specific. HYAL1 and HYAL2 are ubiquitously expressed in somatic tissues (56) and are considered the two major HA-degrading hyaluronidases (57, 58) with optimal activity at pH lower than 4 (59). Since decades, HA degrading model proposed that HYAL2 starts HA degradation at the membrane level; the residues are then endocytosed and totally degraded by HYAL1 within the lysosomes. More recent studies have shown that HA turnover within the pericellular matrix involves not only HYAL2 but also several other enzymes and receptors such as HYAL1, HYAL3, SPAM1 (60-64), CD44 (65-68), TMEM2 (69), NHE1 (70) and KIAA1199 (71). HYAL2 has also been localized in lysosome and endosome as well as anchored at the plasma membrane by glycosyl phosphatidylinositol-(GPI-) where it exerts an extracellular HA-degrading activity (61, 70, 72, 73).

In their model, Chowdhury et al. suggest four pathways for HA-degradation (Figure 6) (74).

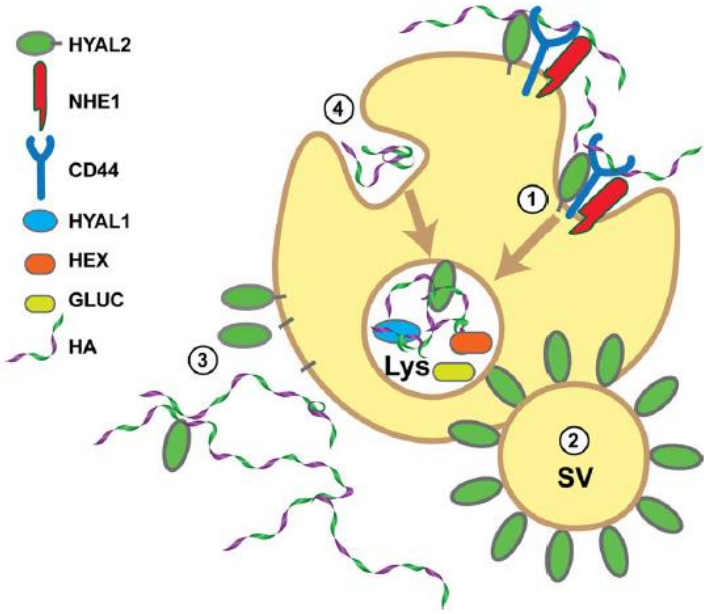

Figure 6 : Model of hyaluronan degradation by Chowdhury et al. (2015) (74).
HA degradation occurs through 4 pathways (1-4).
In pathway 1, cell surface HYAL2 initiates HA hydrolysis in partnership with a receptor, possibly CD44. NHE1 (Sodium-hydrogen antiporter 1) allows HYAL2 activity by local acidification. HA fragments are endocytosed and transported to the lysosome (Lys) where they are degraded by endoglycosidase HYAL1 and exoglycosidases, β-hexosaminidase (HEX) and β-glucuronidase (GLUC).
In pathway 2, secretory vesicles (SV) within specialized epithelial cells are surrounded by HYAL2. Upon secretion, these vesicles degrade extracellular HA.
In pathway 3, cell surface HYAL2 is detached from the surface or released through by lipase or protease to form a soluble form of HYAL2.This enzyme can enter the blood stream or diffuse from the surface to degrade HA distal from the site of HYAL2 expression.
In pathway 4, HA is internalized by a non-HYAL2-dependent route and transported to the lysosome for degradation.

In the first pathway, HYAL2 with its GPI-anchor interacts with CD44 and NHE1 which acidifies the extracellular medium to allow HYAL2 activity (70). HYAL2 is thought to cleave HMW HA into fragments of approximatively

20kDa (+/- 50 disaccharides) (57) that are endocytosed to lysosomes. In these organelles, HYAL2 continues HA lysis and HYAL1, with β-D-glucuronidase and β-hexosaminidase, cleaves the rest of HA into its constituent monosaccharides (56, 75, 76). The second and third pathways suggest an extracellular role for HYAL2 either transported within secretory vesicles or excreted directly in soluble form.

Chowdhurry et al. suggest, in the fourth pathway, that HA could be endocytosed by a non-HYAL2-dependent way and transported to lysosomes for HYAL1 and HYAL2 degradation. This implies the possible involvement of another enzyme that could contribute to both local and circulating HA degradation (74).

Apart from HYAL1 and HYAL2, little is known about the role of other hyaluronidases in HA degradation. According to Atmuri et al., HYAL3 does not play a major role in constitutive HA degradation (77). For the moment, there is no evidence that HYAL4 can degrade HA and HYALP1, a pseudogene with a premature stop codon, is not translated into mRNA (32). The last hyaluronidase which can be helpful to degrade HA is SPAM1 and it can play a role in the fourth pathway described above.

SPAM1 was initially considered to be only a sperm surface protein, detected within testis and epididymis (78-80). Its hyaluronidase activity plays two functional roles in mammalian fertilization: it permits the sperm to traverse the cumulus oophorous (81-83) and is involved in the secondary binding of sperm to the egg (84-86). It seemed to be GPI-anchored to the plasma membrane of the sperm head (81, 87, 88). Currently, SPAM1 is recognized

as a multifunctional enzyme with a more diffuse expression than in the only male reproductive tract. Indeed, its expression has been highlighted in normal breast tissue (89), female reproductive tract (90), chondrocytes, synoviocytes, and dermal fibroblasts (31, 64). It has been associated with tumoral dissemination because its HA degrading activity results in the disruption of basement membrane integrity (64, 89, 91). Unlike HYAL1 and HYAL2, SPAM1 shows a bimodal activity, at neutral and acidic pH, attributed to its two isoforms (52, 64, 81). Moreover, like HYAL2, SPAM1 is a GPI-anchored protein (52) capable of degrading HA and ChS (92, 93), it could be released as free SPAM1 and its expression is upregulated by IL-1 (64).

All these characteristics make SPAM1 a potential actor in the degradation of HA. Its activity at neutral pH could allow it to initiate HA degradation in the extracellular matrix or could also form a complex with CD44/HYAL2 at the cell membrane level.

1.1.2. HA functions in cartilage

In adult cartilage, association of HA with aggrecans permits to retain aggrecans at the high concentration needed to confer the cartilage its compressive resilience (31). As reviewed by Passi and Vigetti, HA are highly hydrophilic and can bind to a large amount of water molecules to form a hydrogel with good lubricant properties (94). The more concentrated HA solution is, the more its viscosity increases; its elasticity is directly proportional to the polymer size.

HA also interacts with cells through different receptors, among which CD44 is the most widespread. CD44 isoforms (95, 96) are expressed by different cells, including chondrocytes and bone cells (73, 97-100). The link between chondrocyte CD44 and HA can generate anabolic effects including cell adhesiveness, migration and wound healing, and thereby contributes to maintain normal cartilage homeostasis (68, 94, 101, 102). As described above, chondrocytes have the capacity to bind and internalize HA via a CD44 dependent mechanism (65, 67, 68, 103). CD44 expressed on chondrocyte membrane is upregulated by pro-inflammatory cytokines that promote matrix remodelling, intracellular HA accumulation and chondrocyte survival modifications or apoptosis (68, 101, 102, 104). Other HA receptors, such as HARE, LYVE-1, SPAM1, HYAL2, and layilin, are able to endocytose HA (64, 72, 105-112). Once internalised, HA is degraded by hyaluronidases in lysosomes (56, 74).

The molecular weight (MW) of HA, resulting from the balance between HAS and HYALs activities, plays a key role in HA physiology. Depending on its high (HMW) or low (LMW) molecular weight and the tissues in which it is found, HA has opposite actions (44, 113-121). HMW HA protects the articular cartilage by its lubricating properties (122) and could be anti-angiogenic (37, 123), anti-inflammatory, immune-suppressive and healing initiator (37, 123). HMW HA is considered the physiological protector of cells. On the contrary, HA degradation by enzymatic or nonenzymatic mechanisms results in the presence of LMW HA fragments which stimulate defensive cellular

responses (124), such as production of growth factors, chemokines and proinflammatory cytokines, as well as ECM remodelling (123, 125-127).

1.2. Calcified cartilage

Calcified cartilage is the deepest layer of articular cartilage and ensures the transition between its uncalcified layers and the underlying subchondral bone. It results from endochondral ossification and persists after growth plate closure (3, 128). The tidemark, which separates uncalcified and calcified cartilage, is considered the scar of the subchondral growth plate (129). This calcified cartilage presents hypertrophic chondrocytes and collagen type X. This collagen is involved in the matrix mineralization and its biological function seems to maintain tissue stiffness and interact with hypertrophic chondrocytes (7, 130, 131). Calcified cartilage and subchondral bone form a biocomposite that is adapted to distribute and transfer mechanical forces. Under physiological loading conditions, only a small fraction of the load forces is absorbed by calcified cartilage. With aging, proliferation of nerves and blood vessels, arising from the subchondral bone, can be observed within the calcified cartilage (14).

1.3. Subchondral bone

The subchondral bone is composed of superimposed subchondral plate and trabecular bone. Right beneath the calcified cartilage, the subchondral plate consists in compact bone, weakly porous and poorly vascularized. Its density and thickness are adapted by remodelling according to modification in mechanical forces (132, 133).

The subchondral trabecular bone, also referred to as cancellous bone, is located under the subchondral plate. Its porosity and anisotropy provide a structural network which is adapted to the local forces. The boundary between the subchondral plate and the subchondral trabecular bone is not always clearly defined, which explains why it is not often mentioned.

Under normal conditions, the two parts of the subchondral bone adapt their structural properties through regulated processes called modelling and remodelling. Modelling, mostly active in skeletal growth and development, contributes to bone shape (134). It involves directly and independently osteoblast or osteoclast activity in order to, respectively, add or remove bone from existing surfaces, without coupling bone resorption and formation (135). Bone remodelling is the lifelong process which involves the functional coupling of osteoblasts and osteoclasts in a bone multicellular unit (BMU). BMU remodels bone by five coordinated phases: quiescence, activation initiated by osteoblastic lineage and leading to osteoclast recruitment, resorption by osteoclasts, reversal phase, with apoptosis of osteoclasts and recruitment of osteoblasts, and formation of new bone matrix by osteoblasts (134). These processes allow bone adaptation to

modification in local soluble mediators, in biochemical factors, in loading forces or in case of mechanical injuries. Both modelling and remodelling are activated during the evolution of OA and play key roles in the alterations of skeletal architecture and function (3, 136, 137).

Osteocytes, in particular, play a multifunctional role in orchestrating bone remodelling by regulating both osteoclast and osteoblast function (138-142). Derived from osteoblasts, they are the most numerous bone cells and reside in lacunae within the mineralized bone matrix. Their numerous processes into canaliculi form a lacunocanalicular network by which they connect to each other as well as to lining cells and vessels (139). Since osteocyte and its processes are constantly exposed to fluid flow shear stresses into the lacunocanalicular system, they are considered mechanosensory to several possible stimuli (143-147). It has also been shown that the osteocyte lacuna acts as a strain concentrator which amplifies macroscopic strain applied over the whole bone (143, 148).

2. Osteoarthritis and the osteochondral unit

According to the Osteoarthritis Research Society International (OARSI), osteoarthritis is “a disorder involving movable joints characterized by cell stress and extracellular matrix degradation initiated by micro- and macro-injury that activates maladaptive repair responses including pro-inflammatory pathways of innate immunity. The disease manifests first as a molecular derangement (abnormal joint tissue metabolism) followed by anatomic, and/or physiologic derangements (characterized by cartilage degradation, bone remodelling, osteophyte formation, joint inflammation and loss of normal joint function), that can culminate in illness“ (149).

Osteoarthritis (OA) can affect all the joints in the body but preferentially resides in the weight-bearing spine, hip, knee, ankle and foot joints, and in those that are often used such as small hand joints. Its main feature is the degradation of the articular cartilage, but this only corresponds to the tip of the iceberg. Indeed, weakness of the periarticular muscles, ligament hyperlaxity, traumatic or not, synovial inflammation, as well as remodeling of the subchondral plate and trabecular bone which can lead to the formation of osteophytes and calcified nodules, are also associated with OA. All of them result from an imbalance between the mechanisms of degeneration and repair of joint tissues.

It is difficult to estimate the prevalence and incidence of OA, which depend on the OA consequences analyzed, the populations and joints studied, the presence of a traumatic event, physical activity or repeated occupation, etc. The incidence is recognized to increase with age, especially after the age of

50, with higher rates in women than in men. James et al (2018) estimate that about 300 million people are affected by the disease worldwide (150).

Among musculoskeletal disorders, OA is the second most prevalent one right after “low back pain without leg pain” and before “neck pain” (150). The prevalence of OA depends on different factors such as age, gender, ethnicity, genetics, sociodemographic factors, obesity, level and type of physical activities, occupation, joint malalignment or trauma, etc., some of which will be detailed in the following section (OA etiology).

The first symptoms of OA are joint pain leading to movement limitation and subsequently joint stiffness. These symptoms lead to disability for patients who lose their independence, may become sedentary and gain weight, which increases the risk of cardiovascular disease. OA may also have a negative impact on mental health. Studies demonstrated that people with lower limb OA had greater odds of developing depressive symptoms due to the lack of movement and independence; OA could be associated with a greater odd of suicidal ideation, with a perceived memory loss partially due to sleep and mood impairments (151, 152). Inevitably, OA burdens the patient and the community and has been shown to be correlated with higher hospitalization and emergency rooms occupancy rates (153, 154).

2.1. OA etiology

As mentioned above, OA is a multifactorial disease which can have various origins. The natural OA development is correlated with age because of numerous individual factors such as oxidative damage, thinning of cartilage, muscle weakening and a reduction in proprioception. Moreover, basic

cellular mechanisms that maintain tissue homeostasis decline with aging, leading to an inadequate response to stress or joint injury and consecutive joint tissue destruction and loss (155).

Early OA development can be observed in people who engage in regular and intense physical activity such as running, gymnastics, ballet or breakdance, among others. Other physical activities such as sports involving many impacts or twisting movement (boxing, football, basketball, skiing, baseball, etc.) can also lead to early OA because they are often associated with joint injuries, like sprains, torn ligaments, impaction or intra-articular bone fractures (155).

Consistent with this, higher muscle strength and OA may also be associated. For instance, higher knee extensor strength can generate knee OA and increase in patellofemoral cartilage loss (156, 157). Repetitive activities inherent in certain occupations such as construction and domestic work, load bearing, firefighting, or praying, are associated with greater risk of OA (158-160). For instance, prolonged squatting or kneeling is correlated with increased risk of posterior knee OA (155). Early OA can also result from traumatic or physiological joint malalignment (161). Malalignment following meniscus tear or rupture of cruciate or collateral ligaments of the knee causes joint instability and leads to rapid and excessive deterioration of certain parts of the joint. In the absence of a prior injury, incorrect bone or joint shape, such as hip dysplasia or *genu varum*, may contribute to the risk of OA (159, 162-164). These joint misalignments modify the distribution of mechanical loads on the cartilage and, subsequently, lead to bone marrow lesions and cartilage degradation and loss, as observed in MRI (163, 165).

Another non-traumatic parameter possibly correlated with increased prevalence and incidence of OA is the bone mineral density (BMD) (159, 162). High systemic BMD was recently shown to predicate structural OA features in knee (166), like increased iliac crest stiffness and BV/TV had been associated with OA grades II-IV in hand joints (167). It is also known that the early phase of OA is characterized by increased bone resorption (168, 169) followed, later in OA development, by bone regeneration, subchondral bone sclerosis and osteophytes formation (133, 170).

Beside musculoskeletal contributing factors, approximately 30-65% of the risk of OA is genetically determined (2, 159, 160, 171). Women appear to have a higher risk to develop hand, hip and knee OA than men. African-American ethnicity was shown to experience severe knee OA development and progression (160, 172-174). As reviewed recently by Reynard & Barter (2020), hypothesis-free genome wide association studies (GWAS) identified 56 new loci giving novel insights into OA disease, with potential drug targets, and allowing the use of polygenic risk scores in selecting individuals for clinical trials (175). Briefly, once a DNA region harboring OA genetic risk has been identified by GWAS, functional studies permit to highlight prioritized OA candidate genes, potential mechanisms of action and the role of target genes in cartilage homeostasis and disease. OA genetic risk loci might play a role during skeletal development by slightly changing the joint shape; the subsequent alterations in joint biomechanics could result in individual predisposition to OA (175, 176). For example, some DNA variants were shown to be associated with weight, high body mass index, shape and

developmental dysplasia of the hip, as well as knee and/or hand OA (177-181).

Obesity, defined by body mass index > 30kg/m^2, is a common metabolic syndrome, whose prevalence has doubled from 1980 to 2016 (182). This multifactor condition is characterized by excessive fat accumulation in the body due to disorders of fat metabolism and changes in habits of life, including sedentarism and consumption of processed and caloric food (183, 184). Because of its systemic effects owing to metabolic and inflammatory alterations, obesity is associated with OA (184) and considered a possible onset of OA and pain intensifier or complicator (185). Several studies demonstrated an association between obesity and knee, spine or hip OA (186-188). Excessive accumulation of fat tissue increases weight bearing by the intervertebral discs and the lower limb joints and enhances the production of adipokines, including adiponectin, leptin, resistin and chemerin, and pro-inflammatory cytokines, such as IL-6 and TNF-α, which contribute to inflammatory and autoimmune diseases (189, 190). Adipokines, synthetized by adipocytes, as well as chondrocytes, bone and immune cells, seem to contribute to cell differentiation, growth, apoptosis and regulation of inflammatory cytokines, matrix-metalloproteinases (MMPs) and A Disintegrin and Metalloproteinases with Thrombospondin motifs (ADAMTS) (191-195). Obesity appears to play a role in knee OA by enlarging the infrapatellar fat pad (IFP); that IFP volume is correlated with age in osteoarthritic patients (196). This articular fat pad, located between the joint capsule and the synovium, could act as paracrine tissue via its local

production of IL-6 which is 2-fold increased compared to normal expression in subcutaneous adipose tissue (197).

2.2 Cartilage changes in osteoarthritis

Macroscopic changes in the cartilage consist in progressive occurrence of superficial cracks. As OA worsens, cartilage degradation spreads by extending cracks to the deeper layers, which can lead successively to exfoliation of cartilage fragments, destruction of the articular cartilage and exposure of calcified cartilage or subchondral bone.

One of the first microscopic osteoarthritic changes is the swelling of the cartilage (198). This is due to the increase in water content following proteoglycan degradation by aggrecanase ADAMTS-5. Cleavage of the aggrecan core protein frees the GAG side chains which attract ions and water and create a high osmotic swelling pressure (199). Moreover, the ECM is prone to collapse as a result of increased mechanical stress and production of MMP-13 which impairs the collagen network (200). The content in HA is also diminished by the increase in hyaluronidase expression, especially HYAL2 (201). During OA development, the three major components of the cartilage ECM are then gradually degraded by MMPs, ADAMTS and Hyals. These enzymes are produced by chondrocytes but also by subchondral bone cells and synovial cells in response to local biomechanical and biochemical perturbations (202).

During OA progression, chondrocytes also show changes in their phenotype as a result of excessive mechanical loading, expression of degradative and/or

proinflammatory cytokines and cell-surface mechanosensors allowing them to interact with each other. First, during the early stages of OA, chondrocytes increase their synthetic activity in an attempt to repair the ECM degradation, as attested by enhanced proteoglycan staining around cells (203). With OA progression, clonal clusters of chondrocytes suggest proliferative events (16). At late stage of OA, chondrocytes show signs of apoptosis, including nucleus fragmentation, cell-membrane "ghosts" and hypertrophy (204). In association with cell death, chondrocytes and various cell types increase their production of proinflammatory cytokines, chemokines and MMPs, which leads to ECM disruption but also to the secretion of Damage Associated Molecular Patterns (DAMPs) and alarmins triggering further deregulation of chondrocyte function through Toll-like receptors (205). In consequence, synovial tissue induces inflammation and expresses reactive oxygen species (ROS) that feed back to the chondrocytes to worsen the catabolic state. Chondrocytes adapt to the development of OA by changing to a hypertrophic phenotype and modifying their synthetic activity (206-208). Hypertrophic chondrocytes are believed to promote bone formation thanks to four characteristics: the mineralization of their ECM through expression of collagen X instead of collagen II, their VEGF production which attracts blood vessels, their size and their apoptosis allowing infiltration of osteoblasts and bone formation. The new vascular channels at the depth of calcified cartilage are accompanied by nerves that could take part in the pathogenesis of OA joint pain (11, 209, 210).

2.3. Subchondral bone changes in osteoarthritis

In OA, disruption of the whole biochemical and biomechanical balance of the joint involves not only cartilage but also subchondral bone and synovium (211). OA bone impairment is generally considered to be due to persistent abnormal mechanical stresses that generate microfractures of the osteochondral junction allowing pathological interactions between synovium and subchondral bone. It has been shown that a change in the inflammatory pattern of the subchondral bone through reciprocal interactions with altered cartilage can lead to OA progression (212). The tidemark is normally a barrier to this type of crosstalk; loss of its integrity is therefore critical in the progression of OA (4).

As reviewed by Hügle and Geurts, new imaging technologies show that subchondral bone remodeling and synovial inflammation are actively involved in OA development and are often visible prior to cartilage degradation (213). Bone marrow lesions (BMLs), highlighted by magnetic resonance imaging (MRI), are one of the first signs of OA and can precede cartilage damage (188). BMLs appear to result from remodeling of subchondral bone associated with malalignment and mechanical overload (214, 215). Absence or regression of BMLs could be associated with a decreased risk of cartilage loss (216).

Subchondral plate and subchondral trabecular bone react to the development of OA by distinct changes in their structure and biochemical activities (132). The first adaptation is the thickening of subchondral plate and is followed by increase in trabecular number, thickness and volume

resulting in an increase in the amount of trabecular bone and a decrease in its bone mineral density. These modifications are driven by cellular and biomolecular responses of osteochondral tissues (4). During OA, both osteoclast and osteoblast activities are increased (212). However, osteoblasts derived from bone marrow mesenchymal stem cells (MSCs) are different from mature lining osteoblasts in subchondral bone by their slower proliferation and their hypomineralization phenotype (217, 218). Several experimental studies also showed that the interaction between osteoblasts and osteoclasts leads to a first temporary decrease in trabecular bone volume before an increase of these parameters (168, 219, 220). Trabecular bone adjusts to increased weight-bearing or mechanical stress by increasing the number and thickness of trabeculae (221-223). The site of bone changes corresponds to that of cartilage lesions, which indicates that both tissues adapt to loading and stress (136, 137). *In vitro* and *ex vivo* studies analysed the behaviour of osteoblasts in order to understand their interactions during OA development and showed that osteoblasts from OA patients expressed less ACAN, which encodes for aggrecan, SOX9 which is required for cartilage formation, and COL2A1, but more MMP3 and MMP13 than non-OA osteoblasts (224-227).

At later stages of OA, osteophytes appear at the joint margins and are easily detected with X-rays. They result from cartilage outgrowths which undergo endochondral ossification (188, 228, 229). More precisely, chondrophytes, or abnormal cartilage masses, are produced by the periosteal cells located at the joint periphery in answer to abnormal mechanical stress. Their

chondrocytes hypertrophy, leading to endochondral ossification and transformation of chondrophyte into osteophyte, which is connected to the subchondral bone and recovered with cartilage. Even though osteophyte formation is associated with OA worsening, their role is not known. Osteophyte formation was recently shown to be strongly correlated with changes in joint laxity and range of motion (ROM) after knee injury in mice (230). Based on earlier studies, initial joint instability following knee injury was hypothesized to lead to osteophyte formation, which in return restabilizes the joint and reduces joint ROM.

2.4. Synovium and osteoarthritis

Changes in chondrocyte phenotype and osteoblast pattern expression are not the only causes of the disturbed crosstalk between cartilage and subchondral bone. Indeed, another major characteristic of OA is a low-grade inflammation affecting the entire joint (231, 232). The synovial fluid of osteoarthritic joint is enriched with inflammatory mediators such as cytokines IL-6, IL-1β and TNF-α (233), adipokines (234, 235), etc. These inflammatory mediators can be released by chondrocytes (236), osteoblasts (237), intra-articular adipocytes (234, 235), synovial cells and other cells like immune cells and infiltrated macrophages (228).

The synovial membrane is the third major component of joint that plays a role in maintaining its delicate balance. This specialized membrane lines the inner surface of the diarthrodial joint membrane, as well as tendon sheaths and bursae. It is composed of two layers of synoviocytes and is highly

vascularized and innervated. Fibroblast-like synoviocytes elaborate the synovial fluid containing lubricin and HA, which lubricates and nourishes cartilage; macrophage-like synoviocytes contribute to intra-articular immune defence and ensure painless movement (238, 239). Joint overuse or local irritation can lead to synovial membrane inflammation, or synovitis. Synovitis could then cause the formation of BMLs and lead to cartilage degradation (240). As reviewed by Goldring and Otero, inflammatory synovial membrane produces IL-1β, IL-6 and TNF-α which diffuse into cartilage and subchondral bone through the synovial fluid; synovial macrophages and monocytes produce cytokines, including BMP-2, BMP-4 and TGF-β1, that stimulate osteoblast proliferation and differentiation (241). It has been shown that IL-1β and TNF-α induce chondrocyte synthesis of enzymes that degrade their matrix; expression of IL-1β also inhibits the formation of ECM aggrecan and type II collagen (242). Moreover, pannus, a highly vascularized infiltrating connective tissue within inflammatory synovium, increases the fibroblast expression of MMPs and IL-1, which can penetrate cartilage and subchondral bone (243, 244). Adamopoulos et al. hypothesized that synovial macrophages can differentiate into functional osteoclasts that can take part in subchondral bone remodelling (245).

Research objectives

Since OA is characterized by decreased content and MW of HA, the hyaluronidase SPAM1, which is a potential actor in HA degradation, could play a key role in the progression or persistence of this joint disease. Its activity at neutral pH could allow it to initiate HA degradation in the extracellular matrix or to form a complex with CD44/HYAL2 at the cell membrane level. Therefore, we used Spam1-/- mice in order to study knee osteochondral unit before and after OA induction. We hypothesized that Spam1 knockout would decrease OA onset and development and, conversely, that Spam1 plays a significant role in OA. Our research tried to answer three questions:

- does Spam1 knockout mitigate the natural course of knee osteoarthritis development in mouse? (Chapter 1)
- does the absence of Spam1 also reduce the knee cartilage degradation after experimental post-traumatic osteoarthritis in mouse? (Chapter 2)
- does the absence of Spam1 in mouse chondrocyte reduce in vitro expression of matrix degrading enzymes, in both physiological and inflammatory conditions? (Chapter 3)

CHAPTER ONE: Knockout of hyaluronidase Spam1 reduces age-related bone and cartilage changes in mouse knee

Knockout of hyaluronidase Spam1 reduces age-related bone and cartilage changes in mouse knee

S. Lafont[1], Y. Achouri, M. Cardinal[1], T. Roels[1], C. de Ville de Goyet[1], C. Behets[1], D. Manicourt[2]

[1]Pole of Morphology and [2]Pole of Systemic and Inflammatory Rheumatic Diseases – Institut de recherche expérimentale et Clinique - Université Catholique de Louvain, Brussels, Belgium

Lafont S, Achouri Y, Cardinal M, et al. Knockout of hyaluronidase Spam1 reduces age-related bone and cartilage changes in mouse knee [published online ahead of print, 2020 Mar 26]. *Morphologie*. 2020; S1286-0115(20)30024-2. doi:10.1016/j.morpho.2020.03.001

Abstract

Objective: to investigate the role of Spam1 hyaluronidase in age-related cartilage loss in the mouse knee.

Design: Spam1$^{-/-}$ and WT mice were euthanized at different ages from 10 to 52 weeks. The right hindlimbs were dissected, scanned with peripheral Quantitative Computed Tomography (pQCT) and then decalcified for histological analysis (modified Mankin score). In other mice, cartilages of both tibiae were sampled at 10, 30 and 52 weeks of age for RNA extraction and qPCR analysis. We assessed the expression of hyaluronidases Hyal1 and Hyal2, hyaluronan synthase HAS2, extracellular matrix proteases Mmp13 and Adamts-5, and type 2 collagen.

Results: Spam1$^{-/-}$ mice did not exhibit specific morphological characters up to 52 weeks of age. From 20 weeks, the proximal tibia of Spam1$^{-/-}$ mice had a significantly lower bone mineral density than WT mice. At 52 weeks, the modified Mankin score was significantly lower in Spam1$^{-/-}$ than WT mice. Spam1$^{-/-}$ chondrocytes expressed significantly less Hyal2 than WT ones at all ages and less Mmp13 at 52 weeks. Through all the experiment, the Hyal1 expression of Spam1$^{-/-}$ chondrocytes remained similar as that of WT chondrocytes.

Conclusion: Spam1 knockout reduced significantly cartilage degradation in mouse knee whereas the chondrocyte expression of Hyal 1, Hyal 2 and Mmp13 was modified, suggesting a role of this hyaluronidase in cartilage metabolism.

Introduction

Hyaluronan (HA) is a multifunctional high molecular weight glycosaminoglycan (GAG) and is a major constituent of vertebrate extracellular matrices (ECM) of connectives tissues, such as cartilage (36, 37). In mammals, HA is produced at the plasma membrane by three different HA synthases (HAS1, HAS2 and HAS3) and is degraded by multiple hyaluronidases (Hyal1, Hyal2, Hyal3, Hyal4, PH-20/Spam1, Hyalp1). These latter enzymes are clustered on two different chromosomes (36, 45, 46, 75, 119, 246). Hyal1, Hyal2 and Hyal3, located on chromosome 3p21.3, have already been studied extensively. Indeed, decreases in HA content and molecular weight in the articular cartilage are features of cartilage ageing and osteoarthritis (OA). Briefly, Hyal1$^{-/-}$ mice have been shown to accumulate HA in articular cartilage and exhibit early osteoarthritis (62). In Hyal2$^{-/-}$ mice, cartilage degradation was aggravated with ageing (60, 247). Hyal3$^{-/-}$ mice did not display any evidence of HA accumulation in tissues analyzed and did not exhibit gross phenotypic changes. Hyal3 do not seem to play a major role in constitutive HA degradation (77). Furthermore, a dialogue likely occurs between these enzymes. When one of them is knocked-out/down, the expression of another one is increased (60, 62).

PH-20/Spam1 is localized on chromosome 7q31.3 and usually known as the major testicular hyaluronidase (55). Contrary to Hyal1 to 3 which are active at acid pH, this hyaluronidase is active at near neutral pH (64). It seems to be expressed in low quantity in synoviocytes, fibroblasts and chondrocytes but its role in cartilage physiology is not further known.

This study investigated the role of Spam1 hyaluronidase in age-related articular changes by analyzing subchondral bone and articular cartilage of proximal tibia in PH-20/Spam1$^{-/-}$ mice from 10 to 52 weeks of age.

Methods

Animals

Spam1$^{-/-}$ CD1 mice were received from RIKEN research institution (Tokyo, Japan). Wild type CD1 mice (WT) were provided by Janvier Labs (Le Genest-Saint-Isle, France). Mice were raised in our lab and genotyped following a classical protocol. The local ethics committee for animal care of the Université Catholique de Louvain (authorization number 2014/UCL/MD/021) approved all experiments. Animals were housed according to the guidelines of the Belgian federal law (SPF Santé publique, Sécurité de la chaîne alimentaire et Environnement).

WT and Spam1$^{-/-}$ mice were weighed every week and measured from 10 to 52 weeks of age. They were euthanized with Isofluran® at 10, 12, 14, 18, 20, 30 and 52 weeks of age.

Bone mineral density analysis

After euthanasia, the right hindlimb was sampled (n=10/age/group) and stored in 4% neutral Formaldehyde solution (Sigma-Aldrich®) for 14 days. Each hindlimb was then scanned with peripheral Quantitative Computed Tomography (pQCT, XCT Research SA+, Norland Stratec, Germany) to obtain 10 frontal slices, separated by 25µm, with an in-plane voxel size of 70µm.

The subchondral bone of the proximal plateau of the tibia was selected as ROI in order to assess the BMD using the XCT 5.4 software.

Histological and immunohistochemistry analysis

After pQCT processing, the right hindlimbs were decalcified (quick decalcifier - Osteoral, RALA320715-2500, VWR) for 72 hours, embedded in paraffin and sectioned (5µm) in the frontal plane. The slices from the middle and the posterior compartments of the knees were stained using Safranin O and mounted on glass plates for Modified Mankin score analysis.

All sections were analysed using Leica SCN400 (Meyer Instruments Inc., Houston, Texas, USA). The modified Mankin score was assessed independently by two blinded observers. Inter-rater reliability was analyzed using Cohen's kappa coefficient and Pearson's correlation. Inter-rater reliability was moderate to perfect [κ 0.6 – 1.0] and Pearson's correlation from 0.913 to 1. We used the mean of both these measures as individual data, so the mean obtained in each group corresponded to the mean of the individual means.

Tibial Cartilage RNA extraction and qPCR

In other WT and Spam1$^{-/-}$ mice euthanized at 10, 30 and 52 weeks of age (n=10/age/group), cartilage of both tibiae was separated from subchondral bone and stored in liquid nitrogen. For each mouse, both cartilages were wrapped in aluminum foil and crushed in liquid nitrogen with a pestle. Cartilage powder was stored in TriPure Isolation Reagent (Sigma-Aldrich®) before classical RNA extraction. The RNA obtained was suspended in RNAse free water and stored at -20°C. RNA quality and quantity were measured

using a NanoDrop 1000 Spectrophotometer (Thermo Scientific™). The samples were submitted to a classical reverse transcription (RT) protocol. Changes in gene expression were analysed by quantitative PCR using gene specific primers: ACTIN MOUSE – forward GCTTCTAGGCGGAGTGTTACTGA – reverse GCCATGCCAATGTTGTCTCTTAT; TYPE 2 COLLAGEN – forward CAGGTGAACCTGGACGAGAG - reverse ACCACGATCTCCCTTGACTC; HYAL2 – forward CTACCATCGGTGAGAGTGCC – reverse CAGGTCTCCATACTTGAAGCGT; ADAMTS5 – forward CGAGTACTCAGGCCCAAATG – reverse GGCATCATTCATGTGACACC; HAS2 – forward TGCTGGTTCAGCCATCTCAG – reverse GACGACAGGCACCTTACCAA; MMP13 – forward AGAAGTGTGACCCAGCCCTA – reverse GAGGCGCCAGAAGAATCTGT; HYAL1 – forward TGAATGGCCGGTTGGATACC – reverse CTTCAGTCCTGAGGTTTCCCC.

Each reaction was runned in triplicate under the following conditions: 1 cycle at 95°C for 3min and 40 cycles (95°C for 15sec and 57°C for 30sec). The reaction was carried out at least three times for each sample depending on the quantity of RNA extraction.

Statistical analysis

Data are expressed as mean ± SD unless stated otherwise and were analysed using GraphPad Prism 8 (GraphPad Software Inc.). Means at the different experimental times were compared using ANOVA with post-test Tukey. F test was used to compare variances. Cohen's kappa coefficient and Pearson's correlation were calculated using SPSS. A p value < 0.05 was set for statistical significance.

Results

Spam1 playing a role in reproduction, the litters were significantly less numerous in Spam1$^{-/-}$ than WT mice (3.9 ± 2.76 pups versus 13.4 ± 3.2, respectively; $p < 0.0001$). No difference was noted between the percentage of males and females inside the litters. We did not observe specific external morphological characters in Spam1$^{-/-}$ mice. The body weight and length of Spam1$^{-/-}$ and WT mice followed similar curves from 10 to 52 weeks of age (data not shown). At necropsy, organs, tissue morphology and joints appeared similar in both groups from 10 and up to 52 weeks.

Tibial subchondral bone mineral density (BMD)

BMD of proximal tibial plateau, assessed with pQCT, was 965 to 1009 mg HAP/cm³ in WT mice from 10 to 52 weeks of age (Fig. 1). In Spam1$^{-/-}$, BMD was 935 to 893 mg HAP/cm³ but these values tended to decrease with age. At 18 weeks, the difference was at the limit of significance (-6.15% for Spam1$^{-/-}$ mice, $p = 0.0909$) before accentuating significantly at 20 weeks (-7.8%), 30 weeks (-9.5%) and even more at 52 weeks (-11.5%). It has to be noted that BMD tended to increase from week 10 to week 52 in WT mice and to decrease in Spam1$^{-/-}$ mice, but these differences were not significant within both phenotypes.

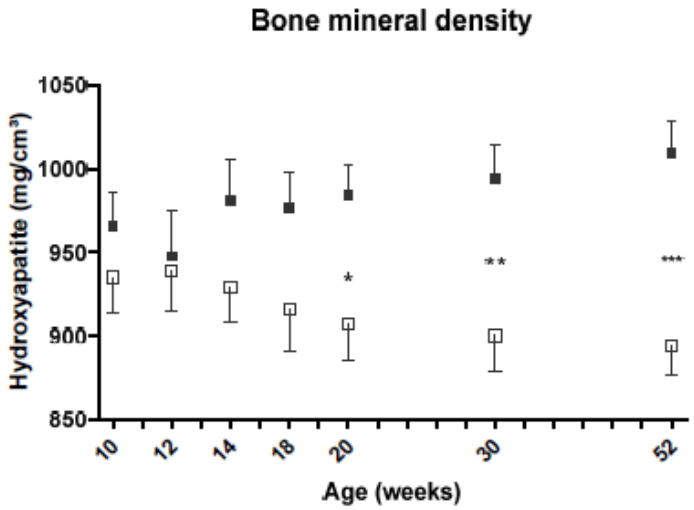

Figure 1: BMD of proximal tibia subchondral bone assessed with pQCT in WT (black squares) and Spam1$^{-/-}$ (white squares) mice from age 10 to 52 weeks (n = 10/group/age). Data are expressed as Mean + SEM for WT and Mean – SEM for Spam1$^{-/-}$ mice. *: $p < 0.05$; **: $p < 0.01$; ***: $p < 0.001$.

Cartilage histology

Histological analysis of Safranin-O stained frontal sections through tibial proximal epiphysis allowed to distinct articular cartilage and subchondral bone. No difference was observed between WT and Spam1$^{-/-}$ mice at 10 weeks of age, as confirmed by the low modified Mankin score (Fig. 2A). At 30 weeks, although the architecture of the subchondral bone remained similar in both groups, we sometimes noticed a slight reduction in matrix staining and some surface irregularities in cartilage of both groups. The modified Mankin score increased but the increase was significant only in the WT group. At 52 weeks, the modified Mankin score was considerably increased in both groups but was significantly lower in Spam1$^{-/-}$ than WT

mice (3.1 ± 0.9 vs. 5.6 ± 1.2; $p < 0.001$). At this age, cartilage of WT mice showed severe reduction in matrix staining, diffuse hypercellularity or some cells clusters, and surface irregularities, as compared with moderately reduced matrix staining, some surface irregularities and some diffuse hypercellularity in cartilage of Spam1$^{-/-}$ mice (Fig. 3). Only in WT mice, the subchondral bone appeared somewhat more abundant at 52 weeks. No ectopic calcification or osteophyte formation was visible in the frontal sections of both groups (Fig. 2B).

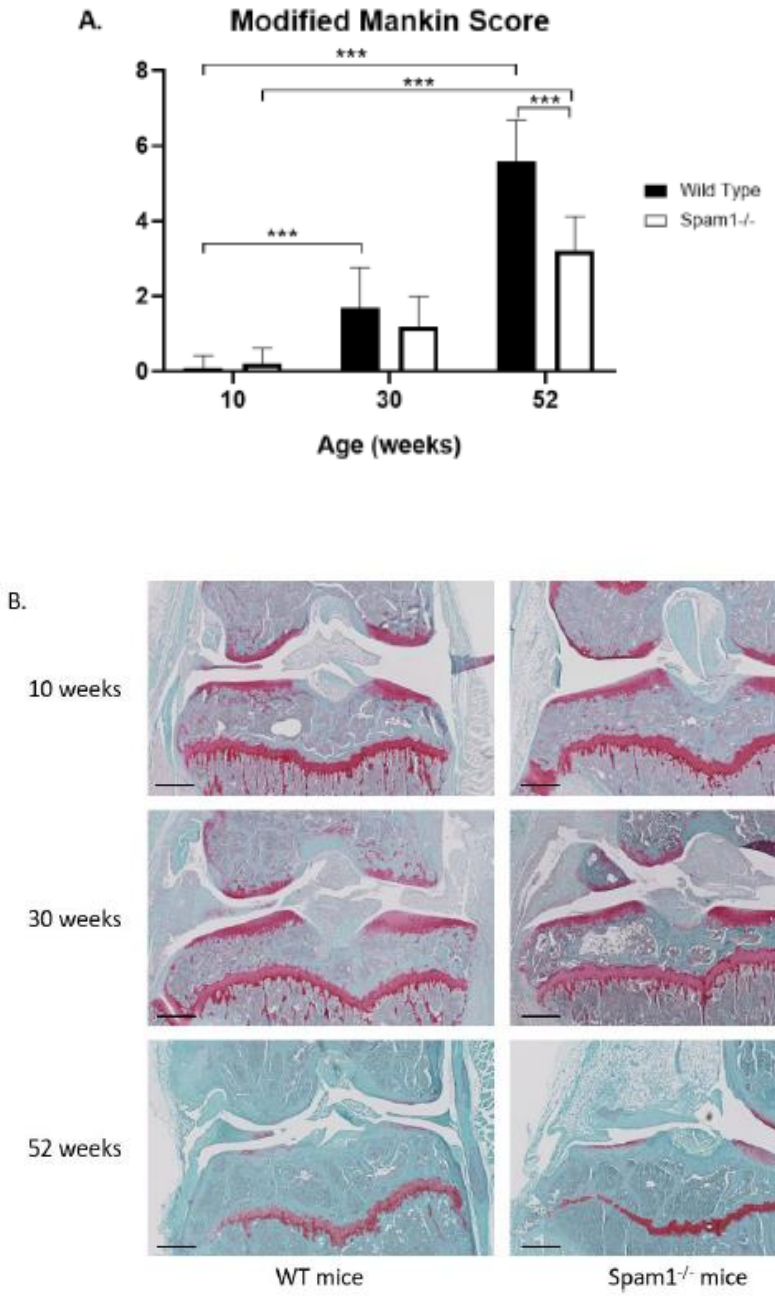

Figure 2: Histological analysis of the right knee of WT and Spam1-/- mice aged 10, 30 and 52 weeks. (A) Modified Mankin Score. (B) Safranin-O stained frontal sections (scale bar = 400 µm). Data are expressed as mean + SD. n = 10/age/group. ***: $p < 0.001$.

qPCR analysis of cartilage

As highlighted by qPCR, WT chondrocytes expressed significantly more Hyal2 at 52 weeks than at 10 weeks of age ($p < 0.05$) (Table I). The chondrocytes of Spam1$^{-/-}$ mice expressed significantly less Hyal2 than WT chondrocytes at 10 weeks (- 35%; $p < 0.05$), 30 weeks (- 41.3%; $p < 0.01$) and 52 weeks (- 54.7%; $p < 0.001$). Contrary to WT, in Spam1$^{-/-}$ chondrocytes the Hyal2 expression remained constant throughout the experiment.

Spam1$^{-/-}$ chondrocytes expressed more Hyal1 than WT chondrocytes at 10 weeks, but this difference was not significant (Table I). This difference decreased with time because WT mice expressed significantly more Hyal1 at 52 than 10 weeks ($p < 0.05$). Through all the experiment, the Hyal1 expression of Spam1$^{-/-}$ chondrocytes remained approximatively the same.

At 10 weeks of age, we did not observe any difference in the expression of Mmp13 between Spam1$^{-/-}$ and WT chondrocytes. This expression increased significantly in WT chondrocytes with time. At 52 weeks, WT chondrocytes expressed significantly more Mmp13 than Spam1$^{-/-}$ chondrocytes ($p < 0.05$) and WT chondrocytes at 10 weeks ($p < 0.05$).

Table I. Expression of Hyal1, Hyal2, Mmp13, Adamts-5, Collagen Type II, HAS-2 by WT and Spam1$^{-/-}$ chondrocytes as assessed by qPCR at 10, 30 and 52 weeks of age.

		Age					
	Genotype	10 weeks		30 weeks		52 weeks	
Hyal1	WT	1 ± 0.21		1.14 ± 0.18		1.37 ± 0.26	$
	Spam1$^{-/-}$	1.29 ± 0.19	n.s.	1.27 ± 0.14	n.s.	1.29 ± 0.16	n.s.
Hyal2	WT	1 ± 0.13		1.09 ± 0.16		1.26 ± 0.24	$
	Spam1$^{-/-}$	0.65 ± 0.08	*	0.64 ± 0.13	**	0.57 ± 0.25	***
Mmp-13	WT	1 ± 0.46		1.24 ± 0.37		1.56 ± 0.29	$
	Spam1$^{-/-}$	0.96 ± 0.38	n.s.	1.06 ± 0.27	n.s.	1.15 ± 0.27	*
Adamts-5	WT	1 ± 0.4		1.03 ± 0.25		1.15 ± 0.27	
	Spam1$^{-/-}$	0.99 ± 0.33	n.s.	1.06 ± 0.28	n.s.	1.05 ± 0.23	n.s.
Collagen Type II	WT	1 ± 0.26		0.95 ± 0.16		0.92 ± 0.21	
	Spam1$^{-/-}$	0.97 ± 0.19	n.s.	1.02 ± 0.21	n.s.	0.94 ± 0.18	n.s.
HAS2	WT	1 ± 0.18		1.06 ± 0.24		1.03 ± 0.23	
	Spam1$^{-/-}$	1.03 ± 0.24	n.s.	1.01 ± 0.18	n.s.	0.98 ± 0.22	n.s.

Data are the mRNA expression of enzymes/actin as mean ± SD; n=10/group/age; each sample was assessed in triplicate. Ns: non-significant; *: $p < 0.05$, **: $p < 0.01$, ***: $p < 0.001$ between WT and Spam1$^{-/-}$ at the same age; $: $p < 0.05$ between WT 52 weeks and WT 10 weeks.

The expression of Adamts-5, type 2 collagen and has2 did not appear different between both groups and did not change from 10 to 52 weeks (Table I).

Discussion

According to our results, Spam1$^{-/-}$ mice did not show specific external or joint morphological character. However, the subchondral bone of their tibial plateau had a lower BMD than that of WT mice; this difference was significant from 20 weeks of age and was accentuating until 52 weeks. At this age, Spam1$^{-/-}$ mice had a significantly lower Modified Mankin score of the knee than WT mice. Those results were associated with a significantly lower chondrocyte expression of Hyal2 and Mmp13 in Spam1$^{-/-}$ than in WT chondrocytes.

First of all, we used a knockout model instead of a conditional knockdown one (31) because Spam1$^{-/-}$ mice are viable and, except testis, Spam1 expression is very low in other cells, including chondrocytes. Furthermore, the main hyaluronidases, Hyal1 and Hyal2, were also studied with knockout mice (62, 247). As expected, Spam1$^{-/-}$ litters were extremely significantly smaller than WT ones. Indeed, Spam1 is the major testicular hyaluronidase (55) and allows the spermatozoids to penetrate the oocyte-cumulus complex (248). Until now, no study has focused on the general phenotype of the Spam1$^{-/-}$ mouse. Our morphological data (mice weight and size, external characters) did not highlight any phenotype difference between WT and Spam1$^{-/-}$ mice. Similarly, Hyal1$^{-/-}$ mice presented no difference in size, tissue morphology and organ weight until 12 months of life (62). On the contrary, Hyal2$^{-/-}$ mice can be recognized among litters by their characteristic shortened nose as early as 3 to 4 weeks and display craniofacial and cervical vertebrae abnormalities (247).

pQCT analysis revealed that BMD of the tibial plateau of Spam1$^{-/-}$ mice was lower than that of WT mice throughout the experimental period. This difference was associated with a significantly lower modified Mankin score of the knee in Spam1$^{-/-}$ than WT mice at 52 weeks. At this time, we observed some increase in bone mass of the tibial plateau in WT mice only. Since both subchondral bone and cartilage modifications are typical of OA, the knockout of Spam1 seems to have a protective effect on the joint towards age-related cartilage loss. By comparison, according to previous studies, Hyal1$^{-/-}$ mice accumulated HA in articular and epiphyseal cartilage and exhibited OA. A decrease in Safranin O staining was observed in Hyal1$^{-/-}$ mice as early as 3 months up to 20 months compared to WT mice (62). Recently, Higuchi et al. (60) showed that a conditional knockdown of Hyal2 in articular cartilage aggravated age-related cartilage degradation as well as OA induced by destabilization of the medial meniscus.

As previously highlighted by some authors, the knockout of one hyaluronidase can affect the expression of other enzymes that degrade the ECM. In Hyal1$^{-/-}$ mice, the expression of Hyal3 was elevated suggesting a compensation role in HA degradation in all tissues, except skeletal ones (62). Nevertheless, Atmuri et al. (77) concluded that Hyal3 is not a major contributor to constitutive HA degradation. In Hyal2$^{-/-}$ mice, besides the increased OA progression, Hyal1 expression in articular cartilage was not modified, but expression of Mmp13 and Adamts-5 was increased (60). Recently, Chowdhury et al. (74) suggested the existence of Hyal2-independent pathway of HA degradation. Spam1, clustered on another

chromosome than hyaluronidases Hyal1 to 3, is expressed in human and mice chondrocytes (31, 64). Furthermore, Spam1 is the only hyaluronidase active at neutral pH and able to degrade HA (64, 249). According to our data, Spam1$^{-/-}$ chondrocytes expressed significantly less Hyal2 than WT chondrocytes and their expression remained constant throughout the experiment, whereas WT chondrocytes expressed significantly more Hyal2 with ageing. On the other hand, we did not find any significant difference in Hyal1 expression between the two groups at the different ages, although only WT chondrocytes expressed significantly more Hyal1 at 52 weeks than at 10 weeks. So, Hyal1 and Hyal2, which are widely expressed and considered the major HA-degrading enzymes in somatic tissues (31, 32, 52) are not more expressed by Spam1$^{-/-}$ chondrocytes with ageing. Since the complex CD44-Hyal2 deals with first step of HA degradation (75), the knockout of Spam1 could decrease the HA degradation with ageing.

Besides hyaluronidases, the matrix proteases Adamts-5 and Mmp13 are upregulated during OA development and play a role in the hypertrophic differentiation of articular chondrocytes (250). We did not observe any difference in the expression of Adamts-5 between both genotypes whatever their age. At 52 weeks of age, however, Spam1$^{-/-}$ chondrocytes expressed significantly less Mmp13 than WT chondrocytes. Only WT chondrocytes increased significantly their Mmp13 expression with ageing. Mmp13 being a regulator of inflammation (206), its lower expression in Spam1$^{-/-}$ chondrocytes at 52 weeks of age might protect the joints by preserving ECM.

One limitation of our study is the difficulty to obtain RNA in enough amounts. To avoid using too many mice, it might be useful to consider an in-vitro Spam1$^{-/-}$ chondrocyte model to analyse the expression of enzymes that degrade or synthesize the ECM. This model could also be useful for studying the reaction of Spam1$^{-/-}$ chondrocytes in inflammatory conditions. A second limitation concerns the bone analyses. The tibial subchondral bone architecture could be evaluated more accurately using Micro-CT instead of pQCT.

In conclusion, our data show that the absence of Spam1 seems to have a protective effect on the joint components towards age-related cartilage loss. Furthermore, Spam1 knockout appears to have an impact on the chondrocyte expression of the two main hyaluronidases Hyal1 and Hyal2, as well as of Mmp13.

CHAPTER TWO: Mouse SPAM1 knockout prevents subchondral bone loss and cartilage degradation

Sébastien Lafont[1], Mickael Cardinal[1], Thomas Roels[1], Catherine Behets[1], Daniel Manicourt[2]

[1]Pole of Morphology and [2]Pole of Systemic and Inflammatory Rheumatic Diseases – Institut de recherche expérimentale et Clinique - Université Catholique de Louvain, Brussels, Belgium

Manuscript submitted in Journal of Clinical Investigation

Conflict of interest statement

The authors have declared that no conflict of interest exists.

Abstract

Hyaluronan [HA] is crucial for cartilage structure and functions. Hyaluronidases Hyal1 and Hyal2 and HA synthase 2 [HAS2] determine its levels. We reported the depletion of HA in osteoarthritic [OA] cartilage and the chondrocyte expression of the neutral-active Hyal-Spam1/PH-20. Recently, we showed that, at 52-weeks of age, Spam1$^{-/-}$ mice had a two-fold reduction in Mankin histologic-histochemical OA score [MS]. This 10-weeks-study weekly explored the cartilage and subchondral bone defects induced by knee destabilization in Spam1$^{-/-}$ and WT mice. MS increased at week-2 to reach, by week-10, 6.5/15 in Spam1$^{-/-}$, and 13.6/15 in WT. On day-3, subchondral tibial bone mineral density and bone volume fraction decreased in WT and unexpectedly increased in Spam1$^{-/-}$. Trabecular changes in number [Tb.N] and thickness [Tb.Th] accounted for these differences. Later, on day-7, BMD remained higher in WT. Changes in BV/TV, Tb.N, and Tb.Th were not significant. The volume and number of osteophytes in Spam1$^{-/-}$ were lower than in WT. The rise in enzyme expression in WT versus Spam1$^{-/-}$ was 21-fold vs. 6-fold for MMP13, 4-fold vs. 2-fold for Hyal1, and 2-fold vs. 0-fold for Hyal2. HAS2 collapsed with time post-surgery in both genotypes. Spam1 might be an important new target for OA prevention and therapy.

1. Introduction

Hyaluronan [HA] is an unbranched linear covalent polymer alternating glucuronic acid-N-acetylglucosamine [GlcA-GlcNAc] and reaching a molecular mass [MM] of 10^5-10^7 Da (36, 63, 251). HA is essential for the assembly of the sophisticated extracellular matrix [ECM] that brings physical scaffolding to the cells and initiates biomechanical and biochemical cues for tissue morphogenesis, differentiation, and homeostasis. In body fluids, the polyanionic HA chain attracts cations and water and adopts an expanded random coil conformation. These intra-and intermolecular interactions produce a viscoelastic gel that hydrates, shapes, and gives turgor to the tissues while facilitating cellular migration and proliferation (252). Many cells have an HA-rich protective pericellular matrix [PM] (253). The interactions HA with CD44, Toll-like, and other transmembrane proteins are essential for tissue homeostasis (254). The results depend on the HA size. Typically, high MM HA reduces joint enzymatic degradation (255-258). Conversely, low MM HA promotes angiogenesis, inflammation, and bone resorption (31, 119, 259-261). In the ECM further remote from the cell, HA binds tissue-specific proteins to form large complexes. In cartilage, HA binding to aggrecan retains it at high concentrations within the collagen network to provide compressive resilience (104, 262). Breakdown and loss of HA as occur in osteoarthritic [OA] cartilage alter joint biomechanics and contribute to the destruction of cartilage and subchondral bone (168, 263). We know little about the regulation of HA metabolism, partly because of technical difficulties. There 15 g of HA in a 70-kg individual, of which 5 g is replaced daily (63, 264). HA half-life varies among and within tissues and

can be as short as 2-5 minutes in the blood and as long as 18 days when bound to cartilage aggrecans (264, 265). In chondrocyte cultures, HA half-life is shorter in the cell-associated matrix than in the ECM further remote from the cells (266). Cells strictly regulate the synthesis and degradation of HA to maintain the homeostasis of this critical component of the ECM. HA synthases are transmembrane proteins. Eucaryotes express three isoforms (45). HAS2 produces very high MM HA [≥ 4 MDa], whereas HAS3 and HAS1 provide smaller polydisperse chains with an average MM of 0.8 and 1 MDa, respectively. HAS gene usage is tissue-specific, and regulation of HA synthesis multi-faceted. HAS2 predominates in cartilage and HAS1 in the synovium (267). Complete deficiency of HAS2 causes embryonic lethality (63). The repair of cartilage injury is ineffective in $HAS1^{-/-}$ mice. HAS1 ablation does not alter the HA content of cartilage but enhances apoptosis and IL-17/IL-6 signaling (268). In human OA, chondrocytes increase their rate of HA synthesis significantly compared to normal (269). Thus, the reduction in the content of HA seen in OA cartilage results from enhanced HA catabolism. Free radicals and hyaluronidases [Hyals] degrade HA (254, 270). Hyals are endo-β-N-acetyl-hexosaminidases in mammals. Humans have six HYAL genes that are clustered at 3p21.3 [HYAL2-HYAL1-HYAL3], and 7q31.3 [SPAM1-HYAL4- HYALP1] (56, 63, 271). The mouse orthologs have a similar organization on chromosome 9F1-F2 and 6A2, respectively. HYALP1 is active in mice and a pseudogene in humans (272). Rodents have an additional HYAL5, that maps downstream of SPAM1 (273, 274). As they are ubiquitously expressed, Hyal1 and Hyal2 are likely candidates for the constitutive degradation of HA (31, 63, 74, 275). Hyal1 is acid-active and

found in both lysosomes and body fluids. Hyal2 is a GPI-anchored protein. *In vitro*, Hyal2 activity occurs at pH 4-7 and requires the presence of CD-44 (107). Both Hyals degrade high MM HA, but Hyal1 yields tetrasaccharides, and Hyal2 generates 20 kDa products. Within a proposed model (63, 275), Hyal2 initiates HA degradation extracellularly by cleaving the high MM HA that is bound to a cell surface receptor such as CD44, HARE or LYVE1. The resulting 20 kDa fragments are then internalized by receptor-mediated endocytosis to enter the endosomal/lysosomal pathway. In lysosomes, Hyal1 cleaves the 20 kDa fragments to smaller pieces that become substrates for the sequential action β-glucuronidase and β-N-acetylhexosaminidase that give GlcA and GlcNAc, respectively. The HA fragments escaping cellular endocytosis within their native tissue gain the lymphatics where most HA degradation occurs in the lysosomes of the lymph node (264). HA avoiding local and lymphatic breakdown enters the blood to be remote by blood-filtering organs. In cartilage, HA is degraded by HYALs intracellularly or extracellularly, depending partly on its association with aggrecan (273). HA free of aggrecan or aggrecan G1 domains bound to HA can be internalized via CD44 (65, 67). By contrast, chondrocytes cannot internalize high MM intact aggrecan-HA complexes before enzymatic cleavage. As hyaline cartilage is paucicellular, HA of the inter-territorial matrix remote from the chondrocyte might escape endocytosis. Cartilage explants release HA, link protein, and aggrecan G1 fragments concomitantly into their media (259, 276). Pulse-chase labelling studies revealed that one-fourth of the pulse labelled [L] HA escaped into the medium the first day of the chase with no further release at later times

(277). Also, the average size of the tissue L HA was higher than that of the resident unlabelled [RU] HA at early chase times but decreased toward the size of the RU HA with a half-life of 1-2 weeks. These studies suggest extracellular degradation of HA. Among the candidate enzymes for the extracellular degradation of cartilage HA at pH values of 6.8-7, we disqualify the acid-soluble Hyal1 as Hyal1$^{-/-}$ mice exhibit OA of the knee joints as early as three months of age (62). We also eliminate the weakly expressed Hyal3. Mice deficient in Hyal3 are viable and do not accumulate HA (77). However, Hyal3 may compensate for Hyal1 in HA degradation as Hyal1 null mice raise their Hyal3 expression (62). Further, Hyal4 is just a chondroitinase that does not express any Hyal activity (278). By contrast, Spam1 or PH-20 is a likely candidate for the degradation of HA in cartilage ECM. The enzyme was initially found in sperm as it assists in sperm penetration through the HA-rich cumulus oophorus surrounding the oocyte (90). Rodents express the additional neutral sperm Hyals: Hyal5 and Hyalp1 (272, 273). Spam1 cleaves HA at both acidic and neutral pH and is the most active mammalian Hyal. The enzyme degrades HA of any size into tetrasaccharides. Male and female genital tracts both express Spam1 (32, 90). Also, Spam1 is present in the kidney (279), and we reported its expression in dermal fibroblasts, synoviocytes, and chondrocytes (64).

Accordingly, overexpression of Spam1 by chondrocytes may contribute to the depletion of HA in articular cartilage and the development of OA. We recently show that the absence of Spam1 reduces age-related cartilage changes (280).

To test this hypothesis, we destabilized the medial meniscus and transected the anterior cruciate knee ligament in 10-week-old Spam1$^{-/-}$ and WT mice. We sampled knees at different times between 3- and 70-days post-surgery and graded OA damage in cartilage and subchondral bone by using histology, pQCT, µCT, and immune-histochemistry.

2. Results

2.1. Survival and bodyweight

All mice completed the 70-day study. On days 0 and 7, there was no difference in mean body mass between Spam1$^{-/-}$ and WT mice, whether operated on, sham-operated or non-operated. On day 70, the operated [OA], sham-operated, and non-operated Spam1$^{-/-}$ mice, as well as the sham-operated and non-operated WT mice, also had a similar mean body mass of 33.6 g. Only, the operated [OA] WT mice had a higher mean body mass of 35.8 g. As operated WT mice moved more slowly and rested much often than mice of the other groups, the discrepancy in the level of physical activity might contribute to explain the higher body weight of operated WT mice.

2.2. Mankin Score changes

Figure 1 gives the severity of OA lesion in the tibial plateau of operated WT and Spam1$^{-/-}$ mice at different time points after surgery. From day 0 to day 3, the score was ≤ 2/14 in all WT and Spam1$^{-/-}$ mice, whether operated or belonging to control groups [sham-operated and non-operated for each genotype]. On day 7, the maximum score was 3/14 in 20% of operated WT mice and 10% of operated Spam1$^{-/-}$ mice, all other mice of the four control groups having a maximum score of 2/14. In operated Spam1$^{-/-}$mice, the mean score of OA changes enhanced by 250% [from 1.6 to 5.6] between day 7 and day 28 post-surgery and then plateaued [from 5.6 to 6.5] until the study ended on day 70. The situation was worse in WT mice. Between day 7 and day 14, their mean OA score increased abruptly by 477% [from 1.3 to

7.5] before rising at a slower pace [mean increase 87%; from 7.5 to 14] between day 14 and day 70. Thus, at the end-of-study, the rise in the Mankin score of operated WT mice was 2 to 3-fold higher compared to operated Spam1$^{-/-}$. In the two control groups of both WT and Spam1$^{-/-}$ mice, the mean histological OA score never exceeded the value of 3 during the 70-day study.

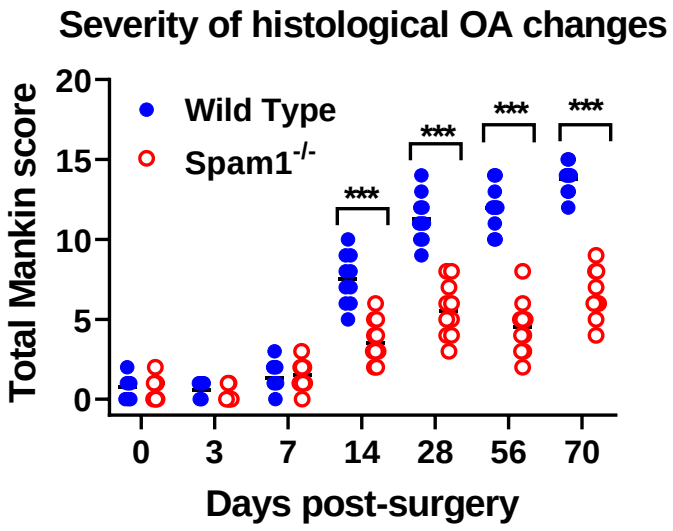

Figure 1. Grading of the severity of OA lesion with the modified Mankin scoring system in WT (blue closed circles) and Spam1$^{-/-}$ (red open circles) mice.
The severity of the OA lesion in the tibial plateau was graded on a scale 0-14 using the modified Mankin scoring system. Each point represents the mean of six assessments assessed in one mouse at a time point. N = ten mice per group and experimental day. *** $p<0.001$ by Fisher test. We only give the statistically significant differences between Spam1$^{-/-}$ mice and WT mice.

2.3. Bone mass of the tibial plateau

Before surgery, the pQCT-based mean BMD of the medial tibial plateau in Spam1$^{-/-}$ mice was reduced by 5% compared to WT [p = 0.03]. As compared to values on day 0 [Figure 2, upper panel], the mean BMD of operated WT knees decreased by 8% on day 3 and by 9% on day 7 before recovering the day 0 value on day 14. Then, a second drop in BMD occurred by days 28 [-3.5%], 56 [-4.8%] and day 70 [-6.5%]. In sham-operated knees, the mean BMD decreased by 4% on day 3, by 3% % on day 7, and reached the day 0 level on day 14. Then, the BMD increased by 1.1% on day 56 and by 1.5% on day 70.

The story was different in operated [OA] Spam1$^{-/-}$ mice [Figure 2, lower panel]. Surprisingly, the BMD was increased by 5.3% on day 3 and decreased by 4.7% on day 7. The BMD then regained the day 0 level on day 28 before reducing by 2.6% on day 56 and by 7.7% on day 70. In sham-operated Spam1$^{-/-}$ mice, the BMD dropped by 1.5% on day 3 and by 2.7% on day 7, returned to day 0 levels on day 14, and then decreased by 1.2% on day 28, by 2.6% on day 56, and by 5% on day 70. The loss in BMD between day 0 and day 70 was 7% in operated [OA] WT knees, and 8% operated [OA] Spam1$^{-/-}$ knees.

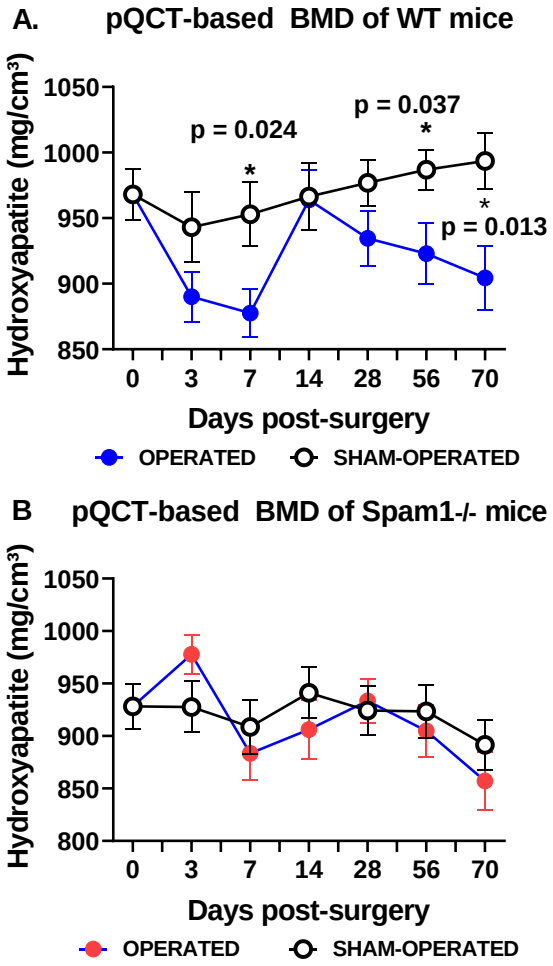

Figure 2. Changes in pQCT-based BMD of the right medial tibial plateau in WT [upper panel] and Spam1$^{-/-}$ [lower panel] mice from day 0 to day 56 after knee destabilization
The value given at each time point for a group represents the Mean ± SEM of the values obtained in ten animals of this given group. Upper panel: closed blue circles = operated WT; open white circles = sham-operated WT. Lower panel: closed red circles = operated Spam1$^{-/-}$; open white circles = sham-operated Spam1$^{-/-}$. * = $p<0.05$ between operated and sham-operated.

2.4. Micro-CT analysis of tibial subchondral bone

To get a better insight into the early postoperative discrepancies in BMD changes between [OA] WT and Spam1$^{-/-}$ knees, we performed µ-CT analyses on the cancellous ROI defined in the medial horizontal subchondral bone of medial tibial plateau specimens. Table 1 and Figure 3 give the results obtained for BMD, bone volume per tissue volume [BV/TV], the trabecular number [Tb. N], trabecular spacing [Tb. Sp], and trabecular thickness [Tb. Th] at different postsurgical time points.

On day 0 and as compared to WT [Figure 3A], the cancellous bone of Spam1$^{-/-}$ exhibited enhanced Tb. N [+23%] as well as a decreased BMD [-5%], BV/TV [-12%], and Tb. Th [-23%]. All these changes were statistically significant, and the magnitude of the relative decrease in BMD was similar to that obtained by pQCT. On day 3, BMD [Figure 3A] and BV/TV [Figure 3B] both decreased dramatically in operated [OA] WT mice [-6.5% and -7.6%, respectively] and increased markedly in operated [OA] Spam1$^{-/-}$ OA mice [+3% and +10%, respectively]. It was the only time point during which BMD and BV/TV in OA Spam1$^{-/-}$ mice were significantly higher compared to OA WT. Parallel modifications in Tb Th mainly drove these differences in BMD and BV/TV [-16% in WT and +25% in Spam1$^{-/-}$; Figure 3D]. There were less marked inverse changes in Tb. N [+10% in WT and -12% in Spam1$^{-/-}$; Figure 3C].

Then, on day 7 and in each genotype, the mean BMD values returned to their corresponding day 0 values [Figure 3A]. However, as compared to day 0 [Table 1], the mean Tb. N was enhanced by 4% in WT and reduced by 7.4% in Spam1$^{-/-}$, whereas the mean Tb. Th was decreased by 8% in WT and increased by 11% in Spam1$^{-/-}$.

The results highlight marked differences in the way each genotype adapts the microarchitecture of its subchondral bone rapidly to drastic changes in joint biomechanics.

The representative µCT images of tibial plateaus [Figure 4] from WT [left panels] and Spam1$^{-/-}$ [right panels] mice show the profound changes in BMD occurring during the first week post-surgery. According to the color scale, the medial plateaus of WT specimens are blue-green [high BMD values] on day 0 and day 7, and green-red [medium BMD values] on day 3. In contrast, the medial plateaus of Spam1$^{-/-}$ specimens are green-red [medium BMD values] on day 0 and day 7, but full green [low BMD values] on day 3.

In the absence of contrast medium specific to cartilage, we also show safranin-O-stained sections of the femorotibial joint compartment. During the first postoperative week, the significant microarchitectural changes in the subchondral bone contrasted with the small histological OA lesions observed in corresponding cartilage slices. The Mankin score of 3/14 was similar to that seen in control knees [sham-operated and non-operated]. Also, the histological sections witness the severing of the cruciate ligament and the translocation of the medial meniscus.

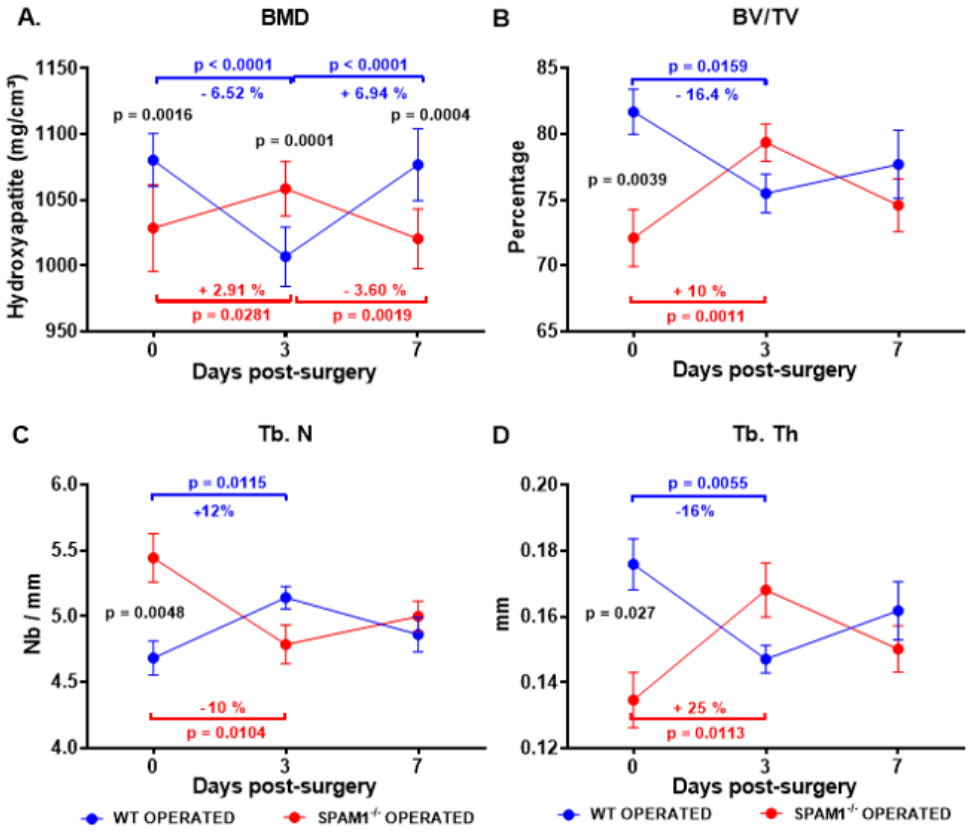

Figure 3. Micro-CT analysis of tibial subchondral bone in OA WT [closed blue circles] and OA Spam1$^{-/-}$ [closed red circles] mice during the first seven postoperative days.

A. Bone mineral density (BMD). B. Bone volume fraction (BV/TV). C. Trabecular number (Tb.N). D. Trabecular thickness (Tb.Th). We only give statistically significant differences and the percentage of increase (+) or decrease (-). P-value alone represents the difference between the two murine groups on the same experimental day. P-value + percentage represent the change of the parameter within the same group between two consecutive experimental times. We give data as mean ± SEM. N = ten mice per group and experimental day.

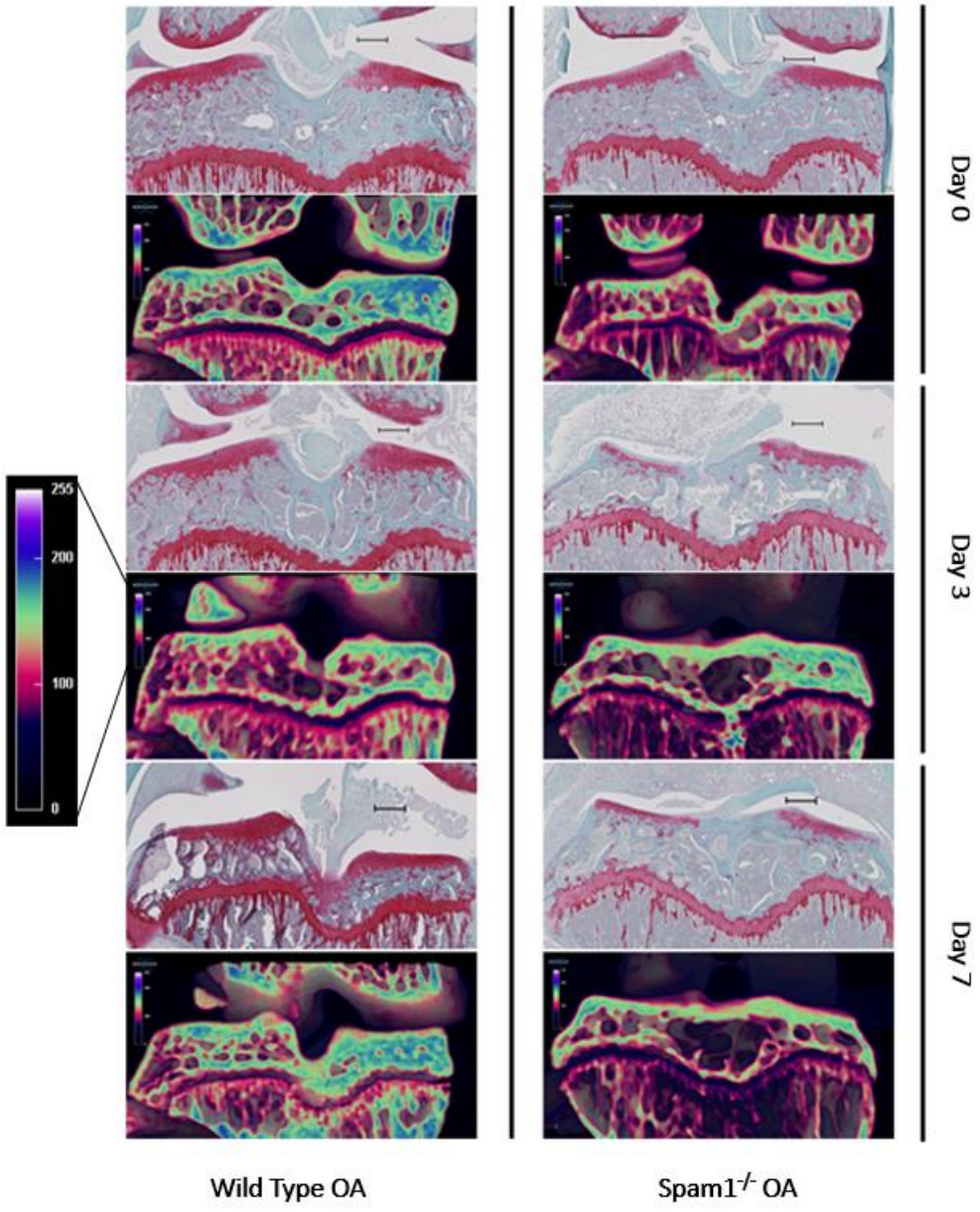

Figure 4. Histological and micro-CT frontal sections through proximal tibias of destabilized knees from Wild Type OA and Spam1$^{-/-}$ OA mice on day 0, day 3, and day 7 post-surgery. The color scale corresponds to BMD values. The changes in BMD of the medial plateau on day 3 are evident: as compared to similar specimens sampled on day 0 and day 3, the BMD of day 3 samples deceased in WT OA and increased in Spam1$^{-/-}$ OA.

Table 1. Micro-CT analysis of right tibias of Spam1$^{-/-}$ OA and WT OA mice at days 0, 3, 7, 14, 28, 56 and 70 after OA induction.

		Micro-CT parameters									
Experimental time	Mice	BMD (mg hydroxyapatite/cm³)	p-value	BV/TV (%)	p-value	Tb. N (1/mm)	p-value	Tb. Sp (µm)	p-value	Tb. Th (µm)	p-value
Day 0	WT	1080.3 [1063.4 - 1097.1]		81.7 [77.6 - 85.7]		4.7 [4.4 - 5]		106.1 [99.1 - 113]		175.9 [157.6 - 194.2]	
	Spam1 $^{-/-}$	1028.6 [1003.3 - 1054]	**0.0016**	72.1 [67.1 - 77.1]	**0.0039**	5.4 [5 - 5.9]	**0.0048**	107.31 [101.6 - 113]	0.7458	134.6 [115.3 - 153.9]	**0.0027**
Day 3	WT OA	1006.9 [988.06 - 1025.9]		75.5 [72 - 79]		5.1 [4.9 - 5.3]		106.77 [97.6 - 115.9]		147 [137.1 - 157]	
	Spam1 $^{-/-}$ OA	1058.6 [1043.8 - 1073.4]	**0.0001**	79.4 [76.2 -82.6]	0.0789	4.8 [4.5 - 5.1]	0.0671	107.86 [102.6 - 113.1]	0.8040	168 [149.4 - 186.7]	0.0514
Day 7	WT OA	1076.8 [1055.8 - 1097.8]		77.7 [71.9 - 83.6]		4.9 [4.6 - 5.1]		110.9 [102.4 - 119.4]		161.7 [141.8 - 181.7]	
	Spam1 $^{-/-}$ OA	1020.5 [1001.5 - 1039.5]	**0.0004**	74.6 [68.8 - 79.3]	0.3740	5 [4.7 - 5.3]	0.4543	104.3 [92.9 - 115.6]	0.2858	150.1 [133.4 - 166.8]	0.3370
Day 14	WT OA	1067.4 [1049.1 - 1085.7]		81.2 [77.2 - 85.3]		4.3 [4.2 - 4.4]		121.9 [104.8 - 139.1]		189.6 [175.5 - 203.7]	
	Spam1 $^{-/-}$ OA	1029.8 [1012.1 - 1047.6]	**0.0036**	70.1 [63.1 - 77]	**0.0071**	4.8 [4.6 - 5]	**0.0004**	138.6 [123.6 - 153.7]	0.1070	145.3 [131 - 159.7]	**0.0001**
Day 28	WT OA	1074.2 [1056 - 1092.4]		75 [70.5 - 79.5]		4.6 [4.3 - 4.9]		134.2 [115.4 - 152.9]		164.9 [146.6 - 183.4]	
	Spam1 $^{-/-}$ OA	1020.9 [1008.5 - 1033.2]	**< 0.0001**	67.7 [59.6 - 75.8]	0.0709	4.3 [3.9 - 4.7]	0.1765	145.5 [134.2 - 156.7]	0.2855	159.4 [131.6 - 187.3]	0.6951
Day 56	WT OA	1032.9 [1018.6 - 1047.3]		63.8 [60.5 - 67.1]		4.2 [4 - 4.5]		149.7 [136.4 - 163]		151.4 [139.4 - 163.5]	
	Spam1 $^{-/-}$ OA	1022.9 [1014.1 - 1031.8]	0.2188	56.1 [51.7 - 60.4]	**0.0041**	3.9 [3.6 - 4.3]	0.1143	177.4 [162.3 - 192.4]	**0.0059**	143.6 [130.1 - 157.1]	0.3341
Day 70	WT OA	1001.6 [983.33 - 1019.9]		63.3 [60.1 - 66.5]		4.1 [3.9 - 4.4]		153.4 [145.6 - 161.2]		154.3 [139 - 169.7]	
	Spam1 $^{-/-}$ OA	984.8 [958.82 - 1010.7]	0.2242	54.1 [49.5 - 58.7]	**0.0011**	4 [3.7 - 4.3]	0.5013	167.2 [153.9 - 180.4]	**0.0442**	135.2 [120.4 - 150.1]	0.0600

Measurements included bone mineral density (BMD), bone volume fraction (BV/TV), trabecular number (Tb.N), trabecular separation (Tb.Sp) and trabecular thickness (Tb.Th). Results are expressed as Mean [95% confidence interval]. Statistical differences between Spam1$^{-/-}$ OA and WT OA mice were calculated for each parameter at each experimental time. N=10/group/experimental time.

2.5. Osteophyte volume and ectopic calcifications

3D reconstruction of micro-CT slices features osteophytes [OSP] and ectopic calcifications [EC] in the operated knees [Figure 5, upper panel]. OSPs usually occupied the posteromedial side of the knee and were found as early as on day 14 post surgery in both genotypes.

In OA WT mice, the OSP frequency was already 100% as early as on day 28 [Figure 5, left lower panel] whereas, in OA Spam1$^{-/-}$ mice, their incidence averaged 60-70% from day 14 to day 56 and reached 90% on day 70. OSPs had a similar mean volume in the two genotypes, both on days 14 and 28. By contrast, and as compared to OA Spam1$^{-/-}$, the size of OA WT osteophytes was twice as broad on day 56 [$p = 0.0276$] and about four times as large on day 70 [$p = 0.0011$].

From day 0 to day 14, we did not find any EC as defined as inappropriate biomineralization occurring in joint soft tissues, not connected with the tibia or the femur, and different from the patella, fabella, and anterior horns of menisci (53, 54). By contrast, we detected mineralized nodules on day 28 post surgery [Figure 5, right lower panel], and there was no difference in their mean number between OA WT and OA Spam1$^{-/-}$mice. Mineralized nodules were more numerous in OA WT mice compared to Spam1$^{-/-}$mice on both day 56 [$p = 0.0003$] and day 70 [$p = 0.0037$].

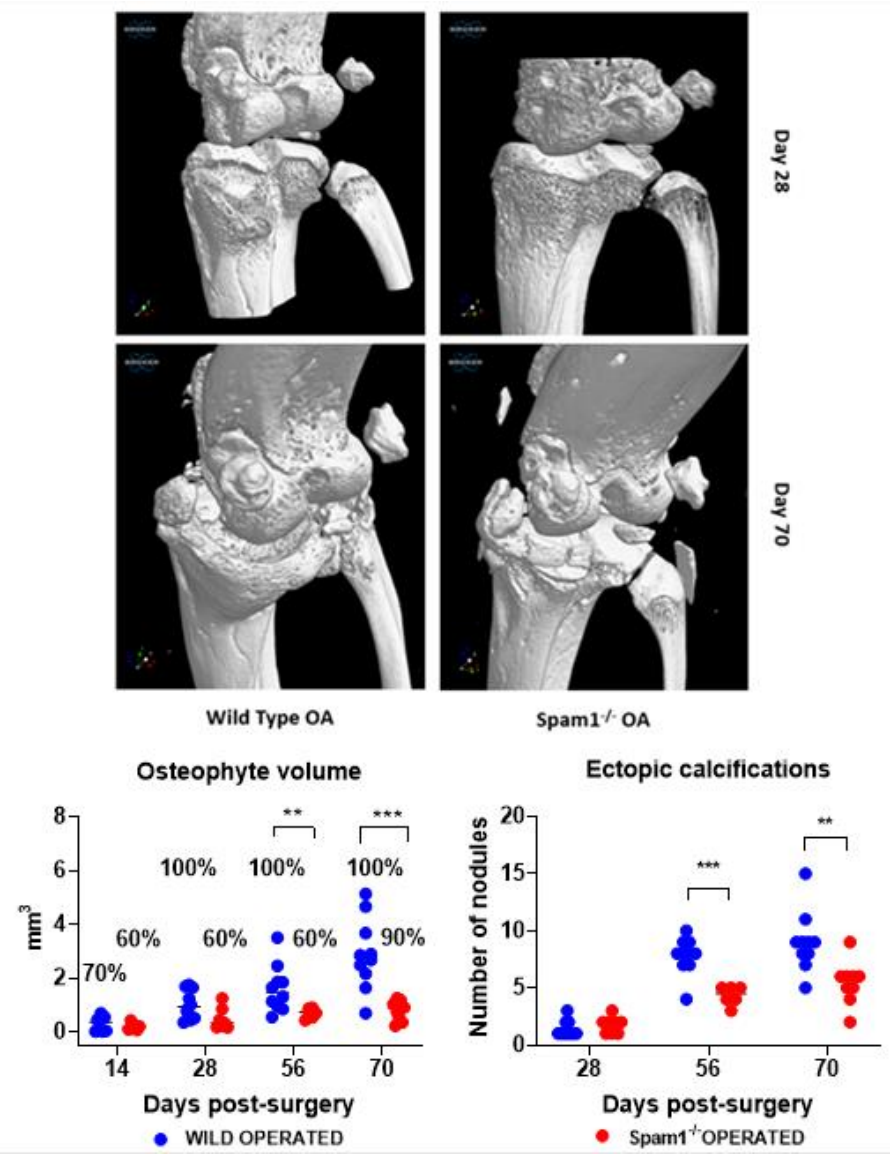

Figure 5. Micro-CT analysis of the right knees of WT OA and Spam1$^{-/-}$ mice. Upper panel: 3D reconstruction (CTvox – Bruker) at days 28 and 70 post-surgery. Posteromedial view. Lower panels. Left: Osteophyte volume (mm³) and incidence (%) at different experimental time points post-surgery. Right: Number of ectopic calcifications at different experimental times. **: p<0.05; ***: p<0.01. N = ten mice per group and experimental day.

2.6. Immunohistochemistry [IHC] of matrix enzymes

Figure 6 [panels A] illustrates the chromogenic staining for Mmp-13 in histological slices of cartilage sampled from operated [OA] WT and Spam1$^{-/-}$ knees. As Mmp-13 plays a significant role in the degradation of cartilage collagen during the early stages of OA (281, 282), it is worth noting that the staining for Mmp-13 increased in surface and intensity with time post-surgery in operated [OA] WT cartilage. Interestingly, at each of the five-time points of the study, the strength and expanse on Mmp-13 staining were markedly reduced in Spam1$^{-/-}$ histological slices compared to WT.

The results of semi-quantitative IHC scores given in panels B to E of Figure 6 are in close agreement with the subjective visual scoring of slice staining given above for Mmp-13. At days 0, 14, 28, 56, and 70, the IHC score for HAS2 [panel B] was similar in both WT and Spam1$^{-/-}$ cartilages. Also, as compared to their IHC score for HAS2 on day 0, the WT and Spam1$^{-/-}$ cartilage specimens exhibited a significant decrease in their HAS2 score on day 14 [-54 and -41%, respectively], 28 |-63 and -49%], 56 [-70 and -54%], and 70 [-77 and-62%]. Thus, the expression of HAS2, the most abundant HAS in chondrocyte, collapsed with time post-surgery in both WT and Spam1$^{-/-}$ tibial plateau cartilage.

WT and Spam1$^{-/-}$ cartilages did not differ in their IHC score for Hyal1 [C] on day 0. Likewise, the two cartilages did not differ in their IHC score for Hyal2 [D] on day 0. The IHC score for Hyal1 in WT cartilages became significantly higher compared to Spam1$^{-/-}$ on days 56 [$p = 0.0027$] and 70 [$p<0.0001$]. WT cartilages also had a significantly higher IHC for Hyal2 on days [56; p =

0.0035] and 70 [p<0.0001]. As compared to day 0 values, the HIC score for Hyal1 in WT specimens increased significantly at all time points, i.e., by 200% on day 14, 343% on day 56, and 477% on day 70. In Spam1$^{-/-}$ specimens, a smaller but significant increase in Hyal1 score |+95%] occurred at day 70. As far as Hyal2 is concerned, its IHC score in Spam1$^{-/-}$ cartilages did not change significantly from day 0 to day 70. By contrast, WT cartilage exhibited a significant gain in their HIC score for Hyal2 |+85%] at day 70.

At baseline, WT and Spam1$^{-/-}$ cartilages had a similar IHC score for Mmp-13. The score raised in all operated mice but at a different pace. In WT specimens, the expression of Mmp-13 bursted [+878%] as early as on day 14 and kept climbing by 2271% on day 56 and 1720% by day 70. We had a lower positive slope for Mmp-13 expression in Spam1$^{-/-}$ specimens. As compared to day 0 values, the IHC score increased by 212% on day 14, 440% on day 28, 510% on day 56, and 623% on day 70. Thus, the expression level of Mmp-13 had increased by 18-24 times in [OA] WT cartilages, and only by 6-7 times in [OA] Spam1$^{-/-}$ specimens.

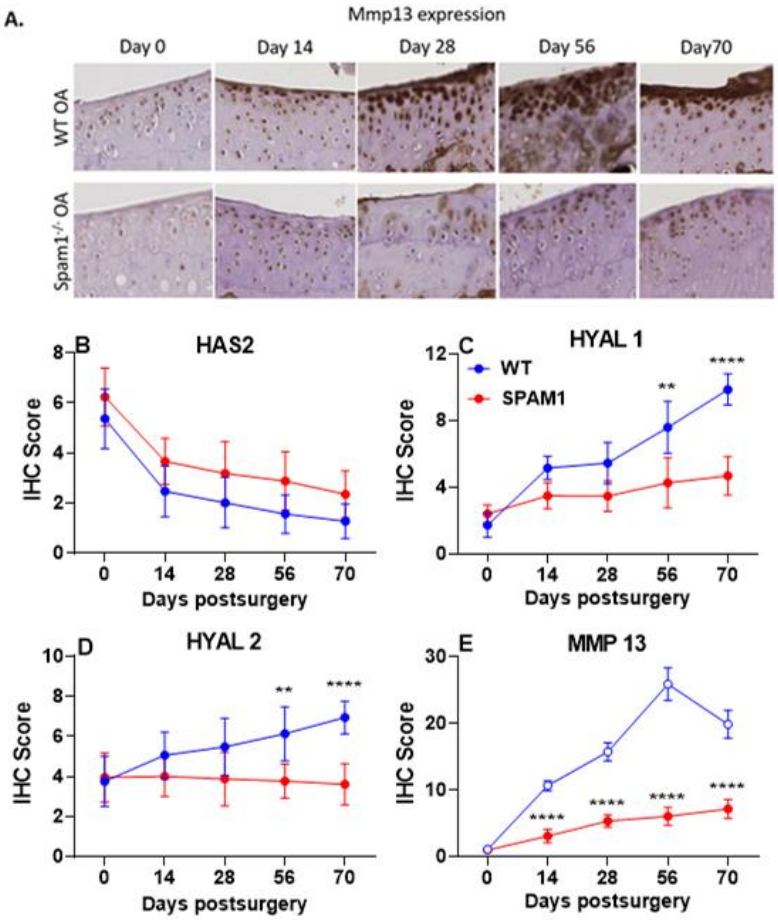

Figure 6. Immunohistochemistry of ECM enzymes in the cartilage of the medial tibial plateau from operated WT mice [closed blue circles] and operated Spam1$^{-/-}$ mice [closed red circles]

A. Two upper panels: chromogenic immunohistochemistry (IHC) staining of Mmp-13 in cartilage sections sampled from the knees of WT mice [top row] and Spam1$^{-/-}$ mice [lower row] at day 0, day 14, day 28, day 56, and day 70 after surgery. The higher the brown color, the higher the tissue content in Mmp-13

Lower panels: Evolution of immunoreactive score (IRS) for Hyaluronan synthase 2 |HAS2; B], hyaluronidase 1 [Hyal1; C], hyaluronidase 2 [Hyal2; D] and Mmp-13 (E) with time post-surgery. In cartilage from operated WT and Spam1$^{-/-}$ knees. The IRS represents [the ratio of the positive staining area to the total tissue area] *100. N = ten mice per group for each genotype and at each time point of the study. We express the results as Mean [95% confidence interval]. [95% confidence interval]. We give the p-value between WT and Spam1$^{-/-}$ specimens at the same time point. ** = p< 0.01; **** = p<0.0001

3. Discussion

The results presented herein indicate that inactivation of Spam1/PH-20 reduces the development of OA lesions markedly in the knee cartilage and subchondral bone in a model of severe OA utilizing surgical instability (283). On day 70 post-surgery, the Mankin histologic-histochemical OA score in operated Spam1$^{-/-}$ knees was mild to moderate at 6.5/14 and contrasted with the severe rating of 13.4/14 observed in operated WT knees. As compared to OA WT chondrocytes, Spam1$^{-/-}$ chondrocytes expressed 3 to 4 times fewer Mmp-13 as well as two times less Hyal1 and Hyal2. Also, the postsurgical defects in subchondral bone microarchitecture were worse in WT tibial plateaus than in Spam1$^{-/-}$. Yet, we had raised the challenge by combining risk factors of murine OA. We indeed chose CD1 mice known to have a more severe aging-associated spontaneous OA compared to other usual laboratory strains (284). We also included male mice that develop more severe OA than females (285). Besides, we enhanced the maximum loading and malalignment of the knee joint by combining two surgical instability procedures, namely the anterior cruciate ligament transection [ACLT] and a destabilization of the medial meniscus [DMM] (283). Both processes produce lesions primarily on the central weight-bearing region of the medial tibial plateau and medial femoral condyle. The posterior drawer caused by ACLT also causes injuries in the posterior aspect of the tibial plateau.

Spam1$^{-/-}$ mice do not exhibit overt specific morphological characters for up to 52 weeks of age (280). We noted a 7% reduction in their tibial plateau

BMD that amounted to 7% at 30 weeks of age and 12% at 52 weeks of age. The knee cartilage of 52-week-old specimens also exhibited a Mean ± SD Mankin histologic-histochemical OA score of 3.2 ± 0.9 that contrasted significantly with the score 5.6 ± 1.1 in WT [$p < 0.001$] found in control WT specimens of the same age. This observation suggests that silencing Spam1 might have a protective role for cartilage in health and disease. As expected, Spam1$^{-/-}$ litters were smaller than regular ones with four pups versus thirteen pups in control WT. Though Spam1 assists in sperm penetration through the HA-rich cumulus oophorus surrounding the oocyte (90), rodents partly overcome their lack of Spam1 by expressing two additional neutral active sperm Hyals, namely Hyal5 and Hyalp1 (272, 273, 286).

The phenotypic effects of silencing other Hyals was explored. The defect in Hyal1 results in mucopolysaccharidosis IX, a lysosomal storage disorder. Hyal1$^{-/-}$ chondrocytes display intense pericellular and cytoplasmic HA staining leading to early osteoarthritis (62). We do not detect any elevation of HA in Hyal1$^{-/-}$ serum and non-skeletal tissues. By contrast, murine Hyal2 deficiency results in enhanced serum HA levels and severe cardiopulmonary dysfunction (74). Hyal3 deficient mice are viable and fertile, with no accumulation of HA in tissues and body fluids (63, 77). However, its overexpression in cultured kidney cells increased Hyal1 activity, suggesting a role for Hyal3 in HA metabolism (63, 287).

Maintaining normal HA levels within the cartilage matrix is essential for the structure and function of the articular tissue. For instance, OA and disuse articular cartilage both have a marked depletion in their aggrecan content

and enhanced amounts of aggrecan-degrading enzymes (288). Still, the two tissues differ in their HA content that is normal in disuse and reduced in OA, a difference that may account for the reversibility of disuse and the apparent irreversibility of OA.

The degradation of HA within cartilage may differ between the pericellular matrix and the interterritorial matrix further remote from the cells (22). In the pericellular matrix, HA free of aggrecan or aggrecan G1 domains bound to HA can be internalized via CD44 (65, 67). Csoka et al. proposed a model for HA degradation that suggests co-ordination between Hyal1 and Hyal2 activities (56). Within this model, Hyal2 bound to a cell surface receptor such as CD44 initiate HA degradation extracellularly to generate 20 kDa fragments that are then internalized by receptor-mediated endocytosis and transported to lysosomes (63). Once inside the lysosome, further degradation takes place through the action of acid-active Hyal1 and exoglycosidases. The delivery of HA to lysosomes by CD44 mediated endocytosis is well documented for cartilage (67). This model might contribute to explain why the conditional knockdown of Hyal2 in mice causes OA by enhancing the cartilage and pericellular content in HA, as observed in Hyal1$^{-/-}$ mice (60).

By contrast, chondrocytes cannot internalize high MM intact aggrecan-HA complexes before enzymatic cleavage. Also, cartilage is pluricellular, and the HA molecules present in the inter-territorial matrix far from the cell might escape endocytosis. Studies provide convincing evidence for extracellular degradation of HA in cartilage (31, 259, 276). For instance,

catabolic stimuli of cartilage explants induce the simultaneous release of HA, Link protein, and aggrecan G1 fragments into conditioned media (as reviewed by Bastow (31)). Also, pulse-chase labelling studies revealed that one-fourth of the pulse labelled HA escaped into the medium the first day of the chase with no further release at later times (277). Also, the average size of the tissue labeled HA was higher than that of the resident unlabeled HA at early chase times but decreased toward the size of the resident unlabeled HA with a half-life of 1-2 weeks.

Spam1 or PH-20 is a likely candidate for the degradation of HA in cartilage ECM. The enzyme is active in the pH range 4-8. Chondrocytes, synoviocytes, dermal fibroblasts, and chondrosarcoma cells all produce the protein (64), and catabolic agents, such as IL-1, up-regulates their production. As the pro-inflammatory cytokines also up-regulate the expression of the CD44 receptor by chondrocytes, Spam1 activity within cartilage might reduce the size of aggrecan aggregates, and thereby facilitates their chondrocyte endocytosis. Also, by degrading randomly high MM HA, Spam1 to produce HA fragments of different sizes and even tetrasaccharides. By contrast to high MM HA that has anabolic effects, HA molecules of smaller formats have significant catabolic effects. They are potent mediators of inflammation and favor angiogenesis (260, 261). HA fragments of < 8000Da, but not high MM HA, induce osteoclastic bone resorption (289). Thus, the Spam1-mediated production of small MM HA molecules after surgery might contribute to explain the transitory loss in subchondral bone BMD in WT mice during the first postsurgical week. Spam1-mediated degradation of HA did not occur in

Spam1$^{-/-}$ mice and exogeneous High MM HA has an anti-osteoclastogenic effect via Toll-like receptor-4 (290).

Hyaluronan fragments induce the transcription and expression of several metalloproteinases [MMPs], including Mmp-13 (291), the critical degrading enzyme of the cartilage collagen network. Excessive degradation of this network is believed to be the point of no return during the OA disease process. It is worth noting that Spam1 silencing was associated with the down production by chondrocytes of fibrillar collagen degrading collagenases (292), matrix metalloproteinase (MMP)-13 (293), leading to the loss of cartilage matrix, The excessive proteolysis of the fibrillar collagen component of the matrix is closely associated with hypertrophic differentiation of chondrocytes (294).

In conclusion, this study demonstrated that the absence of Spam1 was associated with a significant decrease in the levels of cartilage and subchondral bone defects following joint surgical instability. The mouse model provides a promising tool to investigate the physiopathology of post-traumatic OA. Our data also suggest that Spam1 might be a promising target for the treatment and prevention of OA.

4. Methods

4.1. Animals

Spermatozoids with inactivated SPAM1 were bought from the RIKEN research institution (Tokyo, Japan) and used to generate Spam1$^{-/-}$ CD1 mice in our institution. Janvier laboratories [53940 Le Genest-Saint-Isle, France] provided Wild [WT] type CD1 mice. We performed weaning at four weeks. The genotype of the mice was monitored by PCR amplifying the purified genomic DNA from tail cut samples. According to RIKEN, we used the primers: MHA3: TTGAAGTCCAATCGACAAGCT; MHA3: GGTATTCAGAGGTACGATCAG; IL3NEO: TGATCTGGACGAAGAGCATCA.

4.2. Surgical procedures

As sex hormones significantly impact the progression of OA following medial meniscus destabilization, with males having more severe OA than females (285), we only included male mice in the study. We randomly distributed 10-week-old male WT and Spam1 mice into three groups per phenotype to get the six following groups: operated [OA] WT, operated [OA] Spam1$^{-/-}$, sham-operated WT, sham-operated Spam1$^{-/-}$, non-operated WT, and non-operated Spam1$^{-/-}$.

We anesthetized mice with the mixture ANESKETIN® - ROMPUN® 2% in physiological saline (4ml/kg) from EUROVET Animal Health [Bladel, Nederlands]. We used a surgical microscope and microsurgical instruments, and we followed the procedure described by Glasson et al. (283). In the operated mice [OA WT and OA Spam1$^{-/-}$], we sectioned the anterior cruciate

ligament, and we remote the medial meniscus. We paid close attention not to injure the articular cartilage and peripheral arteries. In the sham-operated group [sham WT sham and sham Spam1$^{-/-}$], we only performed an incision in the skin, the quadriceps femoris, and the joint capsule of the right knee. Animals of the two control groups [WT and Spam1$^{-/-}$] were free of anesthesia and surgical procedure.

4.3. Peripheral Quantitative Computed Tomography [pQCT]

WT and Spam1$^{-/-}$ mice from the three groups were weighed and euthanized at different times (0, 3, 7, 14, 28, 56, and 70 days; n = 10 per group and per experimental time) after the surgery. The right hindlimb was dissected and stored in 4% neutral Formaldehyde solution (Sigma-Aldrich®).

We scanned each specimen with a pQCT Research SA + (Norland Stratec, Birkenfeld, Germany). We defined the subchondral bone of the medial plateau of the tibia as the region of interest [ROI], and we acquired ten frontal slices, separated from each other by 25µm, and with an in-plane voxel size of 70µm. We assessed BMD according to the manufacturer instructions for the XCT 5.4 software. The value retained for each specimen was the average value calculated from measurements made on. The reproducibility (CV) of BMD measurements was 1-2%.

4.4. Micro-computed tomography [µ-CT]

Immediately after death, the intact tibias were remote and stored in a 4 % neutral Formaldehyde solution (Sigma-Aldrich®) for a maximum of fourteen

days. We scanned specimens with a Microtomograph Skyscan 1275 (Bruker microCT, Kontich, Belgium) equipped with an X-ray tube working at 40kV and 250µA. Knees were wrapped in paper, placed in a plastic container, and fixed with plasticine within the µ-CT to avoid any movement. Analysis settings were: a pixel size of 8µm, an exposure time of 100ms, a rotation step of 0.360°, and using a 360° rotation. The duration of each scan was 14 minutes. The NRecon software [version 1.7.1.2.; Bruker microCT, Kontich, Belgium] performed the reconstructions that were then analyzed by using CTAn software (Bruker microCT) and CT Vox (Bruker microCT). The ROI was designed as the medial part of the proximal epiphysis of the tibia between the growth plate and the calcified cartilage.

According to the ASBMR nomenclature (295), we evaluated the relative bone volume (BV / TV; %), bone mineral density [BMD; mg hydroxyapatite/cm^3], trabecular number |Tb.N; 1/mm], trabecular thickness [Tb.Th; µm], trabecular separation [Tb.Sp; µm], number of ectopic calcifications, and osteophyte volume [mm^3]. The CV of repeated measurements is <2%.

4.5. Histological analysis

After µ-CT processing, we decalcified the right hindlimbs of the WT OA and Spam1$^{-/-}$ OA mice using a quick decalcifier (Osteoral, RALA320715-2500, VWR) for 72hours. We then embedded specimens in paraffin before sectioning (5µm) in the frontal plane. The slices from the middle and the

posterior compartments of the knees were stained using Safranin O and finally mounted on glass plates for Modified Mankin score analysis.

The modified semi-quantitative grading histological scale was graded based on the following items: cartilage structure (0 to 6 points), cartilage cells (0 to 3 points), Safranin-O staining (0 to 4 points) and tidemark integrity (0 to 1 point). Two observers, blinded to the label of the slide, scored each slide independently. A scoring table is available in the paper of Mainil-Varlet et al. (296). We then added the score of each item to get a final score per mouse. We used ten mice per group per time point postsurgery, and we analyzed six slices per animal. Thus, for each group at each time point in Figure 1, each point represents the means of six values, and the mean of the group is the mean of sixty values.

4.6. Immunohistochemistry

We conducted a classical immunohistochemical staining protocol for the knee sections adjacent to those used for the Modified Mankin score. Briefly, the sections were incubated with Proteinase K (1/100 in Tris-EDTA pH 8.0, Roche) during 20min at 37°C to unmask the ECM antigenes. Primary antibodies were: Anti-HYAL1 antibody (Hyaluronidase 1; 1mg/ml; Abcam, ab203293), Anti-HYAL2 antibody (Hyaluronidase 2; 1mg/ml; Abcam, ab68608), Anti-MMP13 antibody (Matrix metalloproteinase 13; 1mg/ml; Abcam, ab39012), Anti-Hyaluronan synthase 2 antibody (1mg/ml; Abcam, ab199794), Anti-ADAMTS5 antibody (A disintegrin and metalloproteinase with thrombospondin motifs 5; 1mg/ml; Abcam, ab41037), Anti-Collagen II

antibody (1mg/ml; Abcam, ab34712), Spam1 Antiserum (Department of Biological Sciences, University of Delaware, Newark, DE19716). We used EnVision+ System – HRP (Dako, Carpinteria, CA, USA) as a secondary antibody and DAB peroxidase substrate kit (Vector – Burlingame, CA, USA) for the revelation. In control sections, we used the second antibody without the primary antibody. The slide scanner Leica SCN400 from Meyer Instruments Inc [Houston, Texas, USA] States of America) analyzed the sections. Two blinded observers evaluated each slide independently. We calculated the immunoreactive score [IRS] as the percentage of positive cells * staining intensity (297), the two parameters being measured by using Leica SCN400.

4.7. Statistics.

We present the results as mean ± 95% confidence interval unless stated otherwise. We used GraphPad Prism version 8.0.0 for Windows, GraphPad Software [San Diego, CA, USA]. Unpaired two-tailed t-test compared the means at the different experimental times. F test compared variances. A p-value < 0.05 was set for statistical significance.

4.8. Study approval.

All animal procedures were performed with prior approval from the ethics committee for animal research of the Université Catholique de Louvain (UCLouvain agreement # 2014/UCL/MD/021). We followed the processes required by the Belgian federal law for the management and care of animals.

The mice were kept under controlled light (light 7 a.m. to 7 p.m., dark 7 p.m. to 7 a.m.), temperature (21 ± 2°C) and humidity (55 ± 10%) conditions. They had free access to water and were fed *ad libitum* on Rodent Laboratory Chow. The use of sevoflurane inhalation euthanized the mice.

CHAPTER THREE: Spam1, a new key for unlocking the pathophysiology of osteoarthritic cartilage degradation? Results of a preliminary study in a model of immature murine articular chondrocytes in primary culture

Sébastien Lafont[1], Mickael Cardinal[1], Thomas Roels[1], Catherine Behets[1], Daniel Manicourt[2]

[1]Pole of Morphology and [2]Pole of Systemic and Inflammatory Rheumatic Diseases – Institut de recherche expérimentale et Clinique - Université Catholique de Louvain, Brussels, Belgium

Manuscript in submission

Conflict of interest statement

The authors have declared that no conflict of interest exists.

1. Abstract

The severity of naturally occurring osteoarthritis [OA] during aging is quite lower in Spam1KO mice compared to wild [WT]. To evaluate the pathophysiological relevance of this *in vivo* observation, we used the *in vitro* model of immature murine articular chondrocytes [IMAC] in primary culture. We cultured chondrocytes and osteoblasts with and without IL-1β+TNF-α, and we explored biochemical, morphological, and functional differences between the two genotypes.

Methods: We characterized the phenotype of chondrocytes and osteoblasts, and we examined several biochemical and functional features such as the levels of enzymes involved in the synthesis and degradation of the extracellular matrix.

Results: Our study highlights that, both, chondrocytes and osteoblasts express Spam1 and that the stimulation by IL-1β and TNF-α enhanced the production of Spam1 by 50-55% in WT chondrocytes and by 45-50% in WT osteoblasts. Chondrocytes of both genotypes exhibited a similar level of synthesis expression for Hyal1, Hyal2, and HAS2. Stimulation of WT cells with IL-1β and TNF-α increased their levels of Hyal1 and Hyal2 and decreased their production of HAS2. Conversely, in Spam1KO cells, the two cytokines did not affect levels of Hyal1 and HAS2 and decreased levels of Hyal2. IL-1β and TNF-α enhanced the synthesis of MMP13 in both genotypes, but levels were 3-4 times lower in Spam1KO cells compared to WT. IL-1β and TNF-α increased the production of the aggrecanase ADAMST5 in WT cells and unaffected levels of ADAMST5 in spam1 cells.

2. Introduction

Hyaluronan [HA] is a linear covalent polymer of disaccharide units of N-acetyl-glucosamine and D-glucuronic acid [β-1,3-GlcNac- β-1,4-GlcA] and its molecular mass [MM] is usually higher than 1 million Da (63, 264, 298). HA, not only hydrates and gives turgor to the tissues, but also has a crucial impact on the structure and function of the extracellular matrix [ECM] at both cellular and tissue levels (63, 251, 252). First, HA interacts with versicans, CD-44, other transmembrane proteins, and hyaladherins to form a specialized matrix around the cells. The pericellular matrix [PM] protects the cells from physical loads, initiates signaling pathways, and regulates the cell phenotype (253, 254). The interactions CD44-HA and Toll-like receptors-HA are essential for tissue homeostasis (254). While high MM HA is anabolic (255-258), low MM HA is catabolic (119, 259, 261). Beyond the PM, HA interacts with many matrix molecules to form the complex extracellular matrix [ECM], which brings physical scaffolding to the cells and initiates biochemical and biomechanical cues for tissue differentiation, growth, and homeostasis (36, 251, 299). In articular cartilage ECM, a single HA molecule binds much viscoelastic aggrecan |AGC] molecules to form AGC aggregates of sufficient size to be firmly entrapped within the collagen network. Aggregation provides compressive resilience and protects the subchondral bone (104, 262).

The balance between HA synthesis and degradation is a prerequisite for the maintenance of matrix structural integrity. Mammalian cells have three HA

synthases, which differ in their rates of synthesis and the average sizes of the resulting HA polymers (42). HAS2 synthesizes very high MM HA [≥ 4 MDa], whereas HAS3 and HAS1 synthesize smaller polydisperse chains with an average MM of 0.8 and 1 MDa, respectively (42, 254). Most somatic cells express hyaluronidases [Hyals] 1, 2, and 3 (56, 63). Hyal1 is an acid-active soluble enzyme, whereas Hyal2 has a broader optimum pH range and is a glycosylphosphatidylinositol-[GPI]-anchored protein at the cell surface and in lysosomes (56). Hyal1 yields tetrasaccharides in contrast to Hyal2 that yields 20 kDa products [50 disaccharides]. Hyal3 is unlikely to play a significant role in HA constitutive degradation as Hyal3-deficient mice are fertile with no HA accumulation (77, 287). Hyal4 is a GPI-anchored chondroitin sulfate-specific hydrolase lacking hyaluronidase [Hyal] activity (278).

Initially discovered in sperm and since found in kidneys, placenta, and cancer cell lines, Spam1 is a GPI-anchored Hyal active at both acid and neutral pH that enables the sperm to penetrate the HA-rich cumulus oophorus surrounding the oocyte (56, 81, 82). Dermal fibroblasts, synoviocytes, and chondrocytes also express Spam1 and up-regulate its production upon stimulation with IL-1 (64). Spam1 is the most active mammalian sperm Hyal and can degrade HA molecules of any size into tetrasaccharides (286). In pigs and humans, Spam1 alone can disperse the oocyte-cumulus complex (300). Mice express Hyal5 and Hyalp1, two additional neutral-active Hyals, that cooperate with Spam1 to degrade the HA-rich cumulus oophorus (272-274, 286).

Fully differentiated chondrocytes account for the homeostasis of healthy adult cartilage. By contrast, in osteoarthritis [OA], the most common joint disease, chondrocytes exhibit phenotypic instability and shift toward a degenerative and hypertrophy-like state involving abnormal matrix production and increased activities of aggrecan- and collagen-degrading enzymes (241, 301, 302). IL-1 and TNF-α are the predominant pro-inflammatory cytokines involved in disease initiation and progression. As chondrocytes up-regulate their expression of Spam1 upon stimulation of Il-1β (64) and as IL-1 and TNF-α are involved in OA disease initiation and progression (241), we hypothesized that the enhanced production of Spam1 could contribute to the apparent irreversibility of the OA. Cartilage specimens indeed exhibit a reduced content in HA whether incubated with IL-1α (303), sampled at the time of orthopedic prosthesis (304), or obtained from canine knees after ACLT (263, 305). There must be an increase in the rate of HA degradation, as compared to healthy controls, sampled OA specimens exhibit an increased rate of HA biosynthesis (269, 306). Although free radicals also degrade HA (270), this point is worth investigating since the cleavage of HA molecules destroys AGC aggregates and jeopardizes cartilage tissue strength

To test our hypothesis, we used the model of immature murine articular chondrocyte [IMAC] in primary culture (307). Cells were isolated from the knee joint of healthy newborn WT mice and Spam1KO newborn mice, and we evaluated the effects of the catabolic cytokines IL-1 and TNF-α on the expression of parameters of HA metabolism and cartilage matrix

remodeling. Knockout mice indeed display the consequence of their inactivated gene on the structure and function of body tissues, and functional and molecular parameters can be measured readily in mice (307). Data suggest that Spam1 activity might be an essential player in the control of cartilage matrix turnover.

3. Materials and methods

3.1. Subjects

We conducted this prospective study with prior approval from the Université Catholique de Louvain Committee for Animal Resources (UCLouvain agreement # 2014/UCL/MD/021 and 2020/UCL/MD/01). Subjects were healthy WT PH-20/Spam1($^{+/+}$) CD1mice [Janvier laboratories, Le Genest-Saint-Isle, France], and PH-20/Spam1($^{-/-}$) null [knockout, KO] mice maintained on a CD1 background. We applied the Best Practice Guidelines for mouse experimentation (308, 309), and we reduced the number of mice used per experiment for as long as the cohort sizes provided sufficient statistical power. As the habitat, husbandry conditions, and animal microbiome may impact experimental results (309, 310), we housed the mice used herein in the same room. All mice also had the same husbandry conditions as controlled light (light 7 a.m. to 7 p.m., dark 7 p.m. to 7 a.m.), temperature (21 ± 2°C), and humidity (55 ± 10%). They had free access to water and were fed *ad libitum* on Rodent Laboratory Chow.

3.2. Generation of PH-20/Spam1 KO mice

The Riken BRC provided mouse sperm lacking hyaluronidase PH-20 through the National Bio-Resource Project of the MEXT, Japan. ICR; 129S2-Spam1<tm1Tba> mice are sperm donors. They carry a disruptive null mutation in their PH-20 gene, a neomycin-resistance expression cassette (E. coli) replacing a part of exon two that codes for the hyaluronidase domain of the enzyme (311). We directly added the PH-20 KO sperm to the oviduct of WT CD1 females after breeding with a sterilized male. Because hyaluronidase-5, but not PH-20, is the sperm enzyme critical for degrading the hyaluronan coat surrounding the eggs (273, 311), the inseminated CD1 females became pregnant and gave birth to heterozygous PH-20/Spam1(+/-) mice. By crossing the PH-20 (+/-) heterozygotes to each other, we generated mice harboring either two WT PH-20 alleles ([PH+20(+/+)], two null mutated PH-20 alleles [PH-20(-/-)], or one WT PH-20(+) allele plus one null mutated PH-20(-) allele. The WT and PH-20 null-mutated KO alleles were identified by PCR amplification of tail genomic DNA using MHA3 (5'-TTGAAGTCCAATCGACAAG-CT-3'), MHA16 (5'-GGTATTCAGAGGTACGATCAG-3'), and IL3 NEO (5'-TGATCTGGACGAAGAGC-ATCA-3') as primers. PAGE analyzed the amplified DNA products. DNA fragments with a 500 bp size originated from the KO allele and those with a 145 bp size from the WT allele.

3.3. Isolation, culture, and phenotyping of immature articular chondrocytes

As the small cartilage explants were relatively scarce, challenging to handle, and to aliquot in similar amounts in culture dishes, we opted for cell cultures. We followed the procedure reported by Salvat et al. (2005) to obtain immature murine articular chondrocytes [IMAC] (307). Five-day-old neonatal WT and Spam1KO mice were euthanized by decapitation. The body was placed in the face-down position to ease the removal of the skin and soft tissues. We isolated the femoral heads, femoral condyles, and tibial plateaus before sampling articular cartilage specimens that were, as far as possible, cleaned off soft tissues such as menisci, ligaments, and intra-articular fat. We then incubated cartilage specimens at 37°C and 5% CO2 with collagenase D [3mg/ml] for two rounds of one hour each. The reaction buffer was Dulbecco's Modified Eagle's Medium supplemented with 2mM L-Glutamine, 0.01ml/ml penicillin, and 5,000U/ml streptomycin. After each of the two incubation rounds, the cartilage tissue specimens were agitated to detach soft tissues from the cartilage pieces. When all soft tissues were released free of cartilage into the culture medium, we incubated the cartilage specimens with collagenase D [3mg/ml] for a third-round overnight at 37°C and 5% CO2. The isolated chondrocytes were filtered through a sterile 70-µm nylon mesh before centrifugation for 10 min at 1500rpm. The cells were then suspended in a 5ml culture medium supplemented with 10% FBS and counted. We obtained an average of 1.10^6 chondrocytes per mouse, whatever its genotype.

We seeded IMACs on a culture plate at a density of 8 x 10^3 cells/cm^2, and cells reached confluence by day 7 [Stage P0]. Cells were then subcultured on new culture dishes to reach confluence at 6-8 days later. It is at this stage, termed P1, that we characterized the phenotype and functions of IMACs. For immunofluorescence, cells were fixed in 4% paraformaldehyde before incubating with the primary antibody. For Alcian blue staining, cells were fixed in 4% glutaraldehyde for 15 min and washed in 0.1N HCl before staining with 1% Alcian blue.

At the end of experiments conducted with pro-inflammatory cytokines, stimulated and unstimulated cells were first rinsed in PBS before lysis using radioimmunoprecipitation assay (RIPA) buffer. We then stored lyzed specimens at -80°C until western blotting. Protein concentration was measured using the BCA Protein Assay kit (Millipore).

3.4. Isolation and culture of osteoblasts

We isolated primary osteoblasts from adult mouse long bones following previously described procedures (312, 313). Each cellular preparation required either 3 WT mice or 3 Spam1KO mice. Humeri, femurs, and tibias are collected and trimmed of muscles and soft tissues. We cut diaphyses into pieces of approximately two mm^3, and we washed the bone pieces several times with PBS to remove bone marrow. We then incubate the diaphyseal pieces with collagenase II in DMEM [2mg collagenase II par ml DMEM] for two hours at 37°C in a shaking water bath.

At the end of incubation, we rinse diaphyseal bone pieces three times in the sDMEM culture medium supplemented with 10% FBS, 0.01ml/ml penicillin, and 5,000U/ml streptomycin before transferring them in 25cm² flasks containing 6ml of culture medium. The culture medium is changed every three days for 15-18 days. When cells are confluent [stage P0], we remove bone pieces and pass the cells to T75 flasks containing DMEM. The culture medium is changed every three days, and cells reached subconfluency after 9 to 12 days [stage P1]. As reported by Taylor (2014), osteoblasts deposit a collagen matrix that becomes mineralized after about two weeks (313). We fix osteoblast layers with 2.5% glutaraldehyde for alizarin red staining to detect calcium. Osteoblast layers are fixed with 70% ethanol before collagen staining with Sirius red. Alkaline phosphatase activity is detected using the AP staining kit from System Biosciences (Palo Alto, Ca, USA).

We conduct the functional characterization of osteoblasts when cells are confluent at the stage P1. We herein only report the changes in Spam1 production upon stimulation of osteoblasts with the pro-inflammatory cytokines IL-1β and TNF-α for 24 and 48 hours. Before cytokine stimulation, we starve the osteoblasts for 24 hours (culture medium without FBS). During stimulation, we change every 24 hours the culture medium containing IL-1β and TNF-α [10 ng/ml, each] and lacking FBS. At the end of stimulation, cells are rinsed with sterile phosphate-buffered saline (PBS), lysed with radioimmunoprecipitation assay (RIPA) buffer, and stored at -80°C until western blotting. We assess protein concentrations using the Bicinchoninic

Acid Protein Assay Kit from Pierce. We set the cytokine concentration at 10 ng/ml after pilot studies documenting a reproducible and robust cell response in terms of PGE2 and NO2 release in cell supernatants as previously reported (307). Studies have used similar concentrations (259).

3.5. Immunoblot Analysis-Western Blotting

Chondrocytes were suspended in RIPA lysis buffer. BCA Protein Assay kit (Millipore) assessed the protein concentration of each sample according to the manufacturer's protocol. We loaded ten μg of proteins per well, and the samples migrated under a voltage of 120V. After migration, proteins were transferred onto a nitrocellulose membrane with a constant amperage of 350 mA for 90 minutes. We then incubated the membranes in a TBS-Tween blocking solution containing 5% BSA for one hour at room temperature before incubating the membrane overnight at 4°C in TBS-Tween buffer containing 5% BSA and a primary antibody.

We used the following primary antibodies: anti-HYAL1 (Hyaluronidase 1; 1mg/ml; Abcam, ab203293); anti-HYAL2 (Hyaluronidase 2; 1mg/ml; Abcam, ab68608); anti-MMP13 (Matrix MetalloProteinase 13; 1mg/ml; Abcam, ab39012); anti-Hyaluronan synthase 2 (1mg/ml; Abcam, ab199794); anti-ADAMTS-5 (A Disintegrin And Metalloproteinase with Thrombospondin motifs 5; 1mg/ml; Abcam, ab41037); anti-Collagen I (1mg/ml; Abcam, ab34710); anti-Collagen II (1mg/ml; Abcam, ab34712); and a Spam1 antiserum, generous gift of the Department of Biological Sciences, University of Delaware, Newark, DE19716.

Membranes were washed in TBS-Tween and incubated with the peroxidase-conjugated antibody for 60 minutes at room temperature. Membranes were developed by enhanced chemiluminescence (ECL, Amersham) on CL-Xposure films (Thermo Scientific). We scanned films and semi-quantified protein bands by densitometry using ImageJ software (National Institutes of Health). Levels of proteins of interest were normalized to the values of glyceraldehyde-3-phosphate dehydrogenase [GAPDH], a housekeeping protein. We used the levels of total proteins to normalize the levels of phosphorylated proteins.

3.6. Immunofluorescence

We fixed plated cells using 4% paraformaldehyde for 10 min at room temperature. Then, we flushed cells three times with PBS for 3 min, and one time with PBS containing 0.1% saponin for 3 min, and one time with PBS containing 0.1% saponin and 5% BSA for one hour at room temperature. Then after, we incubated the cells overnight at 4°C with the primary antibody diluted in PBS containing 0.1% saponin and 1% BSA. Cells were then flushed three times for 3 min in PBS containing 0.1% saponin before incubating them for 1 hour at room temperature with the secondary antibody diluted in PBS containing 0.1% saponin and 1% BSA. After the incubation, we flushed the cells with PBS containing 0.1% saponin. We then incubated the cells for 5 min at room temperature with DAPI [1/10.000 in PBS]. After the last flush with PBS, we mounted cells on histological slides.

3.7. Statistics

Data are expressed as mean ± SD unless stated otherwise and were analyzed using GraphPad Prism version 8.0 for Windows, GraphPad Software, San Diego, California USA, www.graphpad.com. ANOVA with post-test Tukey compared means at the different experimental times. We used the F test to compare variances. A p-value < 0.05 was set for statistical significance.

4. Results

4.1. Cells isolated from cartilage have a chondrocyte phenotype

The immature murine articular chondrocytes [IMACs] were isolated from the hip and knee cartilage of both 5-day-old healthy WT mice and PH-20-Spam1KO mice. The cells plated on culture dishes at stage P1 exhibited the rounded morphology of chondrocytes. Previous works report that articular chondrocytes rapidly lose their differentiated phenotype upon prolonged monolayer culturing on plastic and repeated passages (312, 314, 315). The dedifferentiation occurs with the loss of type II collagen and aggrecan synthesis and the production of type I collagen. Thus, we used Alcian blue staining and immunofluorescence with anti-collagen antibodies to characterize the phenotype of WT and Spam1KO IMACs. Alcian blue stained their intercellular matrix, demonstrating the presence of proteoglycans. Immunohistochemistry revealed highly expressed type II collagen in both Spam1KO and WT cells [Figure 1, upper panel, C & D]. By contrast,

immunoreactivity for type I collagen was exceedingly scarce in cells whose genotype was either WT or Spam1KO [upper panels, A & B].

Earlier work shows that the negative impact of IL-1β on type II collagen expression and the positive impact of IL-1β on inducible nitric oxide synthetase [iNOS] depend upon the expression of the differentiated chondrocyte phenotype (301, 316). Therefore, to assess the functional integrity of primary cells (307), we evaluated their ability to enhance iNOS synthesis and to reduce their production of type II collagen in the presence of IL-1β and TNF-α [10 ng/ml each]. After 24 hours of culture and as compared to primary cells incubated without cytokines, the ratio of iNOS protein to GAPDH increased seven times with IL-1β, three times with TNF-α, and thirteen with IL-1β plus TNF-α. Further, incubation with IL-1β and TNFα for 24 hours reduced the production of type II collagen by 67% in WT cells and by 50% in Spam1-KO cells [p =0.0045; Figure 1, lower panel]. The decrease became higher after 48 hours, with -96% for WT cells and -90% for Spam1-KO cells [p =0.0004]. Thus, the negative impact of IL-1β and TNF-α on type II collagen production was observed in both genotypes but was more substantial in WT IMACs than in Spam1KO IMACs. The WT and Spam1KO IMACs at stage P1 had kept their differentiated phenotype. Therefore, IMACs were well-suited to assessing the impact of Spam1 loss on chondrocyte metabolism.

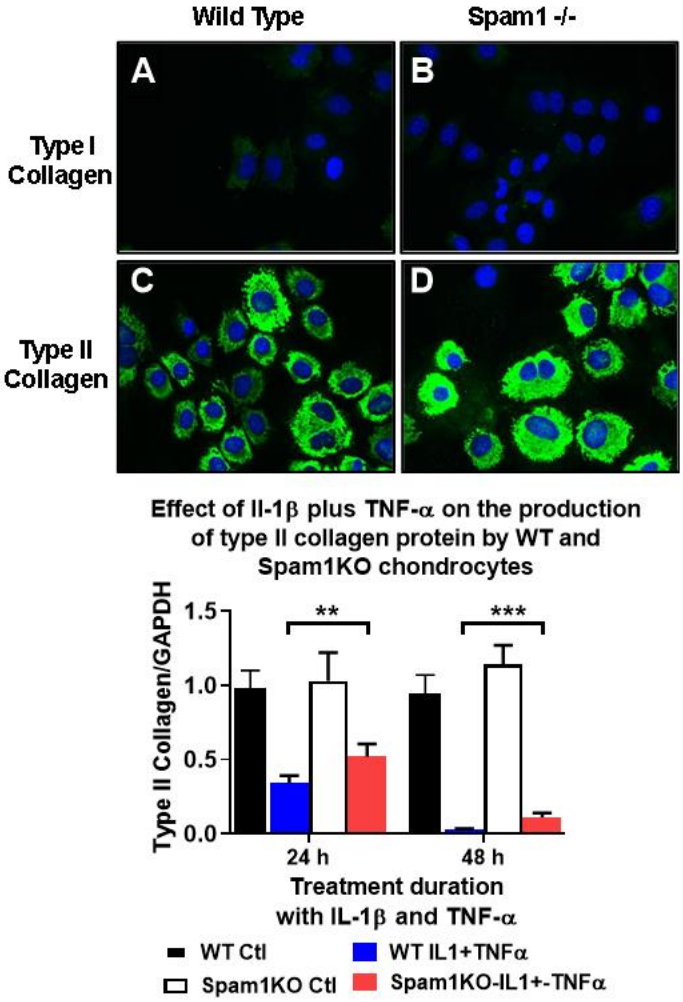

Figure 1. The phenotype of primary chondrocytes

Upper panel. Immunostaining [green] with an anti-type I collagen antibody [A & B] and an anti-type II collagen antibody [C & D] of stage P1 cells harvested from the articular cartilage of 5-days-old WT [A & C] and Spam1KO [B & D] mice. In A & B, the expression of type I collagen is scarce. In C & D, there is a marked expression of type II collagen [intense green color].

Lower panel. WT and Spam1KO cartilage cells were incubated with IL-1β plus TNF-α [10 ng/ml, each] for 24 and 48 hours. Immunoblots evaluated type II collagen and glyceraldehyde-3-phosphate dehydrogenase [GAPDH] protein levels of cell lysates. **: $p<0.01$; ***: $p<0.0001$ by ANOVA. Genotype accounted for 88% of the total variance.

4.2. Cells isolated from long bone diaphysis have an osteoblast phenotype

Immature cells isolated from the diaphysis of long bones and cultured on plastic are likely osteoblastic. They have an ovoidal shape and form a matrix stained with Picrosirius red and thus containing fibril-forming collagen type I and type III, two major structural components of the bone matrix (317). Cells can calcify the bone matrix as it becomes stained with alizarin red to demonstrate the presence of calcium.

As Spam1 and chondrocytes are the main topics of this paper, the functional phenotype of immature osteoblasts was limited to their production of the protein Spam1.

4.3. Pro-inflammatory cytokines and Spam1 production by immature chondrocytes and osteoblasts.

In an earlier study, we showed that IL-1β enhanced Spam1 synthesis in human chondrosarcoma cells and mature human chondrocytes at the P2 -3 stages (64). In the present study, we examined the ability of immature murine WT articular chondrocytes and WT osteoblasts at the P1 stage to produce Spam1 in response to stimulation with IL-1β and TNF-α. We incubated cells with or without IL-1β and TNF-α (10 ng/ml each) for 24 and 48 hours, and we measured the expression of Spam1 protein [Figure 2]. Immunoblots of cell lysates revealed a specific signal for Spam1 in the protein preparations from unstimulated WT chondrocytes and WT

osteoblasts at 24 hours. In the presence of IL-1β and TNF-α, WT chondrocytes enhanced the expression of Spam1 by 52% at 24 hours and by 55% at 48 hours [1.52 ± 0.14 and 1.55 ± 0.25, respectively; $p < 0.001$ each]. Cytokine-stimulated WT osteoblasts also increased Spam1 synthesis by 24% after 24 hours [1.24 ± 0.22; $p = 0.0106$] and by 46% after 48 hours [1.46 ± 0.19; $p<0.0001$]. Levels obtained at 48 hours were higher than those obtained at 24 hours [$p=0.0368$].

The amount of Spam1 detected in Spam1KO cells was less than 5% that found in WT cells [Figure 2]. The addition of IL-1β and TNF-α to Spam1KO cell cultures did not induce Spam1 expression in both Spam1KO immature chondrocytes and osteoblasts.

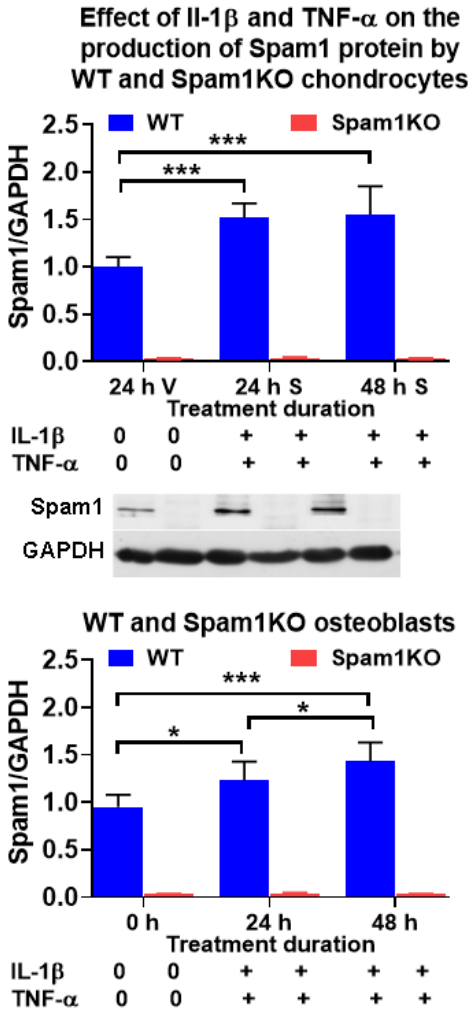

Figure 2. Production of Spam1 by primary chondrocytes and osteoblasts

Primary articular cartilage chondrocytes [stage P1] and primary osteoblasts [stage P1] isolated from WT [blue columns] and Spam1KO [red columns] mice were cultured with [+] or without [0] 10 ng/ml IL-1β and TNF-α [10 ng/ml each] for 24 and 48 hours. Immunoblots evaluated Spam1 and glyceraldehyde-3-phosphate dehydrogenase [GAPDH] protein levels [representative image between the 2 bar graphs]. In Spam1KO cells, levels of Spam1 were scarce, and IL-1β and TNF-α did not affect Spam1 production in both chondrocytes and osteoblasts. By contrast, in WT chondrocytes, IL-1β and TNF-α increased Spam1 production by 52% at 24 hours, and by 55% at 48 hours. In WT osteoblasts, the two cytokines enhanced Spam1 production by 24% at 24 hours, and by 46% at 48 hours. *: $p<0.05$; **: $p<0.01$; ***: $p<0.001$ by ANOVA. Genotype accounted for 91% of the total variance.

4.4. Immature murine articular chondrocytes and other hyaluronidases

Mature murine, bovine, and human chondrocytes produce the hyaluronidases [Hyals] Hyal1, Hyal2, and Hyal3 (31, 63, 254). The three Hyals share several structural parameters with Spam1. They all have uniform amino acid lengths and exhibit a conserved domain representing 63-75% of their amino acids. Also, Spam1 and Hyal2 have a glycosylphosphatidylinositol [GPI] membrane attachment site. These similar features prompted us to test whether immature WT and Spam1KO chondrocytes produce the three Hyals in the presence and absence of pro-inflammatory cytokines and Spam1.

We first measured the expression of Hyal1 proteins. Immunostaining detected Hyal1 in both WT and Spam1KO chondrocytes at 48 hours [Figure 3 upper left panel]. Immunoblots also revealed its signal at both 24 and 48 hours [Figure 3 upper right panel]. IL-1β and TNF-α increased the Hyal1 protein levels of WT cells by 61% at 24 hours and by 69% at 48 hours [$p<0.001$ each]. In contrast, after IL-1β and TNF-α exposure, there was no change in the Hyal1 protein content of Spam1KO cells.

Next, we assessed the expression of Hyal2 protein. Immunofluorescence was positive for Hyal2 in both cell lines after a 48 hours culture [Figure 3 middle left panel].

Earlier, at 24 hours, there was no difference in Hyal2 protein levels between WT and Spam1KO cells, whether incubated with cytokines or the vehicle. Further, after 48-hour incubation with IL-1β and TNF-α, the protein levels of

Hyal 2 were increased by 34% in WT cells [p=0.035] and decreased by 34% in Spam1KO cells [p=0.05].

Whether vehicle-treated or cytokine-treated, WT and Spam1KO chondrocytes did not differ in their expression of Hyal3 at both 24 and 48 hours [Not shown].

4.5. Immature murine articular chondrocytes and hyaluronan synthase 2 [HAS2]

There are three related but distinct forms of hyaluronan synthases [HAS1, HAS2, and HAS3]. They all synthesize HA molecules, but of different sizes and at different rates. Mature bovine chondrocytes cultured in monolayers express mRNA for HAS2 and HAS3. By contrast, monolayer cultures of immature bovine chondrocytes display HAS2 mRNA but virtually no mRNA for both HAS1 and HAS3 (318). Thus, herein, we investigated only the expression of HAS2 in monolayer cultures of immature chondrocytes isolated from WT and Spam1KO mice. Also, as compared to other HAS, HAS2 synthesizes the most massive HA molecules and plays an essential role in producing HA necessary for the organization and retention of the pericellular matrix (31, 45, 104).

As shown in Figure 3, lower panel, the incubation of immature WT and Spam1KO cells with IL-1β and TNF-α decreased the production of HAS2 protein levels in WT cells by 42% at 24 hours [p<0.0001] and by 40% at 48 hours [p=0.0002]. Conversely, the two cytokines did not change the expression of HAS2 in Spam1KO cells significantly [Figure 3, lower panel].

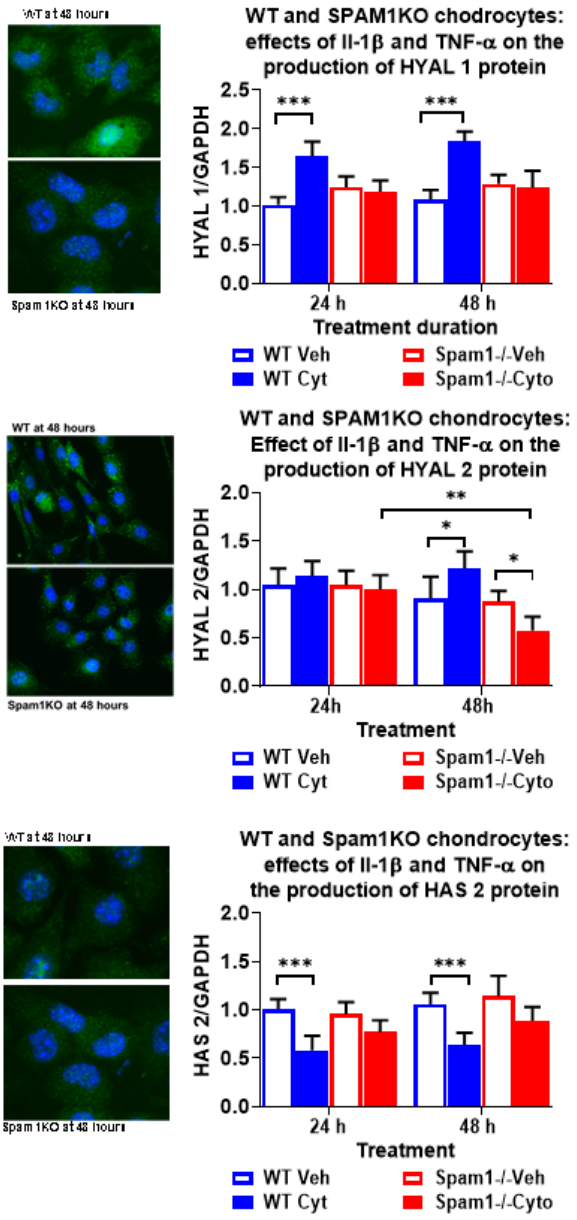

Figure 3. Primary articular chondrocytes and production of Hyal1, Hyal2, and HAS2
Primary articular cartilage chondrocytes [stage P1] isolated from WT [open and closed blue columns] and Spam1KO [open and closed red columns] mice were cultured without [Veh]

or with [Cyt] 10 ng/ml IL-1β and TNF-α [10 ng/ml each] for 24 and 48 hours. We evaluated protein levels of Hyal1, Hyal2, and HAS2 by immunoblots. Levels of glyceraldehyde-3-phosphate dehydrogenase [GAPDH] were used as a reference for normalization. Immunofluorescence were performerd on cells to observe the expression of Hyal1, Hyal2, HAS2.
Upper panel: cytokines increased levels of Hyal1 by 61% at 24 hours and by 69% at 48 hours in WT cells but did not affect Hyal1 levels in Spam1KO cells.
Middle panel: at 48 hours, cytokines enhanced Hyal2 levels by 34% in WT cells and decreased Hyal2 levels by 34% in Spam1KO cells.
Lower panel: cytokines decreased the levels of HAS2 by 42% at 24 hours and by 40% at 48 hours in WT cells but did not affect HAS2 levels significantly in Spam1KO cells. The decrease of 22% observed at 48 in stimulated Spam1KO was at the limit of significance with p=0.0534. *: $p<0.05$; **: $p<0.01$; ***: $p<0.001$ by ANOVA. The impact of genotype for the total variance was 75% for Hyal1, 34% for Hyal2, and 62% for HAS2.

4.6. Immature murine articular chondrocytes and cartilage degrading enzymes

The two main structural elements of articular cartilage are type II collagen and aggrecan. In osteoarthritis, pro-inflammatory cytokines up-regulate the chondrocyte expression of two rate-limiting enzymes in the process of cartilage degradation, namely the collagenase Mmp-13 and the aggrecanase ADAMTS-5 (241, 319, 320).

In the present study, we examined the ability of immature WT and Spam1KO immature chondrocytes [P1] to produce Mmp-13 and ADAMTS-5 in the presence of IL-1β and TNF-α stimulation. In vehicle-treated monolayer cultures, there was no difference in levels of expressed Mmp-13 between WT and Spam1KO cells both at 24 and 48 hours [Figure 4, upper panel, open colums]. IL-1β and TNF-α induced a significant increase in Mmp-13 synthesis in both genotypes and at the two study time points [upper panel, closed columns]. At 24 hours, levels of Mmp-13 were increased by 354% in WT cells

and by 93% in Spam1KO cells [p<0.0001, each]. Likewise, at 48 hours, Mmp-13 levels were enhanced by 454% in WT cells and by 135% in Spam1KO cells [P<0.0001, each]. As compared to WT cells, the relative increase in Spam1KO cells was 3.8 times lower at 24 hours and 3.4 times lower at 48 hours.

As observed for Mmp-13, levels of ADAMTS-5 in vehicle-treated monolayer cultures were similar in both genotypes at the two study time points [Figure 4, lower panel, open columns]. Chondrocyte exposure to IL-1β and TNF-α for 24 hours increased the production of ADAMTS-5 significantly in WT cells [p=0.0395] but not in Spam1KO cells [lower panel, closed columns]. In WT cells cultured for 48 hours, the difference in ADAMTS-5 levels between cytokine-treated and vehicle-treated cells was at the limit of the statistically significant difference [p=0.0535]. There was no difference in ADAMTS-5 levels between cytokine-treated and vehicle-treated Spam1KO cells cultured for 24 and 48 hours.

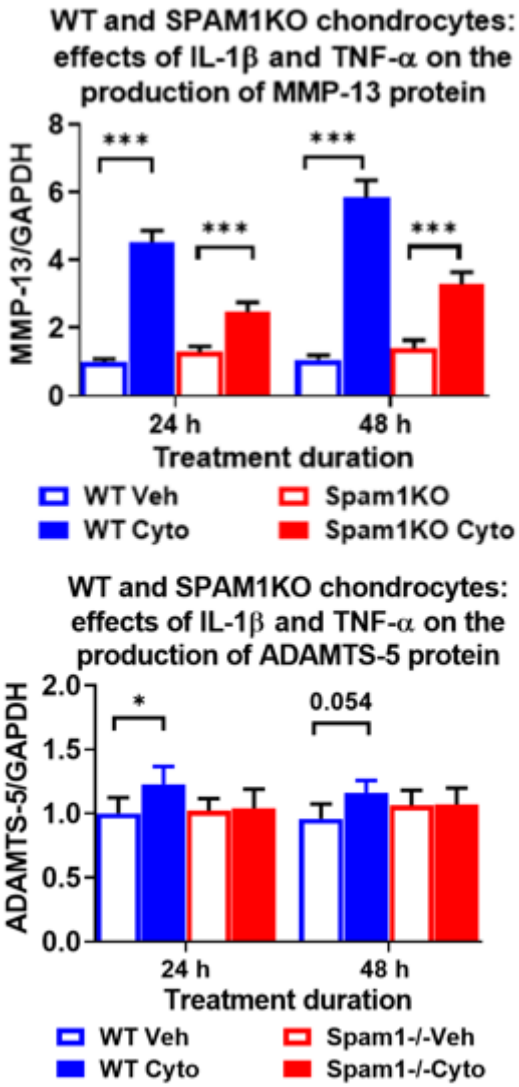

Figure 4. Primary articular chondrocytes and production of MMP-13 and ADAMTS-5.
Primary articular cartilage chondrocytes [stage P1] isolated from WT [open and closed blue columns] and Spam1KO [open and closed red columns] mice were cultured without [Veh] or with [Cyto] 10 ng/ml IL-1β and TNF-α [10 ng/ml each] for 24 and 48 hours. Immunoblots evaluated levels of MMP-13 and ADAMTS-5. Levels of glyceraldehyde-3-phosphate dehydrogenase [GAPDH] were used as a reference for normalization.
Upper panel: Vehicle-treated WT and Spam1KO cells had similar levels of MMP-13 at 24 and 48 hours. Pro-inflammatory cytokines increased levels of MMP-13 markedly in both genotypes and at the two study time points. The relative increase was higher in WT cells

than in Spam1KO cells at both 24 hours [+354% versus +93%, respectively] and 48 hours [+454% versus 135%, respectively].
Lower panel: cytokines enhanced the levels of ADAMTS-5 by 23% at 24 hours [p=0.0395] and by 21% at 48 hours [p=0.0535] in WT cells but did not affect ADAMTS-5 levels significantly in Spam1KO cells; *: $p<0.05$; **: $p<0.01$; ***: $p<0.001$ by ANOVA. The impact of genotype for the total variance was 92% for MMP-13 and 33% for ADAMTS-5.

5. Discussion

Transgenic mice have revolutionized our approach to study gene functions. A null mutation in the SPAM1/PH-20 gene was initially created to assess this neutral-active hyaluronidase's role during the penetration of sperm through the HA-rich cumulus cell layer (311). Unexpectedly, mice carrying the null mutation were fertile as their sperm contain HYAL5, one further neutral-active hyaluronidase [HYAL] (249, 273). As chondrocytes and synoviocytes also express SPAM1 (64), we herein used chondrocytes sampled from wild control cartilage mice and SPAM1-KO mice to address the potential impact of the HYAL on the expression of enzymes implicated in significant joint components turnover. We selected HA synthases, HYAL2, the aggrecanase ADAMTS-5, and the collagenase MMP-13. The presence of the proinflammatory cytokines IL-1β and TNF-α reproduced arthritic conditions. Because there are genetic, physiological, and environmental differences between mice and humans, extrapolating mouse study results in human diseases is not always straightforward. Nevertheless, researchers readily have access to many genetically-modified mouse strains, specific murine antibodies, and probes to unravel many diseases' pathophysiology and identify new therapeutic targets. Recently, combining mouse and human genetic data uncovered a new gene regulating cholesterol (321). Furthermore, the murine model used herein provides millions of primary cells readily subjected to biochemical and molecular biology procedures. It might seem strange that we used immature articular chondrocytes instead of the well-referenced cartilage explant culture system (322), but we

couldn't do otherwise to obtain seven samples per experimental data point! Indeed, we restricted articular cartilage sampling of 5-day-old mice to tibial plateaus, femoral heads, and femoral condyles while avoiding rib and appendicular bone growth plates. Harvested explants were small, scarce, and challenging to handle. Cartilage samples were also inhomogeneous: full-thickness specimens were uncommon, and most specimens were a mixture of superficial, superficial-mid, and mid-deep cartilage layers. Further, Spam1KO mice have low birth rates, and legal grounds prohibited us from using as many mice as we wanted to do. There is no perfect model for in vitro studies. Even cartilage explants are relatively stable for up to ten days, provided the two first days allow the explants to equilibrate (323). After ten days of culture, the cartilage's collagen fibers begin to degrade, and the cartilage could degenerate. Chondrocytes and osteoblasts remained fully differentiated during the duration of the study. Each cell line exhibited its expected morphology and expressed its predicted collagen type and matrix. Also, chondrocytes enhanced their expression of NO in response to IL-1 and TNF-α, whereas dedifferentiated chondrocytes do not (307, 316, 324). Thus, immortalized lines of chondrocytes and osteoblasts were not useful. This point is a real advantage, as there are marked differences between primary cell lines and immortalized ones (325, 326).

The enhanced production of SPAM1 by osteoblasts in the presence of inflammatory cytokines is a new finding. Its relevance remains speculative as the roles of bone endogenous HA synthesis and degradation begins to be defined.

In vitro studies indicate that high MM HA down-regulates osteoclastogenesis (118) and increases osteoblast proliferation and mineralization, whereas low HA increases proliferation and promotes osteoclastic bone resorption (327). As reviewed by Bastow et al., changes in bone HA content, synthesis, retention, and release, in several bone cell types, disease states, and dietary conditions are intimately associated with the control of bone remodeling (31). HA drives osteoclast differentiation through CD44 to increase RANKL in bone marrow stromal cells (328). Isolated osteoblasts synthesize and release HA, the level of release depending upon their origin within the bone and osteogenic stimuli (329, 330).

The IL-1 and TNα induced production of SPAM1 by chondrocytes has been previously reported (64). Up-regulated PH-20 activity at neutral pH may be very deleterious to cartilage matrix, as few cleavages along the central HA backbone of aggregates reduce their viscoelastic properties dramatically. Also, SPAM1 produces HA fragments of various sizes, including HA hexasaccharides that are competitive inhibitors of the binding of hyaluronan to the chondrocyte CD44 surface receptor (331). Also, HA oligosaccharides induce a dose-dependent state of chondrocytic chondrolysis (102), and enhance matrix metalloproteinase 13 via transcriptional activation of NFkappaB and p38 MAP kinase (332). Further, SPAM1 may be responsible for the release of aggrecan ternary complexes made of aggrecans, link protein, and HA from cartilage matrix upon stimulation with retinoic acid, a process that persists when cartilage explants are bathed AG3340 that inhibits

collagenases, aggrecanase-1 and aggrecanase-2 (333). Because the loss of HA from osteoarthritic cartilage explants occurs in spite of an up-regulation in HA biosynthesis (269, 306), a likely explanation is that HA strands are being degraded at an accelerated rate by a hyaluronidase active at near neutral ph. Up-regulation of SPAM1 expression might also contribute to cartilage matrix degradation in arthritides such as rheumatoid arthritis. Indeed, cartilage explants incubated with catabolic stimuli exhibit concomitant release of HA, link protein and aggrecan G1 fragments into media (259, 334, 335).

As previously reported (336), pro-inflammatory cytokines up-regulated the expression of the lysosomal hyaluronidases Hyal1 and Hyal2 in WT chondrocytes. Catabolic factors also enhance the expression of CD44, a cell surface hyaluronan receptor involved in hyaluronan endocytosis (68). Accordingly, small pericellular HA molecules free of aggrecan or complexed to small aggrecan fragments could be internalized via CD44 receptors and degraded intracellularly. Conversely, in SPAM1KO chondrocytes, IL1 and TNF-α unaffected Hyal1 expression and decreased Hyal2 expression suggesting that products of SPAM1 activity might trigger intracellular HA breakdown. In WT cells, but not in Spam1KO cells, the concomitant decrease in HAS2 and increase in both Hyal1 and Hyal2 might be compelling. However, the small oligosaccharides produced by Spam1 might inhibit HAS2 mRNA expression, as observed in a breast cancer cell line (337).

MMP-13 is more active against type II collagen than other collagenases, and the enzyme is predominantly responsible for collagen release from cartilage in degenerative and inflammatory arthritides. IL-1 and TNF-α up-regulated MMP-13 expression markedly in both WT and Spam1KO chondrocytes. However, MMP-13 levels were significantly higher in WT chondrocytes compared to Spam1KO. These data suggest that the inhibition of Spam1 expression reduced the levels of HA degradation products markedly and, thereby, contributed to reducing TLR-4 and CD44 activation and MMP-13 production. Indeed, TNF-α and IL-1 induce the expression of several mediators of the inflammatory reaction, including IL-6, inducible nitric oxide synthase (iNOS), and small HA fragment production (338). The size of HA molecules differently modulates toll-like receptors in mouse chondrocytes (339). Treatment of RA synoviocytes with antioxidants and specific HYAL1, HYAL2, and HYAL3 small interference RNA (siRNAs) significantly reduced TLR-4 and CD44 increase in the mRNA expression and the related protein synthesis, as well as the release of MMP-13 (338).

In conclusion, our in vitro study provides evidence that Spam1 activity might contribute significantly to joint degradation in osteoarthritis and inflammatory arthritides. The uncontrolled and up-regulated activity of the soluble and neutral active hyaluronidase cleaves a significant organizer of cartilage ECM and generate HA oligosaccharides of different sizes known to mediate the expression of matrix-degrading enzymes and to change cell behavior.

Discussion

Our study highlights effects of Spam1 KO in spontaneous and induced OA progression through *in vivo* and *in vitro* experiments. These data have to be interpreted according to the OA models used, with their advantages and limitations. Then, our results arouse interest about the potential role of Spam1 in OA osteochondral unit disturbance, suggesting hypotheses about its involvement in HA turnover.

Experimental models of osteoarthritis

Among many OA animal models, such as mouse, guinea pig, rabbit, dog, pig, goat and horse, as reviewed by Bapat et al., mice present several advantages: a rapid musculoskeletal growth, quick breeding and easy housing (340). However, extrapolation of mice data to humans must take some particularities into account, including lack in intracortical bone remodeling, persistence of growth plate and differences in articular cartilage between mice and humans, such as fewer layers of cells (Introduction, Figure 1), hypercellularity, higher matrix turnover and high speed of cartilage defect progression in small species (340, 341). Nevertheless, mouse is the most widely used animal in OA research with different experimental models available such as spontaneous, surgical, chemical and non-invasive induced ones.

Spontaneous OA occurs during natural mouse ageing or in genetically modified mouse strains.

- Naturally occurring OA is the simplest, constitutive model, requiring no treatment. It mimics the progression of non-traumatic OA in humans and enables researchers to study a completely natural onset and progression of OA (340). However, this OA model is relatively slow and does not ensure systematic OA development, speed of onset and severity of the disease (341). This model was used in our first study on the phenotype of Spam1$^{-/-}$ mice. It allowed us to observe the first signs of osteoarthritis, i.e. a slight reduction in matrix staining and some surface irregularities in cartilage, from the 30th week of age, and typical OA modifications of cartilage and subchondral bone at 52 weeks. Despite this long observation time, some mice of the Spam1$^{-/-}$ strain showed no sign of osteoarthritis at 52 weeks of age.
- Genetically modified mice are more predictable spontaneous OA models. IL-6$^{-/-}$, Col2a1$^{-/-}$, Col9a1$^{-/-}$, Hyal1$^{-/-}$, Hyal2$^{-/-}$, HAS1$^{-/-}$ strain mice (60, 62, 268, 342-344) develop severe OA. On the contrary, knockout of genes encoding ECM-degrading enzymes such as MMP-13 or ADAMTS-5 generates mouse strains with less osteoarthritic features than WT mice (206, 345). To our knowledge, no other study has used Spam1$^{-/-}$ mouse to identify a possible role of Spam1 in joint pathophysiology.

Surgical joint destabilization consists in transection of anterior cruciate ligament (ACTL) and/or medial collateral ligaments, destabilization of the medial meniscus (DMM) or meniscus resection and creation of chondral/osteochondral defects (346-349). These methods lead to post-traumatic OA (PTOA) whose characteristics mirror OA progression in humans. They are challenging due to the necessary consistency of the microsurgical performance across all animals, the high risk of infection and the quickly developing OA (340). In order to ensure the reliability of our model, one single trained operator performed all the surgical experiments, under surgical microscopes and under extremely strict hygienic conditions. The post-operative follow-up of the animals was carried out over one week. The surgical procedure used in our experiment lead to early changes in the subchondral bone, within the first 3 days. Spam1$^{-/-}$ and WT mice displayed opposite subchondral bone reaction to this quickly increasing stress. A less traumatic procedure would allow to properly analyze these early changes, particularly with micro-CT 3D analysis of articular cartilage and subchondral bone. Micro-CT combined with Hexabrix contrast agent made it possible to provide a high resolution and sensitivity to assess GAGs content and 3D distribution in rat femoral cartilage (350). Since Hexabrix is used in human clinical imaging, it could be injected in mice in order to assess OA progression in the same animal at different times.

The surgical disadvantages are reduced when using chemically induced OA models, with injection of collagenase, papain, mono-iodoacetate (MIA) or

quinolones, among others (341, 351-353). These substances compromise the integrity and function of cartilage, ligaments and tendons and thereby destabilize the joint. We did not use these techniques because they do not correlate with pathogenesis of any type of human OA (341).

Non-invasive induced OA models rely on automated single or repeated application of trauma to the joint to mimic human OA injuries (340, 354). Among them, cyclic articular cartilage tibial compression (CACTC), which consists in applying an axial load to displace the tibia relative to the femur, is the preferred method to analyze damages resulting from chronic overuse OA injury (354, 355). These automated mechanisms avoid the disadvantages associated with surgery but require very expensive equipment.

In order to respect the 3R philosophy, i.e. refining, replacing and reducing, *in vitro* models, such as monolayer culture, co-culture, 3D-culture or explant culture (312, 356-359), allow to study cell behavior during early OA development, prior to the peak of the catabolic process (360), although they are not representative of joint complexity. Chondrocyte monolayer, cell scaffold or intact tissue techniques can also influence the cell response to the experimental conditions. Ideally, cartilage tissue should be used as an explant-based model, but this limits the number of samples available (361). This is why the monolayer model is the most widely used due to its rapid response to cytokines or load stimulation. However, its main limitation is

that chondrocytes cannot be used at multiple passages because they dedifferentiate into fibroblasts (356).

Since chondrocytes are sensitive to mechanical stress, they require some load to maintain ECM homeostasis. Load-based *in vitro* OA models permit to analyze the signaling pathway related with mechanotransduction (362). Chondrocytes are embedded into an artificial scaffold which is submitted to weight (363, 364) or to cyclic impacts (365). However, these models require specific devices and high cell numbers that are generally harvested in dogs or horses.

Using reliable monolayer cell cultures protocols (312, 356), we detected not only the expression of Spam1 by murine chondrocytes and osteoblasts, but also changes in this expression after pro-inflammatory cytokine stimulation, which is the most commonly used *in vitro* method of OA induction. As reviewed by Johnson et al., the pro-inflammatory cytokines IL-1β and TNF-α produced following synovial inflammation are known to stimulate, both *in vivo* and *in vitro*, the production of catabolic enzymes MMPs and ADAMTS, as well as VEGF, by humans and animals chondrocytes, synoviocytes and osteoblasts (360). Pro-inflammatory cytokines appear to be ideal candidates for *in vitro* induction of OA-like biological changes in joint cells or tissues (360). In OA human patient synovial fluid, concentrations of IL-1β (<2ng/ml) and TNF-α (<3ng/ml) (366, 367) are very low compared to concentration used *in vitro,* i.e. up to 100ng/ml IL-1β and TNF-α (368, 369). We fixed a 10ng/ml concentration for both IL-1β and TNF-α in our *in vitro* experiment in order to approach the *in vivo* condition.

Spam1 knockout and OA in knee osteochondral unit

Contrary to the other hyaluronidase knockout models, Spam1$^{-/-}$ mice appear to be somewhat protected against age-related and induced OA cartilage degradation, which is the most original and important contribution of our work. Indeed, we observed a significantly lower Modified Mankin score in Spam1$^{-/-}$ than WT mice at 52 weeks of age. From 14 days after surgical OA induction, Spam1$^{-/-}$ mice also showed a significantly lower articular cartilage degradation than WT mice as soon as 14 days after surgical OA induction, as well as they developed smaller osteophytes and less numerous ectopic calcifications than WT mice.

Besides less articular cartilage degradation, subchondral BMD was lower in Spam1$^{-/-}$ mice than in WT mice, which could be another advantage since increasing tibial subchondral BMD was related with evolutive knee OA (370) and high systemic BMD was associated with structural OA features in hand and knee (166, 167, 371).

In early stages of OA, subchondral bone is characterized by increased porosity, decreased BMD and deteriorated subchondral trabeculae, leading to abnormal stress distribution at the cartilage-bone interface and to cartilage degradation but, in return, damaged cartilage influence the deterioration of the underlying subchondral bone (372). Using micro-CT, we observed a temporary decrease in BMD, BV/TV and trabecular thickness in

WT subchondral bone at 3 days after OA induction. This response, which can be explained as a consequence of the quick increase in stress forces on the articular cartilage, is considered a determinant of OA development (168, 220, 373, 374). On the contrary, Spam1$^{-/-}$ mice showed a significant increase in subchondral BV/TV, trabecular thickness and BMD in the first 3 days after OA induction. In contrast to that of WT mice, this reaction could prevent OA development by providing solid support to the articular cartilage undergoing a rapid increase in mechanical stress. After this early period, subchondral BMD of the tibia returned to baseline (Day 0) in both groups and remained lower in the knee of OA Spam1$^{-/-}$ mice. Absence of Spam1 appeared to contribute to optimal interaction between articular cartilage and subchondral bone, thereby reducing the OA severity.

These *in vivo* tissue interferences of Spam1 knockout in age- and OA-related cartilage and subchondral bone damage were associated with specific expression of other matrix degrading enzymes. Hyal2 was significantly less expressed in Spam1$^{-/-}$ chondrocytes than in WT ones from age 10 to 52 weeks. Whereas Hyal1 and Mmp13 expression increased in chondrocytes of 52-week-old WT mice, it remained constant in Spam1$^{-/-}$ ones. After OA induction, articular cartilage of Spam1$^{-/-}$ mice exhibited less Hyal1, Hyal2 and Mmp-13 immunostaining than WT ones. Hyal2 and Mmp-13 were previously identified as playing a key role in cartilage degradation and their expression significantly increases during OA development (200, 201, 375). These results could explain the cartilage preservation in Spam1$^{-/-}$ due to the decreased degradation of the ECM components compared to WT mice. Furthermore,

Spam1 generates HA fragments that are highly angiogenic and potent inducers of inflammatory cytokines in human (376); its absence could have a beneficial impact on cartilage preservation.

To our knowledge, no other study had focused on the cartilage and bone features of Spam1 knockout, whereas this enzyme is related to HA turnover. Like others, we also showed that this murine model is viable and do not show gross morphological particularity, although it presents male subfertility (377, 378). Recently, Park et al. confirmed this impaired sperm activity in double knockout (dKO) Spam1/Hyal5 mice but also observed normal expression of other somatic Hyals by these dKO mice (274).

By comparison, Hyal1$^{-/-}$ mice, the mouse model of human mucopolysaccharidosis IX, showed mainly a lysosomal storage disorder and progressive loss of proteoglycans in the knee joint cartilage from 3 months of age (62). OA appeared to be the main feature, due to increased HA accumulation in the epiphyseal and articular cartilage. Absence of HA elevation in the serum or non-skeletal tissues was suggested to be due to a significant increase of liver Hyal3 expression in Hyal1$^{-/-}$ mice.

Beside localized craniovertebral bone defect, Hyal2$^{-/-}$ mice did not show any accumulation of HA, except in the liver and kidney (247). In addition, the Hyal1 transcript was increased in the kidney and a 2-fold increase was detected in plasma hyaluronidase activity, which was hypothetically attributed to Hyal1 and lead to the conclusion that Hyal2 is needed to maintain normal plasma concentration of HA in mice (247). Recently, Hyal2 conditional deficiency was shown to aggravate cartilage degradation in

ageing mice and after DMM OA induction (60). In these models, Hyal1 expression did not change in articular cartilage whereas Mmp-13 and Adamts-5 expression was significantly increased as well as HA deposition in the chondrocyte pericellular area.

Hyal3 is broadly expressed in mouse (379), has an intracellular localization (287), and plays an important role in HA catabolism. Hyal3$^{-/-}$ mice did not present any gross phenotypic change nor histological changes in joints and their serum HA level was normal (77). Nevertheless, absence of Hyal3 decreased both Hyal2 and Hyal1 expression in liver (77).

Our data indirectly suggest a consistent role of Spam1 in OA development and, consequently, its interaction with HA turnover in normal cartilage. Our *in vitro* experiments allowed to identify Spam1 expression not only in murine chondrocytes, confirming previous report (31), but also in osteoblasts. This original observation is consistent with SPAM1 detection in human connective tissue cells, such as chondrocytes, synoviocytes and fibroblasts (64). As also observed in these latter human cell cultures, cytokine stimulation, that is an *in vitro* model of OA induction, significantly increased Spam1 expression by WT murine chondrocytes, as well as osteoblasts, suggesting its involvement in the whole osteochondral unit disturbance. We further showed that chondrocytes stimulated with pro-inflammatory cytokines produced significantly more Hyal1 and Mmp-13 after 24h, more Hyal2 after 48h and less HAS2 after 24h. These enzymes, which regulate HA metabolism and matrix degradation, are known to vary in such a way during

OA development, which generates imbalance between production and degradation of HA and collagen (201, 380).

Spam1$^{-/-}$ chondrocyte culture provided further support for the hypothesis that Spam1 is interconnected with main actors of HA turnover: under cytokine stimulation, the production of Hyal2 significantly decreased at 48h and the production of HAS2 decreased in a smaller proportion than WT chondrocytes, whereas Mmp-13 production was increased in lower proportion. These data highly suggest that absence of Spam1 lowers HA and collagen degradation, whereas HA synthesis is partly preserved. They are particularly consistent with our in vivo observations.

Perspectives

Our results lead to different perspectives in order to better understand the function of hyaluronidase Spam1. In their model of HA degradation, Chowdhurry et al. suggested a fourth, non-HYAL2-dependent, pathway (74), in which we hypothesized possible involvement of Spam1. Since Hyal2 expression appeared tightly associated with Spam1, interaction of this latter with CD44-Hyal2 complex should be considered. Analysis of the pericellular matrix of chondrocytes could also allow to localize Spam1 and to highlight its relationships with the cell membrane, like Hyal2.

To go further with the role of Spam1 in osteochondral unit, analysis of GAGs concentration and HA molecular weight in articular cartilage of WT and Spam1$^{-/-}$ mice could specify the activity of this hyaluronidase in vivo as well

as in cartilage and even osteochondral unit culture. Expression of Spam1 by osteoblasts and its increase under inflammatory conditions highly suggest investigating their whole protein expression after Spam1 deletion and in osteoarthritic conditions in order to highlight its contribution to osteochondral unit physiopathology and to skeletal health. Indeed, accumulation of GAGs in skeletal tissues could lead to symptoms mimicking mucopolysaccharidoses (60, 62, 77). Decrease or absence of Hyal2 could lead to local bone malformation, as described in Hyal2$^{-/-}$ mice (247).

Spam1$^{-/-}$ mice could also be used to further analyze the activity of this hyaluronidase in liver, kidneys, spleen, skin and lymph nodes, where HA turnover is known to be very active (33, 36, 381). Besides the changes induced in joint tissues, the constitutive absence of Spam1 could lead to adaptations in such organs, with possible over- or under-expression of some hyaluronidases/HAS.

Conclusion

According to our experiments, absence of hyaluronidase Spam1 protects the joint from natural and induced osteoarthritis. This protection includes not only cartilage, but also subchondral bone, which highlights the need for regarding the joint as an organ in the management of OA. Furthermore, Spam1$^{-/-}$ chondrocytes produce significantly less enzymes that degrade the cartilage extracellular matrix, particularly Hyal2. Since Spam1 production by chondrocytes was shown to increase in experimental OA conditions, this hyaluronidase most likely interacts in cartilage HA metabolism and OA physiopathology.

Bibliography

1. OARSI. Osteoarthritis: a serious disease. US Food and Drug Administration. 2016.
2. Kloppenburg M, Berenbaum F. Osteoarthritis year in review 2019: epidemiology and therapy. Osteoarthritis Cartilage. 2020;28(3):242-8.
3. Goldring SR, Goldring MB. Changes in the osteochondral unit during osteoarthritis: structure, function and cartilage-bone crosstalk. Nat Rev Rheumatol. 2016;12(11):632-44.
4. Donell S. Subchondral bone remodelling in osteoarthritis. EFORT Open Reviews. 2019;4(6):221-9.
5. Sophia Fox AJ, Bedi A, Rodeo SA. The basic science of articular cartilage: structure, composition, and function. Sports Health. 2009;1(6):461-8.
6. Nathaniel P. Cohen M, Robert). Foster SVCM, PhD. Composition and Dynamics of Articular Cartilage: Structure, Function, and Maintaining ~ealthy State. JOSPT. 1998;28.
7. Mahjoub M, Berenbaum F, Houard X. Why subchondral bone in osteoarthritis? The importance of the cartilage bone interface in osteoarthritis. Osteoporos Int. 2012;23 Suppl 8:S841-6.
8. Tsang KY, Chan D, Cheah KSE. Fate of growth plate hypertrophic chondrocytes: Death or lineage extension? Development, Growth & Differentiation. 2015;57(2):179-92.
9. Di Bella C, Fosang A, Donati DM, Wallace GG, Choong PF. 3D Bioprinting of Cartilage for Orthopedic Surgeons: Reading between the Lines. Front Surg. 2015;2:39.
10. Armiento AR, Stoddart MJ, Alini M, Eglin D. Biomaterials for articular cartilage tissue engineering: Learning from biology. Acta Biomater. 2018;65:1-20.
11. Hunziker EB, Lippuner K, Shintani N. How best to preserve and reveal the structural intricacies of cartilaginous tissue. Matrix Biol. 2014;39:33-43.
12. Rim YA, Nam Y, Ju JH. The Role of Chondrocyte Hypertrophy and Senescence in Osteoarthritis Initiation and Progression. Int J Mol Sci. 2020;21(7).
13. Simon Ströbel ML, David Wendt, Andreas D Schenk, Christian Candrian, Raija L P Lindberg, Florina Moldovan, Andrea Barbero, Ivan Martin. Anabolic and Catabolic Responses of Human Articular Chondrocytes to Varying Oxygen Percentages. Arthritis Res Ther. 2010;12(2).
14. Houard X, Goldring MB, Berenbaum F. Homeostatic mechanisms in articular cartilage and role of inflammation in osteoarthritis. Curr Rheumatol Rep. 2013;15(11):375.
15. McGlashan SR, Jensen CG, Poole CA. Localization of extracellular matrix receptors on the chondrocyte primary cilium. J Histochem Cytochem. 2006;54(9):1005-14.
16. McGlashan SR, Cluett EC, Jensen CG, Poole CA. Primary cilia in osteoarthritic chondrocytes: from chondrons to clusters. Dev Dyn. 2008;237(8):2013-20.
17. Guilak F, Nims RJ, Dicks A, Wu CL, Meulenbelt I. Osteoarthritis as a disease of the cartilage pericellular matrix. Matrix Biol. 2018;71-72:40-50.
18. Attili S, Richter RP. Self-assembly and elasticity of hierarchical proteoglycan–hyaluronan brushes. Soft Matter. 2013;9(44).
19. Kiani C, Chen L, Wu YJ, Albert JY, Yang BB. Structure and Function of Aggrecan Cell Res. 2002;12 (1).
20. Heinegard D, Saxne T. The role of the cartilage matrix in osteoarthritis. Nat Rev Rheumatol. 2011;7(1):50-6.
21. Quinn TM, Häuselmann HJ, Shintani N, Hunziker EB. Cell and matrix morphology in articular cartilage from adult human knee and ankle joints suggests depth-associated adaptations to biomechanical and anatomical roles. Osteoarthritis and Cartilage. 2013;21(12):1904-12.
22. Gudmann NS, Karsdal MA. Type II Collagen. Biochemistry of Collagens, Laminins and Elastin2016. p. 13-20.

23. Andriacchi TP, Favre J. The nature of in vivo mechanical signals that influence cartilage health and progression to knee osteoarthritis. Curr Rheumatol Rep. 2014;16(11):463.
24. Guo H, Maher SA, Torzilli PA. A biphasic finite element study on the role of the articular cartilage superficial zone in confined compression. J Biomech. 2015;48(1):166-70.
25. Luo Y, Sinkeviciute D, He Y, Karsdal M, Henrotin Y, Mobasheri A, et al. The minor collagens in articular cartilage. Protein Cell. 2017;8(8):560-72.
26. Kvist AJ, Nystrom A, Hultenby K, Sasaki T, Talts JF, Aspberg A. The major basement membrane components localize to the chondrocyte pericellular matrix--a cartilage basement membrane equivalent? Matrix Biol. 2008;27(1):22-33.
27. Gannon JM, Walker G, Fischer M, Carpenter R, Thompson Jr RC, Oegema Jr TR. Localization of Type X Collagen in Canine Growth Plate and Adult Canine Articular Cartilage. J Orthop Res. 1991;9:485-94.
28. Wight TN, Kinsella MG, Qwarnstrom EE. The Role of Proteoglycans in Cell Adhesion, Migration and Proliferation Curr Opin Cell Biol. 1992;4:793-801.
29. Hardingham TE, Muir H. The Specific Interaction of Hyaluronic Acid With Cartillage Proteoglycans Biochim Biophys Acta. 1972;279:401-5.
30. Greene GW, Banquy X, Lee DW, Lowrey DD, Yu J, Israelachvili JN. Adaptive mechanically controlled lubrication mechanism found in articular joints. Proc Natl Acad Sci U S A. 2011;108(13):5255-9.
31. Bastow ER, Byers S, Golub SB, Clarkin CE, Pitsillides AA, Fosang AJ. Hyaluronan synthesis and degradation in cartilage and bone. Cell Mol Life Sci. 2008;65(3):395-413.
32. Csoka AB, Schere SW, Stern R. Expression analysis of six paralogous human hyaluronidase genes clustered on chromosomes 3p21 and 7q31. Genomics. 1999;60 (3):356-61.
33. Laurent TC, Fraser JRE. Hyaluronan. FASEB J. 1992;6:2397-404.
34. Chiara Schiraldi ALGaMDR. Biotechnological Production and Application of Hyaluronan. In: Elnashar M, editor. Biopolymers2010.
35. Knopf-Marques H, Pravda M, Wolfova L, Velebny V, Schaaf P, Vrana NE, et al. Hyaluronic Acid and Its Derivatives in Coating and Delivery Systems: Applications in Tissue Engineering, Regenerative Medicine and Immunomodulation. Adv Healthc Mater. 2016;5(22):2841-55.
36. Fraser JRE, Laurent TC, Laurent UBG. Hyaluronan : its nature, distribution, functions and turnover. Journal of Internal Medecine. 1997;242(1997):27-33.
37. Girish KS, Kemparaju K. The magic glue hyaluronan and its eraser hyaluronidase: a biological overview. Life Sci. 2007;80(21):1921-43.
38. Scott JE, Cummings C, Brass A, Chen Y. Secondary and Tertiary Structures of Hyaluronan in Aqueous Solution, Investigated by Rotary Shadowing-Electron Microscopy and Computer Simulation. Hyaluronan Is a Very Efficient Network-Forming Polymer. Biochem J. 1991;274:699-705.
39. Scott JE. Supramolecular Organization of Extracellular Matrix Glycosaminoglycans, in Vitro and in the Tissues FASEB J. 1992;6:2639-45.
40. Karbownik MS, Nowak JZ. Hyaluronan: towards novel anti-cancer therapeutics. Pharmacol Rep. 2013;65(5):1056-74.
41. Hascall VC, Majors AK, De La Motte CA, Evanko SP, Wang A, Drazba JA, et al. Intracellular hyaluronan: a new frontier for inflammation? Biochim Biophys Acta. 2004;1673(1-2):3-12.
42. Itano N, Kimata K. Mammalian Hyaluronan Synthases. IUBMB Life. 2002;54:195-9.
43. Weigel PH, Hascall VC, Tammi M. Hyaluronan Synthases. J Biol Chem. 1997;272:13997-4000.
44. Spicer AP, Tien JY. Hyaluronan and morphogenesis. Birth Defects Res C Embryo Today. 2004;72(1):89-108.
45. Itano N, Sawai T, Yoshida M, Lenas P, Imagawa M, Shinomura T, et al. Three isoforms of mammalian hyaluronan synthases have distinct enzymatic properties. Journal of Biological Chemistry. 1999;274(35).

46. Vigetti D, Karousou E, Viola M, Deleonibus S, De Luca G, Passi A. Hyaluronan: biosynthesis and signaling. Biochim Biophys Acta. 2014;1840(8):2452-9.
47. Schulz T, Schumacher U, Prehm P. Hyaluronan export by the ABC transporter MRP5 and its modulation by intracellular cGMP. J Biol Chem. 2007;282(29):20999-1004.
48. Knudson W, Ishizuka S, Terabe K, Askew EB, Knudson CB. The pericellular hyaluronan of articular chondrocytes. Matrix Biol. 2019;78-79:32-46.
49. Tammi RH, Passi AG, Rilla K, Karousou E, Vigetti D, Makkonen K, et al. Transcriptional and post-translational regulation of hyaluronan synthesis. Febs j. 2011;278(9):1419-28.
50. Avenoso A, Bruschetta G, D'Ascola A, Scuruchi M, Mandraffino G, Gullace R, et al. Hyaluronan fragments produced during tissue injury: A signal amplifying the inflammatory response. Arch Biochem Biophys. 2019;663:228-38.
51. Schiller J, Fuchs B, Arnhold J, Arnold K. Contribution of Reactive Oxygen Species to Cartilage Degradation in Rheumatic Diseases: Molecular Pathways, Diagnosis and Potential Therapeutic Strategies. Curr Med Chem. 2003;10:2123-45.
52. Stern R, Jedrzejas MJ. Hyaluronidases: their genomics, structures, and mechanisms of action. Chem Rev. 2006;106(3):818-39.
53. Jedrzejas MJ, Stern R. Structures of vertebrate hyaluronidases and their unique enzymatic mechanism of hydrolysis. Proteins. 2005;61(2):227-38.
54. Marković-Housley Z, Miglierini G, Soldatova L, Rizkallah PJ, Müller U, Schirmer T. Crystal Structure of Hyaluronidase, a Major Allergen of Bee Venom Structure. 2000;8:1025-35.
55. Martin-DeLeon PA. Epididymal SPAM1 and its impact on sperm function. Mol Cell Endocrinol. 2006;250(1-2):114-21.
56. Csoka AB, Frost GI, Stern R. The six hyaluronidase-like genes in the human and mouse genomes. Matrix biology. 2001;20:499-508.
57. Lepperdinger G, Strobl B, Kreil G. HYAL2, a Human Gene Expressed in Many Cells, Encodes a Lysosomal Hyaluronidase With a Novel Type of Specificity J Biol Chem. 1998;273:22466-70.
58. Lepperdinger G, Mullegger J, Kreil G. Hyal2--less Active, but More Versatile? . Matrix Biol. 2001;20:509-14.
59. Lokeshwar VB, Rubinowicz D, Schroeder GL, Forgacs E, Minna JD, Block NL, et al. Stromal and epithelial expression of tumor markers hyaluronic acid and HYAL1 hyaluronidase in prostate cancer. J Biol Chem. 2001;276(15):11922-32.
60. Higuchi Y, Nishida Y, Kozawa E, Zhuo L, Arai E, Hamada S, et al. Conditional knockdown of hyaluronidase 2 in articular cartilage stimulates osteoarthritic progression in a mice model. Sci Rep. 2017;7(1):7028.
61. Chow G, Knudson CB, Knudson W. Expression and cellular localization of human hyaluronidase-2 in articular chondrocytes and cultured cell lines. Osteoarthritis Cartilage. 2006;14(9):849-58.
62. Martin DC, Atmuri V, Hemming RJ, Farley J, Mort JS, Byers S, et al. A mouse model of human mucopolysaccharidosis IX exhibits osteoarthritis. Hum Mol Genet. 2008;17(13):1904-15.
63. Triggs-Raine B, Natowicz MR. Biology of hyaluronan: Insights from genetic disorders of hyaluronan metabolism. World J Biol Chem. 2015;6(3):110-20.
64. El Hajjaji H, Cole AA, Manicourt DH. Chondrocytes, synoviocytes and dermal fibroblasts all express PH-20, a hyaluronidase active at neutral pH. Arthritis Res Ther. 2005;7(4):R756-68.
65. Embry JJ, Knudson W. G1 domain of aggrecan cointernalizes with hyaluronan via a CD44-mediated mechanism in bovine articular chondrocytes. Arthritis Rheum. 2003;48(12):3431-41.
66. Ariyoshi W, Knudson CB, Luo N, Fosang AJ, Knudson W. Internalization of aggrecan G1 domain neoepitope ITEGE in chondrocytes requires CD44. J Biol Chem. 2010;285(46):36216-24.
67. Hua Q, Knudson CB, Knudson W. Internalization of Hyaluronan by Chondrocytes Occurs via Receptor-Mediated Endocytosis J Cell Sci. 1993;106:365-75.

68. Chow G, Knudson CB, Homandberg G, Knudson W. Increased Expression of CD44 in Bovine Articular Chondrocytes by Catabolic Cellular Mediators J Biol Chem. 1995;270:27734-41.
69. Yamamoto H, Tobisawa Y, Inubushi T, Irie F, Ohyama C, Yamaguchi Y. A mammalian homolog of the zebrafish transmembrane protein 2 (TMEM2) is the long-sought-after cell-surface hyaluronidase. J Biol Chem. 2017;292(18):7304-13.
70. Bourguignon LY, Singleton PA, Diedrich F, Stern R, Gilad E. CD44 interaction with Na+-H+ exchanger (NHE1) creates acidic microenvironments leading to hyaluronidase-2 and cathepsin B activation and breast tumor cell invasion. J Biol Chem. 2004;279(26):26991-7007.
71. Yoshida H, Nagaoka A, Kusaka-Kikushima A, Tobiishi M, Kawabata K, Sayo T, et al. KIAA1199, a deafness gene of unknown function, is a new hyaluronan binding protein involved in hyaluronan depolymerization. Proc Natl Acad Sci U S A. 2013;110(14):5612-7.
72. Hida D, Danielson BT, Knudson CB, Knudson W. CD44 knock-down in bovine and human chondrocytes results in release of bound HYAL2. Matrix Biol. 2015;48:42-54.
73. Knudson W, Chow G, Knudson CB. CD44-mediated Uptake and Degradation of Hyaluronan. Matrix Biol. 2002;21:15-23.
74. Chowdhury B, Hemming R, Faiyaz S, Triggs-Raine B. Hyaluronidase 2 (HYAL2) is expressed in endothelial cells, as well as some specialized epithelial cells, and is required for normal hyaluronan catabolism. Histochem Cell Biol. 2016;145(1):53-66.
75. Stern R. Hyaluronan catabolism: a new metabolic pathway. Eur J Cell Biol. 2004;83(7):317-25.
76. Gushulak L, Hemming R, Martin D, Seyrantepe V, Pshezhetsky A, Triggs-Raine B. Hyaluronidase 1 and beta-hexosaminidase have redundant functions in hyaluronan and chondroitin sulfate degradation. J Biol Chem. 2012;287(20):16689-97.
77. Atmuri V, Martin DC, Hemming R, Gutsol A, Byers S, Sahebjam S, et al. Hyaluronidase 3 (HYAL3) knockout mice do not display evidence of hyaluronan accumulation. Matrix Biol. 2008;27(8):653-60.
78. Zheng Y, Deng X, Zhao Y, Zhang H, Martin-DeLeon PA. Spam1 (PH-20) mutations and sperm dysfunction in mice with the Rb(6.16) or Rb(6.15) translocation. Mamm Genome. 2001;12(11):822-9.
79. Deng X, He Y, Martin-DeLeon PA. Mouse Spam1 (PH-20): Evidence for Its Expression in the Epididymis and for a New Category of Spermatogenic-Expressed Genes. J Androl. 2000;21:822-32.
80. Zhang H, Martin-DeLeon PA. Mouse Epididymal Spam1 (PH-20) Is Released in Vivo and in Vitro, and Spam1 Is Differentially Regulated in Testis and Epididymis Biol Reprod. 2001;65:1586-93.
81. Cherr GN, Yudin AI, Overtstreet JW. The Dual Functions of GPI-anchored PH-20: Hyaluronidase and Intracellular Signaling. Matrix Biol. 2001;20:515-25.
82. Gmachl M, Sagan S, Ketter S, Kreil G. The Human Sperm Protein PH-20 Has Hyaluronidase Activity FEBS Letters. 1993;336:545-8.
83. Hunnicutt GR, Primakoff P, Myles DG. Sperm Surface Protein PH-20 Is Bifunctional: One Activity Is a Hyaluronidase and a Second, Distinct Activity Is Required in Secondary Sperm-Zona Binding. Biol Reprod. 1996;55:80-6.
84. Lin Y, Mahan K, Lathrop WF, Myles DG, Primakoff P. A Hyaluronidase Activity of the Sperm Plasma Membrane Protein PH-20 Enables Sperm to Penetrate the Cumulus Cell Layer Surrounding the Egg J Cell Biol. 1994;125:1157-63.
85. Overtstreet JW, Lin Y, Yudin AI, Meyers SA, Primakoff P, Myles DG, et al. Location of the PH-20 Protein on Acrosome-Intact and Acrosome-Reacted Spermatozoa of Cynomolgus Macaques. Biol Reprod. 1995;52:105-14.
86. Primakoff P, Hyatt H, Myles DG. A Role for the Migrating Sperm Surface Antigen PH-20 in Guinea Pig Sperm Binding to the Egg Zona Pellucida J Cell Biol. 1985;101:2239-44.
87. Thaler CD, Cardullo RA. Biochemical Characterization of a Glycosylphosphatidylinositol-Linked Hyaluronidase on Mouse Sperm Biochemistry. 1995;34:7788-95.

88. Gacesa P, Civill ND, Harrison RA. PH-20 and Sperm Hyaluronidase: A Conceptual Conundrum in Mammalian Fertilization Biochem J. 1994;303:335-6.
89. Beech DJ, Madan AK, Deng N. Expression of PH-20 in normal and neoplastic breast tissue. J Surg Res. 2002;103(2):203-7.
90. Zhang H, Martin-DeLeon PA. Mouse Spam1 (PH-20) is a multifunctional protein: evidence for its expression in the female reproductive tract. Biol Reprod. 2003;69(2):446-54.
91. Bouga H, Tsouros I, Bounias D, Kyriakopoulou D, Stavropoulos MS, Papageorgakopoulou N, et al. Involvement of hyaluronidases in colorectal cancer. BMC Cancer. 2010;10:499.
92. Csoka AB, Stern R. Mammalian Hyaluronidases. Glycoforum. 2000.
93. Weber GC, Buhren BA, Schrumpf H, Wohlrab J, Gerber PA. Clinical Applications of Hyaluronidase. In: Labrou N, editor. Therapeutic Enzymes: Function and Clinical Implications. Singapore: Springer Singapore; 2019. p. 255-77.
94. Passi A, Vigetti D. Hyaluronan: Structure, Metabolism, and Biological Properties. Extracellular Sugar-Based Biopolymers Matrices. Biologically-Inspired Systems2019. p. 155-86.
95. Screaton GR, Bell MV, Jackson DG, Cornelis FB, Gerth U, Bell JI. Genomic Structure of DNA Encoding the Lymphocyte Homing Receptor CD44 Reveals at Least 12 Alternatively Spliced Exons. Proc Natl Acad Sci U S A. 1992;89:12160-4.
96. Yu Q, Toole BP. A New Alternatively Spliced Exon Between v9 and v10 Provides a Molecular Basis for Synthesis of Soluble CD44. J Biol Chem. 1996;271:20603-7.
97. Fujii Y, Fujii K, Nakano K, Tanaka Y. Crosslinking of CD44 on human osteoblastic cells upregulates ICAM-1 and VCAM-1. FEBS Letters. 2003;539(1-3):45-50.
98. Nakamura H, Kenmotsu S, Sakai H, Ozawa H. Localization of CD44, the hyaluronate receptor, on the plasma membrane of osteocytes and osteoclasts in rat tibiae. Cell Tissue Res. 1995;280(2):225-33.
99. Salter DM, Godolphin JL, Gourlay MS, Lawson MF, Hughes DE, Dunne E. Analysis of human articular chondrocyte CD44 isoform expression and function in health and disease. J Pathol. 1996;179(4):396-402.
100. Kaya G, Rodriguez I, Jorcano JL, Vassalli P, Stamenkovic I. Selective Suppression of CD44 in Keratinocytes of Mice Bearing an Antisense CD44 Transgene Driven by a Tissue-Specific Promoter Disrupts Hyaluronate Metabolism in the Skin and Impairs Keratinocyte Proliferation. Genes Dev. 1997;11:996-1007.
101. Knudson CB, Knudson W. Hyaluronan and CD44. Clinical Orthopaedics and Related Research. 2004;427:S152-S62.
102. Knudson W, Casey B, Nishida Y, Eger W, Kuettner KE, Knudson CB. Hyaluronan oligosaccharides perturb cartilage matrix homeostasis and induce chondrocytic chondrolysis. Arthritis Rheum. 2000;43(5):1165-74.
103. Jiang H, Knudson CB, Knudson W. Antisense inhibition of CD44 tailless splice variant in human articular chondrocytes promotes hyaluronan internalization. Arthritis Rheum. 2001;44(11):2599-610.
104. Nishida Y, Knudson CB, Nietfeld JJ, Margulis A, Knudson W. Antisense Inhibition of Hyaluronan Synthase-2 in Human Articular Chondrocytes Inhibits Proteoglycan Retention and Matrix Assembly. The Journal of biologycal chemistry. 1999;274.
105. Prevo R, Banerji S, Ferguson DJ, Clasper S, Jackson DG. Mouse LYVE-1 is an endocytic receptor for hyaluronan in lymphatic endothelium. J Biol Chem. 2001;276(22):19420-30.
106. Zhou B, Weigel JA, Fauss L, Weigel PH. Identification of the hyaluronan receptor for endocytosis (HARE). J Biol Chem. 2000;275(48):37733-41.
107. Harada H, Takahashi M. CD44-dependent intracellular and extracellular catabolism of hyaluronic acid by hyaluronidase-1 and -2. J Biol Chem. 2007;282(8):5597-607.

108. Weigel JA, Weigel PH. Characterization of the recombinant rat 175-kDa hyaluronan receptor for endocytosis (HARE). J Biol Chem. 2003;278(44):42802-11.
109. Lesley J, English NM, Gal I, Mikecz K, Day AJ, Hyman R. Hyaluronan binding properties of a CD44 chimera containing the link module of TSG-6. J Biol Chem. 2002;277(29):26600-8.
110. Hayflick JS, Kilgannon P, Gallatin WM. The intercellular adhesion molecule (ICAM) family of proteins. New members and novel functions. Immunol Res. 1998;17(3):313-27.
111. Banerji S, Ni J, Wang S, Clasper S, Su J, Tammi R, et al. LYVE-1, a New Homologue of the CD44 Glycoprotein, Is a Lymph-specific Receptor for Hyaluronan. 144. 1999;4:789-801.
112. Bono P, Rubin K, Hynes RO. Layilin, a Novel Integral Membrane Protein, Is a Hyaluronan Receptor. Mol Biol Cell. 2001;12:891-900.
113. Band PA, Heeter J, Wisniewski HG, Liublinska V, Pattanayak CW, Karia RJ, et al. Hyaluronan molecular weight distribution is associated with the risk of knee osteoarthritis progression. Osteoarthritis Cartilage. 2015;23(1):70-6.
114. Ghosh S, Hoselton SA, Dorsam GP, Schuh JM. Hyaluronan fragments as mediators of inflammation in allergic pulmonary disease. Immunobiology. 2015;220(5):575-88.
115. Ghosh P, Guidolin D. Potential Mechanism of Action of Intra-articular Hyaluronan Therapy in Osteoarthritis: Are the Effects Molecular Weight Dependent? Semin Arthritis Rheum. 2002;32(1):10-37.
116. Lee CW, Seo JY, Choi JW, Lee J, Park JW, Lee JY, et al. Potential anti-osteoporotic activity of low-molecular weight hyaluronan by attenuation of osteoclast cell differentiation and function in vitro. Biochem Biophys Res Commun. 2014;449(4):438-43.
117. Vistejnova L, Safrankova B, Nesporova K, Slavkovsky R, Hermannova M, Hosek P, et al. Low molecular weight hyaluronan mediated CD44 dependent induction of IL-6 and chemokines in human dermal fibroblasts potentiates innate immune response. Cytokine. 2014;70(2):97-103.
118. Ariyoshi W, Okinaga T, Knudson CB, Knudson W, Nishihara T. High molecular weight hyaluronic acid regulates osteoclast formation by inhibiting receptor activator of NF-kappaB ligand through Rho kinase. Osteoarthritis Cartilage. 2014;22(1):111-20.
119. Stern R, Asari AA, Sugahara KN. Hyaluronan fragments: an information-rich system. Eur J Cell Biol. 2006;85(8):699-715.
120. Krishnan Y, Grodzinsky AJ. Cartilage diseases. Matrix Biol. 2018;71-72:51-69.
121. Montell E, Stabler T, Vergés J, Kraus VB. Attentuation of Hyaluronan fragment induced inflammatory response in Macrophages by Chondroitin sulphate. Clinical Therapeutics. 2015;37(8).
122. Tamer TM. Hyaluronan and synovial joint: function, distribution and healing. Interdiscip Toxicol. 2013;6(3):111-25.
123. Jiang D, Liang J, Noble PW. Hyaluronan as an immune regulator in human diseases. Physiol Rev. 2011;91(1):221-64.
124. Cowman MK. Hyaluronan and Hyaluronan Fragments. Adv Carbohydr Chem Biochem. 2017;74:1-59.
125. Cyphert JM, Trempus CS, Garantziotis S. Size Matters: Molecular Weight Specificity of Hyaluronan Effects in Cell Biology. Int J Cell Biol. 2015;2015:563818.
126. Heldin P, Lin CY, Kolliopoulos C, Chen YH, Skandalis SS. Regulation of hyaluronan biosynthesis and clinical impact of excessive hyaluronan production. Matrix Biol. 2019;78-79:100-17.
127. D'Agostino A, Stellavato A, Corsuto L, Diana P, Filosa R, La Gatta A, et al. Is molecular size a discriminating factor in hyaluronan interaction with human cells? Carbohydr Polym. 2017;157:21-30.
128. Lyons TJ, McClure SF, Stoddart RW, McClure J. The normal human chondro-osseous junctional region: evidence for contact of uncalcified cartilage with subchondral bone and marrow spaces. BMC Musculoskelet Disord. 2006;7:52.
129. Simkin PA. Consider the tidemark. J Rheumatol. 2012;39(5):890-2.

130. Yang L, Tsang KY, Tang HC, Chan D, Cheah KS. Hypertrophic chondrocytes can become osteoblasts and osteocytes in endochondral bone formation. Proc Natl Acad Sci U S A. 2014;111(33):12097-102.
131. Luckman SP, Rees E, Kwan AP. Partial characterization of cell-type X collagen interactions. Biochem J. 2003;372(Pt 2):485-93.
132. Burr DB. Anatomy and physiology of the mineralized tissues: role in the pathogenesis of osteoarthrosis. Osteoarthritis Cartilage. 2004;12 Suppl A:S20-30.
133. Burr DB, Gallant MA. Bone remodelling in osteoarthritis. Nat Rev Rheumatol. 2012;8(11):665-73.
134. Langdahl B, Ferrari S, Dempster DW. Bone modeling and remodeling: potential as therapeutic targets for the treatment of osteoporosis. Ther Adv Musculoskelet Dis. 2016;8(6):225-35.
135. Eriksen EF. Cellular mechanisms of bone remodeling. Rev Endocr Metab Disord. 2010;11(4):219-27.
136. Goldring MB, Goldring SR. Articular cartilage and subchondral bone in the pathogenesis of osteoarthritis. Ann N Y Acad Sci. 2010;1192:230-7.
137. Goldring SR. The role of bone in osteoarthritis pathogenesis. Rheum Dis Clin North Am. 2008;34(3):561-71.
138. Bonewald LF. The amazing osteocyte. J Bone Miner Res. 2011;26(2):229-38.
139. Dallas SL, Prideaux M, Bonewald LF. The osteocyte: an endocrine cell ... and more. Endocr Rev. 2013;34(5):658-90.
140. Kennedy OD, Laudier DM, Majeska RJ, Sun HB, Schaffler MB. Osteocyte apoptosis is required for production of osteoclastogenic signals following bone fatigue in vivo. Bone. 2014;64:132-7.
141. Schaffler MB, Kennedy OD. Osteocyte signaling in bone. Curr Osteoporos Rep. 2012;10(2):118-25.
142. Schaffler MB, Cheung WY, Majeska R, Kennedy O. Osteocytes: master orchestrators of bone. Calcif Tissue Int. 2014;94(1):5-24.
143. Nicolella DP, Moravits DE, Gale AM, Bonewald LF, Lankford J. Osteocyte lacunae tissue strain in cortical bone. J Biomech. 2006;39(9):1735-43.
144. Jaiprakash A, Prasadam I, Feng JQ, Liu Y, Crawford R, Xiao Y. Phenotypic characterization of osteoarthritic osteocytes from the sclerotic zones: a possible pathological role in subchondral bone sclerosis. Int J Biol Sci. 2012;8(3):406-17.
145. Adachi T, Aonuma Y, Tanaka M, Hojo M, Takano-Yamamoto T, Kamioka H. Calcium response in single osteocytes to locally applied mechanical stimulus: differences in cell process and cell body. J Biomech. 2009;42(12):1989-95.
146. Han Y, Cowin SC, Schaffler MB, Weinbaum S. Mechanotransduction and strain amplification in osteocyte cell processes. Proc Natl Acad Sci U S A. 2004;101(47):16689-94.
147. Nicolella DP, Feng JQ, Moravits DE, Bonivitch AR, Wang Y, Dusecich V, et al. Effects of nanomechanical bone tissue properties on bone tissue strain: implications for osteocyte mechanotransduction. J Musculoskelet Neuronal Interact. 2008;8(4):330-1.
148. Bonivtch AR, Bonewald LF, Nicolella DP. Tissue strain amplification at the osteocyte lacuna: a microstructural finite element analysis. J Biomech. 2007;40(10):2199-206.
149. Kraus VB, Blanco FJ, Englund M, Karsdal MA, Lohmander LS. Call for standardized definitions of osteoarthritis and risk stratification for clinical trials and clinical use. Osteoarthritis Cartilage. 2015;23(8):1233-41.
150. James SL, Abate D, Abate KH, Abay SM, Abbafati C, Abbasi N, et al. Global, regional, and national incidence, prevalence, and years lived with disability for 354 diseases and injuries for 195 countries and territories, 1990–2017: a systematic analysis for the Global Burden of Disease Study 2017. The Lancet. 2018;392(10159):1789-858.

151. Siviero P, Veronese N, Smith T, Stubbs B, Limongi F, Zambon S, et al. Association Between Osteoarthritis and Social Isolation: Data From the EPOSA Study. J Am Geriatr Soc. 2020;68(1):87-95.
152. Innes KE, Sambamoorthi U. The Association of Perceived Memory Loss with Osteoarthritis and Related Joint Pain in a Large Appalachian Population. Pain Med. 2018;19(7):1340-56.
153. Singh JA, Yu S. The burden of septic arthritis on the U.S. inpatient care: A national study. PLoS One. 2017;12(8):e0182577.
154. Singh JA, Yu S. Time Trends, Predictors, and Outcome of Emergency Department Use for Gout: A Nationwide US Study. J Rheumatol. 2016;43(8):1581-8.
155. Dulay GS, Cooper C, Dennison EM. Knee pain, knee injury, knee osteoarthritis & work. Best Pract Res Clin Rheumatol. 2015;29(3):454-61.
156. Goldman LH, Tang K, Facchetti L, Heilmeier U, Joseph GB, Nevitt MC, et al. Role of thigh muscle cross-sectional area and strength in progression of knee cartilage degeneration over 48 months - data from the Osteoarthritis Initiative. Osteoarthritis Cartilage. 2016;24(12):2082-91.
157. Turkiewicz A, Timpka S, Thorlund JB, Ageberg E, Englund M. Knee extensor strength and body weight in adolescent men and the risk of knee osteoarthritis by middle age. Ann Rheum Dis. 2017;76(10):1657-61.
158. Cameron KL, Driban JB, Svoboda SJ. Osteoarthritis and the Tactical Athlete: A Systematic Review. J Athl Train. 2016;51(11):952-61.
159. Neogi T, Zhang Y. Epidemiology of osteoarthritis. Rheum Dis Clin North Am. 2013;39(1):1-19.
160. Johnson VL, Hunter DJ. The epidemiology of osteoarthritis. Best Pract Res Clin Rheumatol. 2014;28(1):5-15.
161. Buckwalter JA, Martin JA. Sports and osteoarthritis. Curr Opin Rheumatol. 2004;16(5):634-9.
162. Allen KD, Golightly YM. State of the evidence. Current Opinion in Rheumatology. 2015;27(3):276-83.
163. Sharma L, Chang AH, Jackson RD, Nevitt M, Moisio KC, Hochberg M, et al. Varus Thrust and Incident and Progressive Knee Osteoarthritis. Arthritis Rheumatol. 2017;69(11):2136-43.
164. Wang B, Liu Q, Wise BL, Ke Y, Xing D, Xu Y, et al. Valgus malalignment and prevalence of lateral compartmental radiographic knee osteoarthritis (OA): The Wuchuan OA study. Int J Rheum Dis. 2018;21(7):1385-90.
165. Wink AE, Gross KD, Brown CA, Guermazi A, Roemer F, Niu J, et al. Varus thrust during walking and the risk of incident and worsening medial tibiofemoral MRI lesions: the Multicenter Osteoarthritis Study. Osteoarthritis Cartilage. 2017;25(6):839-45.
166. Teichtahl AJ, Wang Y, Wluka AE, Strauss BJ, Proietto J, Dixon JB, et al. Associations between systemic bone mineral density and early knee cartilage changes in middle-aged adults without clinical knee disease: a prospective cohort study. Arthritis Res Ther. 2017;19(1):98.
167. Gevers G, Dequeker J, Geusens P, Nyssen-Behets C, Dhem A. Physical and histomorphological characteristics of iliac crest bone differ according to the grade of osteoarthritis at the hand. Bone. 1989;10(3):173-7.
168. Behets C, Williams JM, Chappard D, Devogelaer JP, Manicourt DH. Effects of calcitonin on subchondral trabecular bone changes and on osteoarthritic cartilage lesions after acute anterior cruciate ligament deficiency. J Bone Miner Res. 2004;19(11):1821-6.
169. Burger H, van Daele PLA, Odding E, Valkenburg HA, Hofman A, Grobbee DE, et al. Association of radiographically evident osteoarthritis with higher bone mineral density and increased bone loss with age. Arthritis and Rheumatism. 1996;39(1):91-86.
170. Wong SH, Chiu KY, Yan CH. Review Article: Osteophytes. J Orthop Surg (Hong Kong). 2016;24(3):403-10.

171. Rice SJ, Beier F, Young DA, Loughlin J. Interplay between genetics and epigenetics in osteoarthritis. Nat Rev Rheumatol. 2020;16(5):268-81.
172. Zhang Y, Jordan JM. Epidemiology of osteoarthritis. Rheum Dis Clin North Am. 2008;34(3):515-29.
173. Zhang Y, Jordan JM. Epidemiology of osteoarthritis. Clin Geriatr Med. 2010;26(3):355-69.
174. Vina ER, Ran D, Ashbeck EL, Ratzlaff C, Kwoh CK. Race, sex, and risk factors in radiographic worsening of knee osteoarthritis. Semin Arthritis Rheum. 2018;47(4):464-71.
175. Reynard LN, Loughlin J. Insights from human genetic studies into the pathways involved in osteoarthritis. Nat Rev Rheumatol. 2013;9(10):573-83.
176. Sandell LJ. Etiology of osteoarthritis: genetics and synovial joint development. Nat Rev Rheumatol. 2012;8(2):77-89.
177. Baird DA, Evans DS, Kamanu FK, Gregory JS, Saunders FR, Giuraniuc CV, et al. Identification of Novel Loci Associated With Hip Shape: A Meta-Analysis of Genomewide Association Studies. J Bone Miner Res. 2019;34(2):241-51.
178. Zengini E, Hatzikotoulas K, Tachmazidou I, Steinberg J, Hartwig FP, Southam L, et al. Genome-wide analyses using UK Biobank data provide insights into the genetic architecture of osteoarthritis. Nat Genet. 2018;50(4):549-58.
179. Hatzikotoulas K, Roposch A, Consortium DDHCC, Shah KM, Clark MJ, Bratherton S, et al. Genome-wide association study of developmental dysplasia of the hip identifies an association with GDF5. Commun Biol. 2018;1:56.
180. Kerkhof HJ, Lories RJ, Meulenbelt I, Jonsdottir I, Valdes AM, Arp P, et al. A genome-wide association study identifies an osteoarthritis susceptibility locus on chromosome 7q22. Arthritis Rheum. 2010;62(2):499-510.
181. Styrkarsdottir U, Lund SH, Thorleifsson G, Zink F, Stefansson OA, Sigurdsson JK, et al. Meta-analysis of Icelandic and UK data sets identifies missense variants in SMO, IL11, COL11A1 and 13 more new loci associated with osteoarthritis. Nat Genet. 2018;50(12):1681-7.
182. Kulkarni K, Karssiens T, Kumar V, Pandit H. Obesity and osteoarthritis. Maturitas. 2016;89:22-8.
183. Xie C, Chen Q. Adipokines: New Therapeutic Target for Osteoarthritis? Curr Rheumatol Rep. 2019;21(12):71.
184. Oliveira MC, Vullings J, van de Loo FAJ. Osteoporosis and osteoarthritis are two sides of the same coin paid for obesity. Nutrition. 2020;70:110486.
185. Blagojevic M, Jinks C, Jeffery A, Jordan KP. Risk factors for onset of osteoarthritis of the knee in older adults: a systematic review and meta-analysis. Osteoarthritis Cartilage. 2010;18(1):24-33.
186. Jin WS, Choi EJ, Lee SY, Bae EJ, Lee TH, Park J. Relationships among Obesity, Sarcopenia, and Osteoarthritis in the Elderly. J Obes Metab Syndr. 2017;26(1):36-44.
187. Misra D, Fielding RA, Felson DT, Niu J, Brown C, Nevitt M, et al. Risk of Knee Osteoarthritis With Obesity, Sarcopenic Obesity, and Sarcopenia. Arthritis Rheumatol. 2019;71(2):232-7.
188. Felson DT. Relation of Obesity and of Vocational and Avocational Risk Factors to Osteoarthritis. J Rheumatol. 2005;32:1133-5.
189. Giles JT, van der Heijde DM, Bathon JM. Association of circulating adiponectin levels with progression of radiographic joint destruction in rheumatoid arthritis. Ann Rheum Dis. 2011;70(9):1562-8.
190. Frommer KW, Zimmermann B, Meier FM, Schroder D, Heil M, Schaffler A, et al. Adiponectin-mediated changes in effector cells involved in the pathophysiology of rheumatoid arthritis. Arthritis Rheum. 2010;62(10):2886-99.
191. Huang ZM, Du SH, Huang LG, Li JH, Xiao L, Tong P. Leptin promotes apoptosis and inhibits autophagy of chondrocytes through upregulating lysyl oxidase-like 3 during osteoarthritis pathogenesis. Osteoarthritis Cartilage. 2016;24(7):1246-53.

192. Halade GV, El Jamali A, Williams PJ, Fajardo RJ, Fernandes G. Obesity-mediated inflammatory microenvironment stimulates osteoclastogenesis and bone loss in mice. Exp Gerontol. 2011;46(1):43-52.
193. Yaykasli KO, Hatipoglu OF, Yaykasli E, Yildirim K, Kaya E, Ozsahin M, et al. Leptin induces ADAMTS-4, ADAMTS-5, and ADAMTS-9 genes expression by mitogen-activated protein kinases and NF-kB signaling pathways in human chondrocytes. Cell Biol Int. 2015;39(1):104-12.
194. Gómez R, Scotece M, Conde J, Gómez-Reino JJ, Lago F, Gualillo O. Adiponectin and leptin increase IL-8 production in human chondrocytes. Ann Rheum Dis. 2011;70(11):2052-4.
195. Yang WS, Lee WJ, Funahashi T, Tanaka S, Matsuzawa Y, Chao CL, et al. Weight reduction increases plasma levels of an adipose-derived anti-inflammatory protein, adiponectin. J Clin Endocrinol Metab. 2001;86(8):3815-9.
196. Chuckpaiwong B, Charles HC, Kraus VB, Guilak F, Nunley JA. Age-associated increases in the size of the infrapatellar fat pad in knee osteoarthritis as measured by 3T MRI. J Orthop Res. 2010;28(9):1149-54.
197. Distel E, Cadoudal T, Durant S, Poignard A, Chevalier X, Benelli C. The infrapatellar fat pad in knee osteoarthritis: an important source of interleukin-6 and its soluble receptor. Arthritis Rheum. 2009;60(11):3374-7.
198. Calvo E, Palacios I, Delgado E, Sanchez-Pernaute O, Largo R, Egido J, et al. Histopathological correlation of cartilage swelling detected by magnetic resonance imaging in early experimental osteoarthritis. Osteoarthritis Cartilage. 2004;12(11):878-86.
199. Fosang AJ, Beier F. Emerging Frontiers in cartilage and chondrocyte biology. Best Pract Res Clin Rheumatol. 2011;25(6):751-66.
200. Wang M, Sampson ER, Jin H, Li J, Ke QH, Im HJ, et al. MMP13 is a critical target gene during the progression of osteoarthritis. Arthritis Res Ther. 2013;15(1):R5.
201. Yoshida M, Sai S, Marumo K, Tanaka T, Itano N, Kimata K, et al. Expression analysis of three isoforms of hyaluronan synthase and hyaluronidase in the synovium of knees in osteoarthritis and rheumatoid arthritis by quantitative real-time reverse transcriptase polymerase chain reaction. Arthritis Res Ther. 2004;6(6):R514-20.
202. Loeser RF, Goldring SR, Scanzello CR, Goldring MB. Osteoarthritis: a disease of the joint as an organ. Arthritis Rheum. 2012;64(6):1697-707.
203. Lorenzo P, Bayliss MT, Heinegard D. Altered patterns and synthesis of extracellular matrix macromolecules in early osteoarthritis. Matrix Biol. 2004;23(6):381-91.
204. Hwang HS, Kim HA. Chondrocyte Apoptosis in the Pathogenesis of Osteoarthritis. Int J Mol Sci. 2015;16(11):26035-54.
205. Liu-Bryan R, Terkeltaub R. Emerging regulators of the inflammatory process in osteoarthritis. Nat Rev Rheumatol. 2015;11(1):35-44.
206. Singh A, Rajasekaran N, Hartenstein B, Szabowski S, Gajda M, Angel P, et al. Collagenase-3 (MMP-13) deficiency protects C57BL/6 mice from antidoby-induced arthritis. Arthritis Res Ther. 2013;15(6).
207. Sun MM, Beier F. Chondrocyte hypertrophy in skeletal development, growth, and disease. Birth Defects Res C Embryo Today. 2014;102(1):74-82.
208. Ripmeester EGJ, Timur UT, Caron MMJ, Welting TJM. Recent Insights into the Contribution of the Changing Hypertrophic Chondrocyte Phenotype in the Development and Progression of Osteoarthritis. Front Bioeng Biotechnol. 2018;6:18.
209. Walsh DA, McWilliams DF, Turley MJ, Dixon MR, Franses RE, Mapp PI, et al. Angiogenesis and nerve growth factor at the osteochondral junction in rheumatoid arthritis and osteoarthritis. Rheumatology (Oxford). 2010;49(10):1852-61.

210. Studer D, Millan C, Ozturk E, Maniura-Weber K, Zenobi-Wong M. Molecular and biophysical mechanisms regulating hypertrophic differentiation in chondrocytes and mesenchymal stem cells. Eur Cell Mater. 2012;24:118-35; discussion 35.
211. Lories RJ. Joint homeostasis, restoration, and remodeling in osteoarthritis. Best Pract Res Clin Rheumatol. 2008;22(2):209-20.
212. Weber A, Chan PMB, Wen C. Do immune cells lead the way in subchondral bone disturbance in osteoarthritis? Prog Biophys Mol Biol. 2019;148:21-31.
213. Hugle T, Geurts J. What drives osteoarthritis?-synovial versus subchondral bone pathology. Rheumatology (Oxford). 2017;56(9):1461-71.
214. Hayashi D, Englund M, Roemer FW, Niu J, Sharma L, Felson DT, et al. Knee malalignment is associated with an increased risk for incident and enlarging bone marrow lesions in the more loaded compartments: the MOST study. Osteoarthritis Cartilage. 2012;20(11):1227-33.
215. Englund M, Guermazi A, Roemer FW, Yang M, Zhang Y, Nevitt MC, et al. Meniscal pathology on MRI increases the risk for both incident and enlarging subchondral bone marrow lesions of the knee: the MOST Study. Ann Rheum Dis. 2010;69(10):1796-802.
216. Roemer FW, Neogi T, Nevitt MC, Felson DT, Zhu Y, Zhang Y, et al. Subchondral bone marrow lesions are highly associated with, and predict subchondral bone attrition longitudinally: the MOST study. Osteoarthritis Cartilage. 2010;18(1):47-53.
217. Bianco D, Todorov A, Cengic T, Pagenstert G, Scharen S, Netzer C, et al. Alterations of Subchondral Bone Progenitor Cells in Human Knee and Hip Osteoarthritis Lead to a Bone Sclerosis Phenotype. Int J Mol Sci. 2018;19(2).
218. Campbell TM, Reilly K, Laneuville O, Uhthoff H, Trudel G. Bone replaces articular cartilage in the rat knee joint after prolonged immobilization. Bone. 2018;106:42-51.
219. Pardy CK, Matyas JR, Zernicke RF. Doxycycline effects on mechanical and morphometrical properties of early- and late-stage osteoarthritic bone following anterior cruciate ligament injury. J Appl Physiol (1985). 2004;97(4):1254-60.
220. Boyde A, Firth EC. High resolution microscopic survey of third metacarpal articular calcified cartilage and subchondral bone in the juvenile horse: possible implications in chondro-osseous disease. Microsc Res Tech. 2008;71(6):477-88.
221. Poulet B, Hamilton RW, Shefelbine S, Pitsillides AA. Characterizing a novel and adjustable noninvasive murine joint loading model. Arthritis Rheum. 2011;63(1):137-47.
222. Crema MD, Roemer FW, Marra MD, Guermazi A. Magnetic resonance imaging assessment of subchondral bone and soft tissues in knee osteoarthritis. Rheum Dis Clin North Am. 2009;35(3):557-77.
223. Hudelmaier M, Wirth W. Differences in subchondral bone size after one year in osteoarthritic and healthy knees. Osteoarthritis Cartilage. 2016;24(4):623-30.
224. Sanchez C, Deberg MA, Piccardi N, Msika P, Reginster JY, Henrotin YE. Osteoblasts from the sclerotic subchondral bone downregulate aggrecan but upregulate metalloproteinases expression by chondrocytes. This effect is mimicked by interleukin-6, -1beta and oncostatin M pre-treated non-sclerotic osteoblasts. Osteoarthritis Cartilage. 2005;13(11):979-87.
225. Sanchez C, Deberg MA, Bellahcene A, Castronovo V, Msika P, Delcour JP, et al. Phenotypic characterization of osteoblasts from the sclerotic zones of osteoarthritic subchondral bone. Arthritis Rheum. 2008;58(2):442-55.
226. Chou CH, Wu CC, Song IW, Chuang HP, Lu LS, Chang JH, et al. Genome-wide expression profiles of subchondral bone in osteoarthritis. Arthritis Res Ther. 2013;15(6):R190.
227. Hilal G, Martel-Pelletier J, Pelletier JP, Ranger P, Lajeunesse D. Osteoblast-like cells from human subchondral osteoarthritic bone demonstrate an altered phenotype in vitro: possible role in subchondral bone sclerosis. Arthritis Rheum. 1998;41(5):891-9.

228. Blom AB, van Lent PL, Holthuysen AE, van der Kraan PM, Roth J, van Rooijen N, et al. Synovial lining macrophages mediate osteophyte formation during experimental osteoarthritis. Osteoarthritis Cartilage. 2004;12(8):627-35.
229. Gelse K, Soder S, Eger W, Diemtar T, Aigner T. Osteophyte development--molecular characterization of differentiation stages. Osteoarthritis Cartilage. 2003;11(2):141-8.
230. Hsia AW, Anderson MJ, Heffner MA, Lagmay EP, Zavodovskaya R, Christiansen BA. Osteophyte formation after ACL rupture in mice is associated with joint restabilization and loss of range of motion. J Orthop Res. 2017;35(3):466-73.
231. Berenbaum F. Osteoarthritis as an inflammatory disease (osteoarthritis is not osteoarthrosis!). Osteoarthritis Cartilage. 2013;21(1):16-21.
232. Robinson WH, Lepus CM, Wang Q, Raghu H, Mao R, Lindstrom TM, et al. Low-grade inflammation as a key mediator of the pathogenesis of osteoarthritis. Nat Rev Rheumatol. 2016;12(10):580-92.
233. Kaneko S, Satoh T, Chiba J, Ju C, Inoue K, Kagawa J. Interleukin-6 and interleukin-8 levels in serum and synovial fluid of patients with osteoarthritis. Cytokines Cell Mol Ther. 2000;6(2):71-9.
234. Dumond H, Presle N, Terlain B, Mainard D, Loeuille D, Netter P, et al. Evidence for a key role of leptin in osteoarthritis. Arthritis Rheum. 2003;48(11):3118-29.
235. Eymard F, Pigenet A, Rose C, Bories A, Flouzat-Lachaniette CH, Berenbaum F, et al. Contribution of adipocyte precursors in the phenotypic specificity of intra-articular adipose tissues in knee osteoarthritis patients. Arthritis Res Ther. 2019;21(1):252.
236. Magne D, Palmer G, Barton JL, Mezin F, Talabot-Ayer D, Bas S, et al. The new IL-1 family member IL-1F8 stimulates production of inflammatory mediators by synovial fibroblasts and articular chondrocytes. Arthritis Res Ther. 2006;8(3):R80.
237. Sanchez C, Gabay O, Salvat C, Henrotin YE, Berenbaum F. Mechanical loading highly increases IL-6 production and decreases OPG expression by osteoblasts. Osteoarthritis Cartilage. 2009;17(4):473-81.
238. Ea HK, Bazille C, Lioté F. Histologie et physiologie de la membrane synoviale. EMC - Appareil locomoteur. 2008;3(3):1-6.
239. Mazor M, Best TM, Cesaro A, Lespessailles E, Toumi H. Osteoarthritis biomarker responses and cartilage adaptation to exercise: A review of animal and human models. Scand J Med Sci Sports. 2019;29(8):1072-82.
240. Yusup A, Kaneko H, Liu L, Ning L, Sadatsuki R, Hada S, et al. Bone marrow lesions, subchondral bone cysts and subchondral bone attrition are associated with histological synovitis in patients with end-stage knee osteoarthritis: a cross-sectional study. Osteoarthritis Cartilage. 2015;23(11):1858-64.
241. Goldring MB, Otero M. Inflammation in osteoarthritis. Curr Opin Rheumatol. 2011;23(5):471-8.
242. Goldring MB, Birkhead J, Sandell LJ, Kimura T, Krane SM. Interleukin 1 suppresses expression of cartilage-specific types II and IX collagens and increases types I and III collagens in human chondrocytes. J Clin Invest. 1988;82(6):2026-37.
243. Ainola MM, Mandelin JA, Liljestrom MJ, Li TF, Hukkanen MVJ, Konttinen YT. Pannus Invasion and Cartilage Degradation in Rheumatoid Arthritis: Involvement of MMP-3 and interleukin-1beta. Clin Exp Rheumatol. 2005;23:644-50.
244. Yuan GH, Tanaka M, Masuko-Hongo K, Shibakawa A, Kato T, Nishioka K, et al. Characterization of cells from pannus-like tissue over articular cartilage of advanced osteoarthritis. Osteoarthritis Cartilage. 2004;12(1):38-45.
245. Adamopoulos IE, Sabokbar A, Wordsworth BP, Carr A, Ferguson DJ, Athanasou NA. Synovial fluid macrophages are capable of osteoclast formation and resorption. J Pathol. 2006;208(1):35-43.

246. Dicker KT, Gurski LA, Pradhan-Bhatt S, Witt RL, Farach-Carson MC, Jia X. Hyaluronan: a simple polysaccharide with diverse biological functions. Acta Biomater. 2014;10(4):1558-70.
247. Jadin L, Wu X, Ding H, Frost GI, Onclinx C, Triggs-Raine B, et al. Skeletal and hematological anomalies in HYAL2-deficient mice: a second type of mucopolysaccharidosis IX? FASEB J. 2008;22(12):4316-26.
248. Jansen S, Ekhlasi-Hundrieser M, Töpfer-Petersen E. Sperm adhesion molecules: structure and function. Cells Tissues Organs. 2001;168 (1-2):82-92.
249. Reitinger S, Laschober GT, Fehrer C, Greiderer B, Lepperdinger G. Mouse testicular hyaluronidase-like proteins SPAM1 and HYAL5 but not HYALP1 degrade hyaluronan. Biochem J. 2007;401(1):79-85.
250. Rigoglou S, Papavassiliou AG. The NF-kappaB signalling pathway in osteoarthritis. Int J Biochem Cell Biol. 2013;45(11):2580-4.
251. Cowman MK, Lee HG, Schwertfeger KL, McCarthy JB, Turley EA. The Content and Size of Hyaluronan in Biological Fluids and Tissues. Front Immunol. 2015;6:261.
252. Toole BP. Hyaluronan is not just a goo! J Clin Invest. 2000;106(3):335-6.
253. Wight TN, Kinsella MG, Evanko SP, Potter-Perigo S, Merrilees MJ. Versican and the regulation of cell phenotype in disease. Biochim Biophys Acta. 2014;1840(8):2441-51.
254. Joy RA, Vikkath N, Ariyannur PS. Metabolism and mechanisms of action of hyaluronan in human biology. Drug Metab Pers Ther. 2018;33(1):15-32.
255. Homandberg GA, Hui F, Wen C, Kuettner KE, Williams JM. Hyaluronic acid suppresses fibronectin fragment mediated cartilage chondrolysis: I. In vitro. Osteoarthritis Cartilage. 1997;5(5):309-19.
256. Takahashi K, Goomer RS, Harwood F, Kubo T, Hirasawa Y, Amiel D. The effects of hyaluronan on matrix metalloproteinase-3 (MMP-3), interleukin-1beta(IL-1beta), and tissue inhibitor of metalloproteinase-1 (TIMP-1) gene expression during the development of osteoarthritis. Osteoarthritis Cartilage. 1999;7(2):182-90.
257. Julovi SM, Ito H, Nishitani K, Jackson CJ, Nakamura T. Hyaluronan inhibits matrix metalloproteinase-13 in human arthritic chondrocytes via CD44 and P38. J Orthop Res. 2011;29(2):258-64.
258. Pohlig F, Guell F, Lenze U, Lenze FW, Mühlhofer HM, Schauwecker J, et al. Hyaluronic Acid Suppresses the Expression of Metalloproteinases in Osteoarthritic Cartilage Stimulated Simultaneously by Interleukin 1β and Mechanical Load. PLoS One. 2016;11(3):e0150020.
259. Fosang AJ, Tyler JA, Hardingham TE. Effect of interleukin-1 and insulin like growth factor-1 on the release of proteoglycan components and hyaluronan from pig articular cartilage in explant culture. Matrix. 1991;11(1):17-24.
260. Slevin M, Krupinski J, Kumar S, Gaffney J. Angiogenic oligosaccharides of hyaluronan induce protein tyrosine kinase activity in endothelial cells and activate a cytoplasmic signal transduction pathway resulting in proliferation. Lab Invest. 1998;78(8):987-1003.
261. Noble PW. Hyaluronan and its catabolic products in tissue injury and repair. Matrix Biol. 2002;21(1):25-9.
262. Heinegård D. Fell-Muir Lecture: Proteoglycans and more--from molecules to biology. Int J Exp Pathol. 2009;90(6):575-86.
263. Manicourt DH, Pita JC. Progressive depletion of hyaluronic acid in early experimental osteoarthritis in dogs. Arthritis Rheum. 1988;31(4):538-44.
264. Fraser JRE, Laurent TC, Laurent UB. Hyaluronan: Its Nature, Distribution, Functions and Turnover. J Intern Med. 1997;242:27-33.
265. Schiller S, Dorfman A. The metabolism of mucopolysaccharides in animals. IV. The influence of insulin. J Biol Chem. 1957;227(2):625-32.

266. D'Souza AL, Masuda K, Otten LM, Nishida Y, Knudson W, Thonar EJ. Differential effects of interleukin-1 on hyaluronan and proteoglycan metabolism in two compartments of the matrix formed by articular chondrocytes maintained in alginate. Arch Biochem Biophys. 2000;374(1):59-65.
267. Recklies AD, White C, Melching L, Roughley P. Differential regulation and expression of HAS in human articular chondrocytes, synovial cells and osteosarcoma cells. The Biochemical Journal. 2001;354:17-24.
268. Chan DD, Xiao WF, Li J, de la Motte CA, Sandy JD, Plaas A. Deficiency of hyaluronan synthase 1 (Has1) results in chronic joint inflammation and widespread intra-articular fibrosis in a murine model of knee joint cartilage damage. Osteoarthritis Cartilage. 2015;23(11):1879-89.
269. Ryu J, Treadwell BV, Mankin HJ. Biochemical and metabolic abnormalities in normal and osteoarthritic human articular cartilage. Arthritis Rheum. 1984;27(1):49-57.
270. Li M, Rosenfeld L, Vilar RE, Cowman MK. Degradation of hyaluronan by peroxynitrite. Arch Biochem Biophys. 1997;341(2):245-50.
271. Wei MH, Latif F, Bader S, Kashuba V, Chen JY, Duh FM, et al. Construction of a 600-kilobase cosmid clone contig and generation of a transcriptional map surrounding the lung cancer tumor suppressor gene (TSG) locus on human chromosome 3p21.3: progress toward the isolation of a lung cancer TSG. Cancer Res. 1996;56(7):1487-92.
272. Miller KA, Shao M, Martin-DeLeon PA. Hyalp1 in murine sperm function: evidence for unique and overlapping functions with other reproductive hyaluronidases. J Androl. 2007;28(1):67-76.
273. Kim E, Baba D, Kimura M, Yamashita M, Kashiwabara S, Baba T. Identification of a hyaluronidase, Hyal5, involved in penetration of mouse sperm through cumulus mass. Proc Natl Acad Sci U S A. 2005;102(50):18028-33.
274. Park S, Kim YH, Jeong PS, Park C, Lee JW, Kim JS, et al. SPAM1/HYAL5 double deficiency in male mice leads to severe male subfertility caused by a cumulus-oocyte complex penetration defect. Faseb j. 2019;33(12):14440-9.
275. Stern R. Devising a pathway for hyaluronan catabolism: are we there yet? Glycobiology. 2003;13(12):105r-15r.
276. Sztrolovics R, Recklies AD, Roughley PJ, Mort JS. Hyaluronate degradation as an alternative mechanism for proteoglycan release from cartilage during interleukin-1beta-stimulated catabolism. Biochem J. 2002;362(Pt 2):473-9.
277. Morales TI, Hascall VC. Correlated metabolism of proteoglycans and hyaluronic acid in bovine cartilage organ cultures. J Biol Chem. 1988;263(8):3632-8.
278. Kaneiwa T, Mizumoto S, Sugahara K, Yamada S. Identification of human hyaluronidase-4 as a novel chondroitin sulfate hydrolase that preferentially cleaves the galactosaminidic linkage in the trisulfated tetrasaccharide sequence. Glycobiology. 2010;20(3):300-9.
279. Grigorieva A, Griffiths GS, Zhang H, Laverty G, Shao M, Taylor L, et al. Expression of SPAM1 (PH-20) in the murine kidney is not accompanied by hyaluronidase activity: evidence for potential roles in fluid and water reabsorption. Kidney Blood Press Res. 2007;30(3):145-55.
280. Lafont S, Achouri Y, Cardinal M, Roels T, de Ville de Goyet C, Behets C, et al. Knockout of hyaluronidase Spam1 reduces age-related bone and cartilage changes in mouse knee. Morphologie. 2020.
281. Wu W, Billinghurst RC, Pidoux I, Antoniou J, Zukor D, Tanzer M, et al. Sites of collagenase cleavage and denaturation of type II collagen in aging and osteoarthritic articular cartilage and their relationship to the distribution of matrix metalloproteinase 1 and matrix metalloproteinase 13. Arthritis Rheum. 2002;46(8):2087-94.
282. Li H, Wang D, Yuan Y, Min J. New insights on the MMP-13 regulatory network in the pathogenesis of early osteoarthritis. Arthritis Res Ther. 2017;19(1):248.
283. Glasson SS, Blanchet TJ, Morris EA. The surgical destabilization of the medial meniscus (DMM) model of osteoarthritis in the 129/SvEv mouse. Osteoarthritis Cartilage. 2007;15(9):1061-9.

284. Ratneswaran A, To B, Russell BA, Beier F. Strain and model specific differences in mouse models of osteoarthritis. Osteoarthritis and Cartilage. 2018;26.
285. Ma HL, Blanchet TJ, Peluso D, Hopkins B, Morris EA, Glasson SS. Osteoarthritis severity is sex dependent in a surgical mouse model. Osteoarthritis Cartilage. 2007;15(6):695-700.
286. Kimura M, Kim E, Kang W, Yamashita M, Saigo M, Yamazaki T, et al. Functional roles of mouse sperm hyaluronidases, HYAL5 and SPAM1, in fertilization. Biol Reprod. 2009;81(5):939-47.
287. Hemming R, Martin DC, Slominski E, Nagy JI, Halayko AJ, Pind S, et al. Mouse Hyal3 encodes a 45- to 56-kDa glycoprotein whose overexpression increases hyaluronidase 1 activity in cultured cells. Glycobiology. 2008;18(4):280-9.
288. Manicourt DH, Thonar EJ, Pita JC, Howell DS. Changes in the sedimentation profile of proteoglycan aggregates in early experimental canine osteoarthritis. Connect Tissue Res. 1989;23(1):33-50.
289. Ariyoshi W, Takahashi T, Kanno T, Ichimiya H, Takano H, Koseki T, et al. Mechanisms involved in enhancement of osteoclast formation and function by low molecular weight hyaluronic acid. J Biol Chem. 2005;280(19):18967-72.
290. Chang EJ, Kim HJ, Ha J, Kim HJ, Ryu J, Park KH, et al. Hyaluronan inhibits osteoclast differentiation via Toll-like receptor 4. J Cell Sci. 2007;120(Pt 1):166-76.
291. Fieber C, Baumann P, Vallon R, Termeer C, Simon JC, Hofmann M, et al. Hyaluronan-oligosaccharide-induced transcription of metalloproteases. J Cell Sci. 2004;117(Pt 2):359-67.
292. Kobayashi M, Squires GR, Mousa A, Tanzer M, Zukor DJ, Antoniou J, et al. Role of interleukin-1 and tumor necrosis factor alpha in matrix degradation of human osteoarthritic cartilage. Arthritis Rheum. 2005;52(1):128-35.
293. Dahlberg L, Billinghurst RC, Manner P, Nelson F, Webb G, Ionescu M, et al. Selective enhancement of collagenase-mediated cleavage of resident type II collagen in cultured osteoarthritic cartilage and arrest with a synthetic inhibitor that spares collagenase 1 (matrix metalloproteinase 1). Arthritis Rheum. 2000;43(3):673-82.
294. Tchetina EV, Squires G, Poole AR. Increased type II collagen degradation and very early focal cartilage degeneration is associated with upregulation of chondrocyte differentiation related genes in early human articular cartilage lesions. J Rheumatol. 2005;32(5):876-86.
295. Dempster DW, Compston JE, Drezner MK, Glorieux FH, Kanis JA, Malluche H, et al. Standardized nomenclature, symbols, and units for bone histomorphometry: a 2012 update of the report of the ASBMR Histomorphometry Nomenclature Committee. J Bone Miner Res. 2013;28(1):2-17.
296. Mainil-Varlet P, Schiavinato A, Ganster MM. Efficacy Evaluation of a New Hyaluronan Derivative HYADD(®) 4-G to Maintain Cartilage Integrity in a Rabbit Model of Osteoarthritis. Cartilage. 2013;4(1):28-41.
297. Fedchenko N, Reifenrath J. Different approaches for interpretation and reporting of immunohistochemistry analysis results in the bone tissue - a review. Diagn Pathol. 2014;9:221.
298. Hascall VC. The journey of hyaluronan research in the Journal of Biological Chemistry. J Biol Chem. 2019;294(5):1690-6.
299. Frantz C, Stewart KM, Weaver VM. The extracellular matrix at a glance. J Cell Sci. 2010;123(Pt 24):4195-200.
300. Yoon S, Chang KT, Cho H, Moon J, Kim JS, Min SH, et al. Characterization of pig sperm hyaluronidase and improvement of the digestibility of cumulus cell mass by recombinant pSPAM1 hyaluronidase in an in vitro fertilization assay. Anim Reprod Sci. 2014;150(3-4):107-14.
301. Goldring MB, Berenbaum F. Human chondrocyte culture models for studying cyclooxygenase expression and prostaglandin regulation of collagen gene expression. Osteoarthritis Cartilage. 1999;7(4):386-8.

302. Singh P, Marcu KB, Goldring MB, Otero M. Phenotypic instability of chondrocytes in osteoarthritis: on a path to hypertrophy. Ann N Y Acad Sci. 2019;1442(1):17-34.
303. Nishida Y, D'Souza AL, Thonar EJ, Knudson W. Stimulation of hyaluronan metabolism by interleukin-1alpha in human articular cartilage. Arthritis Rheum. 2000;43(6):1315-26.
304. Sweet MB, Thonar EJ, Immelman AR, Solomon L. Biochemical changes in progressive osteoarthrosis. Ann Rheum Dis. 1977;36(5):387-98.
305. Müller FJ, Setton LA, Manicourt DH, Mow VC, Howell DS, Pita JC. Centrifugal and biochemical comparison of proteoglycan aggregates from articular cartilage in experimental joint disuse and joint instability. J Orthop Res. 1994;12(4):498-508.
306. Manicourt DH, Druetz-Van Egeren A, Haazen L, Nagant de Deuxchaisnes C. Effects of tenoxicam and aspirin on the metabolism of proteoglycans and hyaluronan in normal and osteoarthritic human articular cartilage. Br J Pharmacol. 1994;113(4):1113-20.
307. Salvat C, Pigenet A, Humbert L, Berenbaum F, Thirion S. Immature murine articular chondrocytes in primary culture: a new tool for investigating cartilage. Osteoarthritis Cartilage. 2005;13(3):243-9.
308. Fenwick N, Griffin G, Gauthier C. The welfare of animals used in science: how the "Three Rs" ethic guides improvements. Can Vet J. 2009;50(5):523-30.
309. Justice MJ, Dhillon P. Using the mouse to model human disease: increasing validity and reproducibility. Dis Model Mech. 2016;9(2):101-3.
310. Nguyen TL, Vieira-Silva S, Liston A, Raes J. How informative is the mouse for human gut microbiota research? Dis Model Mech. 2015;8(1):1-16.
311. Baba D, Kashiwabara S, Honda A, Yamagata K, Wu Q, Ikawa M, et al. Mouse sperm lacking cell surface hyaluronidase PH-20 can pass through the layer of cumulus cells and fertilize the egg. J Biol Chem. 2002;277(33):30310-4.
312. Bakker AD, Klein-Nulend J. Osteoblast isolation from murine calvaria and long bones. Methods Mol Biol. 2012;816:19-29.
313. Taylor SE, Shah M, Orriss IR. Generation of rodent and human osteoblasts. Bonekey Rep. 2014;3:585.
314. Häuselmann HJ, Fernandes RJ, Mok SS, Schmid TM, Block JA, Aydelotte MB, et al. Phenotypic stability of bovine articular chondrocytes after long-term culture in alginate beads. J Cell Sci. 1994;107 (Pt 1):17-27.
315. Lefebvre V, Garofalo S, Zhou G, Metsäranta M, Vuorio E, De Crombrugghe B. Characterization of primary cultures of chondrocytes from type II collagen/beta-galactosidase transgenic mice. Matrix Biol. 1994;14(4):329-35.
316. Lemare F, Steimberg N, Le Griel C, Demignot S, Adolphe M. Dedifferentiated chondrocytes cultured in alginate beads: restoration of the differentiated phenotype and of the metabolic responses to interleukin-1beta. J Cell Physiol. 1998;176(2):303-13.
317. Eyden B, Tzaphlidou M. Structural variations of collagen in normal and pathological tissues: role of electron microscopy. Micron. 2001;32(3):287-300.
318. Hiscock DR, Caterson B, Flannery CR. Expression of hyaluronan synthases in articular cartilage. Osteoarthritis Cartilage. 2000;8(2):120-6.
319. Mehana EE, Khafaga AF, El-Blehi SS. The role of matrix metalloproteinases in osteoarthritis pathogenesis: An updated review. Life Sci. 2019;234:116786.
320. Yang CY, Chanalaris A, Troeberg L. ADAMTS and ADAM metalloproteinases in osteoarthritis - looking beyond the 'usual suspects'. Osteoarthritis Cartilage. 2017;25(7):1000-9.
321. Li Z, Votava JA, Zajac GJM, Nguyen JN, Leyva Jaimes FB, Ly SM, et al. Integrating Mouse and Human Genetic Data to Move beyond GWAS and Identify Causal Genes in Cholesterol Metabolism. (1932-7420 (Electronic)).
322. Goldring MB, Goldring SR. Osteoarthritis. (1097-4652 (Electronic)).

323. Moo EK, Osman Na Fau - Pingguan-Murphy B, Pingguan-Murphy B. The metabolic dynamics of cartilage explants over a long-term culture period. (1980-5322 (Electronic)).
324. Goldring MB, Berenbaum F. The regulation of chondrocyte function by proinflammatory mediators: prostaglandins and nitric oxide. (0009-921X (Print)).
325. Loeser RF, Sadiev S Fau - Tan L, Tan L Fau - Goldring MB, Goldring MB. Integrin expression by primary and immortalized human chondrocytes: evidence of a differential role for alpha1beta1 and alpha2beta1 integrins in mediating chondrocyte adhesion to types II and VI collagen. (1063-4584 (Print)).
326. Finger F, Schörle C Fau - Zien A, Zien A Fau - Gebhard P, Gebhard P Fau - Goldring MB, Goldring Mb Fau - Aigner T, Aigner T. Molecular phenotyping of human chondrocyte cell lines T/C-28a2, T/C-28a4, and C-28/I2. (0004-3591 (Print)).
327. Huang L, Cheng Yy Fau - Koo PL, Koo Pl Fau - Lee KM, Lee Km Fau - Qin L, Qin L Fau - Cheng JCY, Cheng Jc Fau - Kumta SM, et al. The effect of hyaluronan on osteoblast proliferation and differentiation in rat calvarial-derived cell cultures. (1549-3296 (Print)).
328. Cao JJ, Singleton Pa Fau - Majumdar S, Majumdar S Fau - Boudignon B, Boudignon B Fau - Burghardt A, Burghardt A Fau - Kurimoto P, Kurimoto P Fau - Wronski TJ, et al. Hyaluronan increases RANKL expression in bone marrow stromal cells through CD44. (0884-0431 (Print)).
329. Fedarko NS, Termine Jd Fau - Young MF, Young Mf Fau - Robey PG, Robey PG. Temporal regulation of hyaluronan and proteoglycan metabolism by human bone cells in vitro. (0021-9258 (Print)).
330. Midura RJ, Evanko Sp Fau - Hascall VC, Hascall VC. Parathyroid hormone stimulates hyaluronan synthesis in an osteoblast-like cell line. (0021-9258 (Print)).
331. Knudson CB. Hyaluronan receptor-directed assembly of chondrocyte pericellular matrix. (0021-9525 (Print)).
332. Ohno S, Im Hj Fau - Knudson CB, Knudson Cb Fau - Knudson W, Knudson W. Hyaluronan oligosaccharides induce matrix metalloproteinase 13 via transcriptional activation of NFkappaB and p38 MAP kinase in articular chondrocytes. (0021-9258 (Print)).
333. Sugimoto K, Iizawa T Fau - Harada H, Harada H Fau - Yamada K, Yamada K Fau - Katsumata M, Katsumata M Fau - Takahashi M, Takahashi M. Cartilage degradation independent of MMP/aggrecanases. (1063-4584 (Print)).
334. Yasumoto T, Bird Jl Fau - Sugimoto K, Sugimoto K Fau - Mason RM, Mason Rm Fau - Bayliss MT, Bayliss MT. The G1 domain of aggrecan released from porcine articular cartilage forms stable complexes with hyaluronan/link protein. (1462-0324 (Print)).
335. Durigova M, Roughley Pj Fau - Mort JS, Mort JS. Mechanism of proteoglycan aggregate degradation in cartilage stimulated with oncostatin M. (1063-4584 (Print)).
336. Flannery CR, Little Cb Fau - Hughes CE, Hughes Ce Fau - Caterson B, Caterson B. Expression and activity of articular cartilage hyaluronidases. (0006-291X (Print)).
337. Urakawa H, Nishida Y Fau - Knudson W, Knudson W Fau - Knudson CB, Knudson Cb Fau - Arai E, Arai E Fau - Kozawa E, Kozawa E Fau - Futamura N, et al. Therapeutic potential of hyaluronan oligosaccharides for bone metastasis of breast cancer. (1554-527X (Electronic)).
338. Campo GM, Avenoso A Fau - D'Ascola A, D'Ascola A Fau - Scuruchi M, Scuruchi M Fau - Prestipino V, Prestipino V Fau - Nastasi G, Nastasi G Fau - Calatroni A, et al. The inhibition of hyaluronan degradation reduced pro-inflammatory cytokines in mouse synovial fibroblasts subjected to collagen-induced arthritis. (1097-4644 (Electronic)).
339. Campo GM, Avenoso A Fau - Campo S, Campo S Fau - D'Ascola A, D'Ascola A Fau - Nastasi G, Nastasi G Fau - Calatroni A, Calatroni A. Molecular size hyaluronan differently modulates toll-like receptor-4 in LPS-induced inflammation in mouse chondrocytes. (1638-6183 (Electronic)).
340. Bapat S, Hubbard D, Munjal A, Hunter M, Fulzele S. Pros and cons of mouse models for studying osteoarthritis. Clin Transl Med. 2018;7(1):36.

341. Lampropoulou-Adamidou K, Lelovas P, Karadimas EV, Liakou C, Triantafillopoulos IK, Dontas I, et al. Useful animal models for the research of osteoarthritis. Eur J Orthop Surg Traumatol. 2014;24(3):263-71.
342. Lapveteläinen T, Hyttinen M, Lindblom J, Långsjö TK, Sironen R, Li SW, et al. More knee joint osteoarthritis (OA) in mice after inactivation of one allele of type II procollagen gene but less OA after lifelong voluntary wheel running exercise. Osteoarthritis Cartilage. 2001;9(2):152-60.
343. Hu K, Xu L, Cao L, Flahiff CM, Brussiau J, Ho K, et al. Pathogenesis of osteoarthritis-like changes in the joints of mice deficient in type IX collagen. Arthritis Rheum. 2006;54(9):2891-900.
344. Kyostio-Moore S, Nambiar B, Hutto E, Ewing PJ, Piraino S, Berthelette P, et al. STR/ort mice, a model for spontaneous osteoarthritis, exhibit elevated levels of both local and systemic inflammatory markers. Comp Med. 2011;61(4):346-55.
345. Botter SM, Glasson SS, Hopkins B, Clockaerts S, Weinans H, van Leeuwen JP, et al. ADAMTS5-/- mice have less subchondral bone changes after induction of osteoarthritis through surgical instability: implications for a link between cartilage and subchondral bone changes. Osteoarthritis Cartilage. 2009;17(5):636-45.
346. Kamekura S, Hoshi K, Shimoaka T, Chung U, Chikuda H, Yamada T, et al. Osteoarthritis development in novel experimental mouse models induced by knee joint instability. Osteoarthritis Cartilage. 2005;13(7):632-41.
347. Figueroa D, Espinosa M, Calvo R, Scheu M, Valderrama JJ, Gallegos M, et al. [Treatment of acute full-thickness chondral defects with high molecular weight hyaluronic acid; an experimental model]. Rev Esp Cir Ortop Traumatol. 2014;58(5):261-6.
348. Fang H, Huang L, Welch I, Norley C, Holdsworth DW, Beier F, et al. Early Changes of Articular Cartilage and Subchondral Bone in The DMM Mouse Model of Osteoarthritis. Sci Rep. 2018;8(1):2855.
349. Sniekers YH, Weinans H, Bierma-Zeinstra SM, van Leeuwen JP, van Osch GJ. Animal models for osteoarthritis: the effect of ovariectomy and estrogen treatment - a systematic approach. Osteoarthritis Cartilage. 2008;16(5):533-41.
350. Xie L, Lin AS, Guldberg RE, Levenston ME. Nondestructive assessment of sGAG content and distribution in normal and degraded rat articular cartilage via EPIC-microCT. Osteoarthritis Cartilage. 2010;18(1):65-72.
351. Adães S, Mendonça M, Santos TN, Castro-Lopes JM, Ferreira-Gomes J, Neto FL. Intra-articular injection of collagenase in the knee of rats as an alternative model to study nociception associated with osteoarthritis. Arthritis Res Ther. 2014;16(1):R10.
352. Pitcher T, Sousa-Valente J, Malcangio M. The Monoiodoacetate Model of Osteoarthritis Pain in the Mouse. J Vis Exp. 2016(111).
353. Bendele AM. Animal models of osteoarthritis. J Musculoskelet Neuronal Interact. 2001;1(4):363-76.
354. Poulet B. Non-invasive Loading Model of Murine Osteoarthritis. Curr Rheumatol Rep. 2016;18(7):40.
355. Christiansen BA, Guilak F, Lockwood KA, Olson SA, Pitsillides AA, Sandell LJ, et al. Non-invasive mouse models of post-traumatic osteoarthritis. Osteoarthritis Cartilage. 2015;23(10):1627-38.
356. Mirando AJ, Dong Y, Kim J, Hilton MJ. Isolation and culture of murine primary chondrocytes. Methods Mol Biol. 2014;1130:267-77.
357. Vazquez M, Evans BA, Riccardi D, Evans SL, Ralphs JR, Dillingham CM, et al. A new method to investigate how mechanical loading of osteocytes controls osteoblasts. Front Endocrinol (Lausanne). 2014;5:208.
358. Bougault C, Aubert-Foucher E, Paumier A, Perrier-Groult E, Huot L, Hot D, et al. Dynamic compression of chondrocyte-agarose constructs reveals new candidate mechanosensitive genes. PLoS One. 2012;7(5):e36964.

359. Fitzgerald JB, Jin M, Dean D, Wood DJ, Zheng MH, Grodzinsky AJ. Mechanical compression of cartilage explants induces multiple time-dependent gene expression patterns and involves intracellular calcium and cyclic AMP. J Biol Chem. 2004;279(19):19502-11.
360. Johnson CI, Argyle DJ, Clements DN. In vitro models for the study of osteoarthritis. Vet J. 2016;209:40-9.
361. Amin AK, Huntley JS, Simpson AH, Hall AC. Chondrocyte survival in articular cartilage: the influence of subchondral bone in a bovine model. J Bone Joint Surg Br. 2009;91(5):691-9.
362. Mobasheri A, Barrett-Jolley R, Carter SD, Martín-Vasallo P, Schulze-Tanzil G, Shakibaei M. Functional Roles of Mechanosensitive Ion Channels, ß1 Integrins and Kinase Cascades in Chondrocyte Mechanotransduction. In: Kamkin A, Kiseleva I, editors. Mechanosensitivity in Cells and Tissues. Moscow: Academia

363. Henson FM, Vincent T. Chondrocyte outgrowth into a gelatin scaffold in a single impact load model of damage/repair - effect of BMP-2. BMC Musculoskelet Disord. 2007;8:120.
364. Huser CA, Davies ME. Validation of an in vitro single-impact load model of the initiation of osteoarthritis-like changes in articular cartilage. J Orthop Res. 2006;24(4):725-32.
365. Chen CT, Burton-Wurster N, Borden C, Hueffer K, Bloom SE, Lust G. Chondrocyte necrosis and apoptosis in impact damaged articular cartilage. J Orthop Res. 2001;19(4):703-11.
366. Kahle P, Saal JG, Schaudt K, Zacher J, Fritz P, Pawelec G. Determination of cytokines in synovial fluids: correlation with diagnosis and histomorphological characteristics of synovial tissue. Ann Rheum Dis. 1992;51(6):731-4.
367. Fujita Y, Hara Y, Nezu Y, Yamaguchi S, Schulz KS, Tagawa M. Direct and indirect markers of cartilage metabolism in synovial fluid obtained from dogs with hip dysplasia and correlation with clinical and radiographic variables. Am J Vet Res. 2005;66(12):2028-33.
368. Macrory L, Vaughan-Thomas A, Clegg PD, Innes JF. An exploration of the ability of tepoxalin to ameliorate the degradation of articular cartilage in a canine in vitro model. BMC Vet Res. 2009;5:25.
369. López-Armada MJ, Caramés B, Lires-Deán M, Cillero-Pastor B, Ruiz-Romero C, Galdo F, et al. Cytokines, tumor necrosis factor-alpha and interleukin-1beta, differentially regulate apoptosis in osteoarthritis cultured human chondrocytes. Osteoarthritis Cartilage. 2006;14(7):660-9.
370. Bruyere O, Dardenne C, Lejeune E, Zegels B, Pahaut A, Richy F, et al. Subchondral tibial bone mineral density predicts future joint space narrowing at the medial femoro-tibial compartment in patients with knee osteoarthritis. Bone. 2003;32(5):541-5.
371. Castañeda S, Roman-Blas JA, Largo R, Herrero-Beaumont G. Subchondral bone as a key target for osteoarthritis treatment. Biochem Pharmacol. 2012;83(3):315-23.
372. Li G, Yin J, Gao J, Cheng TS, Pavlos NJ, Zhang C, et al. Subchondral bone in osteoarthritis: insight into risk factors and microstructural changes. Arthritis Res Ther. 2013;15(6):223.
373. Bettica P, Cline G, Hart DJ, Meyer J, Spector TD. Evidence for increased bone resorption in patients with progressive knee osteoarthritis: longitudinal results from the Chingford study. Arthritis Rheum. 2002;46(12):3178-84.
374. Intema F, DeGroot J, Elshof B, Vianen ME, Yocum S, Zuurmond A, et al. The canine bilateral groove model of osteoarthritis. J Orthop Res. 2008;26(11):1471-7.
375. Ji B, Ma Y, Wang H, Fang X, Shi P. Activation of the P38/CREB/MMP13 axis is associated with osteoarthritis. Drug Des Devel Ther. 2019;13:2195-204.
376. Liu D, Pearlman E, Diaconu E, Guo K, Mori H, Haqqi T, et al. Expression of hyaluronidase by tumor cells induces angiogenesis in vivo. Proc Natl Acad Sci U S A. 1996;93(15):7832-7.
377. Zhou C, Kang W, Baba T. Functional characterization of double-knockout mouse sperm lacking SPAM1 and ACR or SPAM1 and PRSS21 in fertilization. J Reprod Dev. 2012;58(3):330-7.

378. Reese KL, Aravindan RG, Griffiths GS, Shao M, Wang Y, Galileo DS, et al. Acidic hyaluronidase activity is present in mouse sperm and is reduced in the absence of SPAM1: evidence for a role for hyaluronidase 3 in mouse and human sperm. Mol Reprod Dev. 2010;77(9):759-72.
379. Shuttleworth TL, Wilson MD, Wicklow BA, Wilkins JA, Triggs-Raine BL. Characterization of the murine hyaluronidase gene region reveals complex organization and cotranscription of Hyal1 with downstream genes, Fus2 and Hyal3. J Biol Chem. 2002;277(25):23008-18.
380. Tetlow LC, Adlam DJ, Woolley DE. Matrix metalloproteinase and proinflammatory cytokine production by chondrocytes of human osteoarthritic cartilage: associations with degenerative changes. Arthritis Rheum. 2001;44(3):585-94.
381. Laurent TC, Fraser JR. The properties and turnover of hyaluronan. Ciba Found Symp. 1986;124:9-29.

Appendices

Cartilage structure	
Normal	0
Surface irregularities	1
Pannus and surface irregularities	2
Clefts to transitional zone	3
Clefts to radial zone	4
Clefts to calcified zone	5
Complete disorganization	6
Cartilage cells	
Normal	0
Pyknosis, lipid degeneration hypercellularity	1
Clusters	2
Hypocellularity	3
Safranin-O	
Normal	0
Slight reduction	1
Moderate reduction	2
Severe reduction	3
No staining	4
Tidemark integrity	
Intact	0
Destroyed	1

Modified Mankin's histological Score for cartilage evaluation. Taken from "Efficacy Evaluation of a New Hyaluronan Derivative HYADD ® 4-G to Maintain Cartilage Integrity in a Rabbit Model of Osteoarthritis" Mainil-Varlet, P.; Cartilage. 2013;4(1):28-41 (296).